Activity dynamics lead to diverse structural plasticity at single dendritic spines

Ali Özgür Argunşah

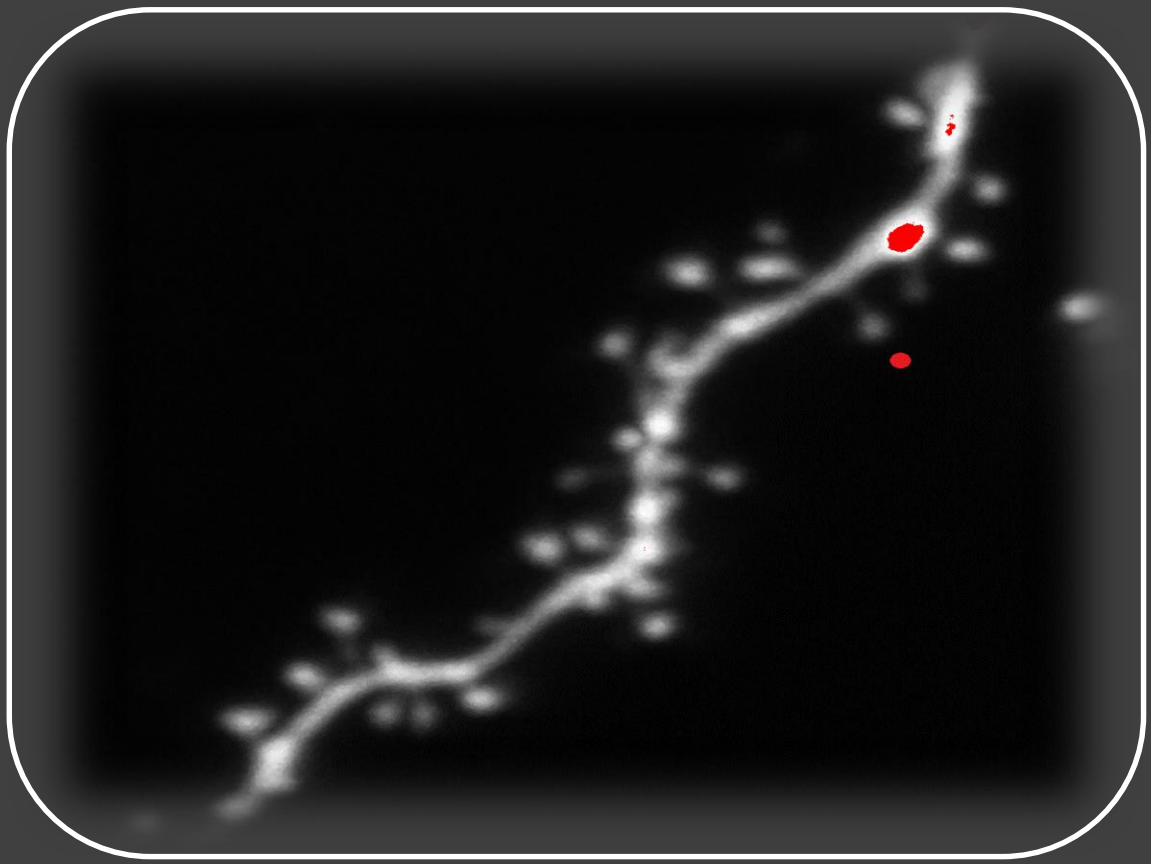

Dissertation presented to obtain the
Ph.D degree in Biology | Neuroscience

Instituto de Tecnologia Química e Biológica António Xavier | Universidade Nova de Lisboa

Oeiras,
July, 2016

INSTITUTO
DE TECNOLOGIA
QUÍMICA E BIOLÓGICA
/UNL

Knowledge Creation

Activity dynamics lead to diverse structural plasticity at single dendritic spines

Ali Özgür Argunşah

Dissertation presented to obtain the
Ph.D degree in Biology | Neuroscience

Instituto de Tecnologia Química e Biológica António Xavier | Universidade Nova de Lisboa

Research work coordinated by:

Oeiras, July, 2016

Activity Dynamics Lead to Diverse Structural Plasticity at Single Dendritic Spines

ALİ ÖZGÜR ARGUNŞAH

A Dissertation
Presented to the Faculty
of Universidade Nova de Lisboa
in Candidacy for the Degree
of Doctor of Philosophy

Inbal Israely

2016

To My Family
Sema, Özge and Hüseyin

Acknowledgments

First and foremost I would like to thank to Champalimaud Neuroscience Programme (CNP) for accepting me to this amazing Ph.D. programme. I cannot think of a better place to pursue a Ph.D. in neuroscience. CNP provided an amazing environment for learning, interactions and discussions, as well as great teachers during the period of courses and fantastic line of seminar speakers throughout my studies.

My supervisor Dr. Inbal Israely accepted me in her lab, neuronal structure and function (NSF), without hesitation, even though I had no experience in experimental neuroscience, not even any wet lab experience including mixing any two solutions. She supported me for the entire period of my studies. She taught me many things from preparing hippocampal slices to thinking like a neuroscientist and most importantly it was her seminar presentation back in the Instituto Gulbenkian de Ciência (IGC) that motivated me to do all the work that is presented in this thesis.

The members of NSF lab have always been the most supportive, helpful and knowledgeable. Dr. Yazmin Ramíro-Cortês, a.k.a. *Dr. Cortex*, without whom this thesis would not exist, has been the *teacher of biology* to this ignorant engineer, a.k.a. *Alisinho*. Hopefully-Dr.-by-the-time-of-this-thesis-defense Anna Felicity Hobbiss has been the source of friendship, emotional support and the voice of scientific-reasoning for the entire period of this Ph.D. road that we walked together. Inês Vaz de Cunha, Ana Vaz and Dr. Cátia Feliciano have always been there when I needed, either with their amazing technical skills or friendship. Last but not least, I would also like to thank Dr. María Royo and Dr. Daniela Pereira for their relatively recent but warm friendships and critical evaluation of my work.

I learned so much from my fellow students from INDP 2009 and PIBS 2009 programmes. Among those, a number of them have had profound implications on my scientific life. My main brainstorming partner Dr.

Bahtiyar Yılmaz and I had many amazingly interesting discussions that at the end confused both of us in a somewhat useful way. Dr. Thiago Santos Gouvêa introduced me the un-ending world of behaviorism, Pedro Garcia da Silva's extensive knowledge of neuroscientific techniques and literature, and his crazy theories motivated me to read and investigate more.

My dear friend Libbi Rickenbacher has just made my life better by her existence and being a giant ball of positivism, so I thank her for that. Dr. Dušica Radoš has always been there for me when I needed, she cheered me up and fed me with delicious pancakes. And finally, I would like to thank Dr. Branka, *the person*, Kolundžija for her ever-present support, friendship, and not to mention the critical reading of the thesis.

I have been very fortunate for being a part of three different research groups before and during my Ph.D. which I believe shaped my scientific career path. I would like to thank Dr. Emery N. Brown who accepted me in his lab. as a visiting researcher and let me watch a real brain surgery for 8 hours. I also want to thank Dr. Thomas J. McHugh for letting me spend two months in his lab, and his lab members, specially Dr. Steven J. Middleton and Roman Boehringer for teaching me how to make tetrode drives, surgeries and their welcoming friendships. Last but not least, my advisors during my masters, Dr. Müjdat Çetin and Dr. Aytül Erçil have been very supportive and encouraging for the neuroscience degree I wanted to pursue, and my colleagues from computer vision and pattern analysis lab., Emrecan Çökelek, Dr. Cemre Zor, Dr. Batu Akan, Dr. Serhan Coşar, Dr. Baran Çürüklü and Dr. Taner Eskil have always been supportive. And special thank to my dearest friend Dr. Saygın Topkaya, a.k.a. *Paşam*, who has been the person I enjoyed sharing ideas the most from any disiplines starting from particle physics to the philosophies found in science fiction literature.

The dendritic spine analysis toolbox Spines that is presented in the thesis is developed in collaboration with a great group of engineers/scientists and I am very happy and thankful for being able to work with such dedicated and motivated people. I want to thank them for putting up with my endless questions and requests starting from Dr. Devrim Ünay who initiated the study with me, Ertunç Erdil who has been the main co-developer and Muhammad Usman Ghani for being the most productive master student ever.

I gratefully acknowledge the funding sources that made this Ph.D. work possible. I was funded by the Fundação para a Ciência e a Techologia (FCT) fellowship for my first 4 years and by NSF lab. at Fundação Champalimaud (FC) for last 3 years.

I am very thankful for having Dr. Alfonso Renart and Dr. Leopoldo Petreanu, to whom I look up to scientifically, for being my thesis committee members and helping me with their constructive criticisms over the years. I am also very happy to have Dr. Armando Miguel Caseiro Pires Remondes and Dr. José A. Esteban for accepting to be a part my thesis discussion.

Lastly, I would like to thank my family for all their unconditional love and support.

Thank you.

Título

Diferentes Padrões de Atividade Induzem Diversas Formas de Plasticidade Estrutural em Espículas Dendríticas

Resumo

As sínapses, locais onde os neurónios se conetam entre si, são os locais onde se supõe que a aprendizagem ocorra através de alterações nestas conecções. LTP (do inglês long-term potentiation) e o LTD (do inglês long-term depression) foram propostos como mecanismos de adaptação das conecções entre neurónios. Através de uncaging de glutamato mediado pela luz, foi elucidada uma relação linear entre a quantidade de corrente que passa por uma sínapse individual e o tamanho da respectiva espícula dendritica, permitindo que as alterações estruturais que ocorrem ao nível das espículas sirva como medida para estimar plastícidade sináptica. Para quantificar de forma eficiente e exata as dinâmicas estruturais observadas em imagens adquiridas em microscópio de dois fotões desenvolvemos uma toolbox baseada Matlab, denomidade SpineS, que analisa automaticamente as alterações de volume das espículas dendriticas ao longo do tempo, baseando-se numa livraria de imagens representativas. Padrões de estimulação regularmente espaçados, como padrões de alta ou baixa frequência (do inglês high-frequency, HFS, e low-frequency stimulation, LFS, respectivamente), que são tradicionalmente usados para induzir plasticidade no hipocampo não são as formas mais comuns de atividade no cérebro. Assim, decidimos estudar quais são as formas funcionais e estruturais que padrões irregulares de atividade geram em espículas dendriticas individuais de neurónios piramidais da região de CA1 do hipocampo. Para isso foram desenhados padrões de estimulação que seguem uma distribuição Poisson e se assemelham aos padrões de atividade recebidos por estes neurónios textitin vivo. Neste estudo descobrimos que a longevidade

induzida por esta estimulação é determinada pela estrutura temporal do padrão de estimulação. Quando a atividade ocorre de forma homogénea ao longo do tempo, é observado um crescimento robusto e de longa duração, até 4 horas, em espículas individuais, que depende de ativação de receptores NMDA e síntese de proteínas. Contrariamente, se a densidade de eventos de atividade se acumular no início ou no fim do padrão de estimulação apenas ocorre um crescimento das espículas de curta duração. Estas experiências demonstram que o fator chave na indução de alterações sinápticas de longa duração em botões individuais é a estrutura temporal do padrão de estimulação, sendo que a duração total do estimulo, o número de eventos de atividade e a quantidade de glutamato libertado não difere entre padrões. De maior relevância foi a observação de que, durante a estimulação destes diversos padrões de atividade, as espículas dendriticas sofrem rápidas alterações estruturais. Recolhemos imagens das alterações que ocorrem durante os 60 segundos de estimulação e descobrimos que o crescimente toal de uma espícula dendritica é altamente variável mesmo em resposta ao mesmo padrão de actividade. Contudo, a quantidade total de crescimento expressa em cada espícula está significativamente relacionada com o facto de uma determinada espícula sofrer plasticidade de longa-duração, independentemente do padrão de estimulação. Isto indica que para determinados padrões de estimulação a integração final que ocorre ao nível da espícula é o que determina em última análise a longevidade da plasticidade sináptica.

Estes resultados elucidam como diferentes padrões de atividade levam a processos fundamentalmente diferentes de plasticidade ao nível das sinapses, permitindo compreender como as alterações da atividade neural *in vivo* têm consequências ao nível das sinapses e ao nível dos circuitos neuronais.

Abstract

Synapses are the sites at which learning is proposed to occur through changes in the strength of neuronal connections. Utilizing 2-photon mediated glutamate uncaging and imaging, the size of a dendritic spine and the amount of current which that synapse conducts has been shown to be linearly correlated and thus allows for structural changes in spine volumes to serve as a proxy for measuring plasticity. In order to efficiently and accurately quantify such structural dynamics, we developed a Matlab-based toolbox, named SpineS, which automatically analyses dendritic spine volume changes more rapidly, and with greater precision, based on a learned library of representative images. Regularly spaced stimulations, such as the high- and low-frequency patterns traditionally used to induce plasticity in the hippocampus, are not the most common forms of activity which occur in the brain. Therefore, we decided to investigate what are the functional and structural correlates of irregular patterns of activity at single spines of hippocampal CA1 pyramidal neurons. To accomplish this, we designed stimulation paradigms that follow a Poisson distribution, resembling the *in vivo* firing properties of the endogenous inputs to these neurons. We found that the longevity of the induced potentiation is determined by the timing structure of the stimulation pattern. When the activity that is delivered is homogeneously distributed over time, we observe robust and long-lasting potentiation and growth of single spines that last for at least 4 hours, requires NMDA activation and new protein synthesis. In contrast to this finding, if the density of events is clustered either towards the beginning or towards the end of the stimulus train, only short-term potentiation is achieved. These experiments demonstrate that a key factor in the induction of long-lasting changes at individual inputs is the structure of the activity, as the total stimulation time, the number of events, and the amount of glutamate delivered are all constant. Of further interest to us was the observation that during the delivery of these vari-

ous activity patterns, we saw that spines were undergoing rapid structural dynamics. We imaged the changes that were taking place during these 60 second stimulation periods and found that the total spine growth is highly variable even in response to the same activity pattern. However, the total amount of growth expressed at a spine was significantly correlated to whether that particular spine will undergo long-lasting plasticity. This indicates that for certain patterns of activity, the final integration which occurs within a spine is ultimately what influences its long-term plasticity outcome.

These results shed light on how different patterns of activity lead to fundamentally different plasticity processes at synapses, providing insight as to how the variety of neural activity patterns *in vivo* will have long-term consequences for synaptic strength and thus circuit organization.

Author Contributions

Experiments conducted in this thesis were designed by Ali Özgür Argunşah and Inbal Israely.

Data were collected and analyzed by Ali Özgür Argunşah.

Dendritic spine analysis software (SpineS) is developed in collaboration with Devrim Ünay, Ertunç Erdil, Muhammad Usman Ghani, Arif Murat Yağcı, Sümeyra Demir Kanık, Müjdat Çetin, Anna Felicity Hobbiss and Yazmín Ramiro Cortés.

Financial Support

This work is supported by Fundação para a Ciência e a Techologia (FCT) with grant number SFRH/BD/51264/2010, Fundação Champalimaud (FC) and Instituto Gulbenkian de Ciência (IGC) and The Scientific and Technological Research Council of Turkey (TÜBiTAK) with grant number 113E603.

Contents

List of Tables

List of Figures

Chapter 1

Introduction

1.1 Neuron Doctrine

In the early 1800s, the brain was thought to be a continuous network of tissue, a theory known as the *reticular theory*. Santiago Ramón y Cajal, widely thought of as the father of modern neuroscience, used Golgi staining technique to show that the brain is made up of discrete elements, named neurons. Having observed discreet spaces at the tips of cerebellar basket cells, he proposed that neurons are the fundamental units of the nervous system, in a theory known as the *neuron doctrine* (López-Muñoz, Boya, & Alamo, 2006). Further research suggested that neurons are connected to each other via synapses, a term coined by Sherrington in 1897 (Foster, 1895; Fulton, 1960; Sabbatini, 2003; Segal, 2004).

The discovery of the discrete nature of brain tissue and the hypothesized role of synapses in the formation of memories raised various questions about how the number of neurons or synapses are involved in the storage of memory, how different forms of activity could be responsible for the encoding and shaping of information storage, and what are the specific mechanisms underlying these processes. In particular, understanding how synapses are formed and whether and how they are modified are questions which the neuroscience community is still trying to understand, and which will be addressed in part by the work presented in the following chapters of this thesis.

1.2 Synaptic Plasticity

With the advent of electron microscope, it was demonstrated that neurons are indeed connected to each other via synapses (Palade, 1954; De Robertis & Bennett, 1955; López-Muñoz et al., 2006). The human brain has on average 10^{11} neurons and an estimated number of 10^{14} synapses connecting them (DeFelipe, Marco, Busturia, & Merchán-Pérez, 1999; Brait-

enberg, 2001; Azevedo et al., 2009). The discovery of synapses between neurons raised the question of how connectivity is established and how communication between neurons takes place. Further, it raised the possibility that the efficacy of these points of connection may be modified, as a means by which to encode the changes during learning. Synaptic plasticity refers to the changes in the efficacy of synaptic connections and the efficacy of synapses changes conditional to activity (Bliss & Lømo, 1973) as well as during learning (Whitlock, Heynen, Shuler, & Bear, 2006), and these changes correlate with the structural alterations of dendritic spines (Asrican, Lisman, & Otmakhov, 2007; Matsuzaki, Honkura, Ellis-Davies, & Kasai, 2004).

Many studies to date have focused on defining how neurons communicate across synapses, beginning with an understanding of the basic organization of the structure. The synapse is a tripartite complex, composed of a pre-synaptic axon terminal, a post-synaptic dendritic spine, and glia (Araque, Parpura, Sanzgiri, & Haydon, 1999). When an action potential reaches the axon terminal, it leads to the opening of voltage-gated calcium channels which further leads to the release of glutamate in a stochastic manner. Glutamate released from the axonal bouton (pre-synaptic partner of a synapse) binds to glutamatergic receptors at spines (Figure 1.2.1). Amino-3-hydroxy-5-methyl-4-isoxazolepropionate (AMPA) and N-methyl-D-aspartate (NMDA) receptors are the two main glutamatergic receptors, crucial for synaptic transmission and plasticity. The binding of glutamate induces conformational changes in receptors leading to ionic exchanges between the inside and outside of the spine. AMPARs predominantly conduct Na ions and have faster channel kinetics compared with NMDARs, which puts them in the first node of the synaptic transmission-chain. NMDARs conduct both Na and Ca ions and Ca^{2+} is required for the induction of synaptic plasticity. Calcium theory of plasticity suggests that the immediate high concentration of Ca^{2+} leads to long-term po-

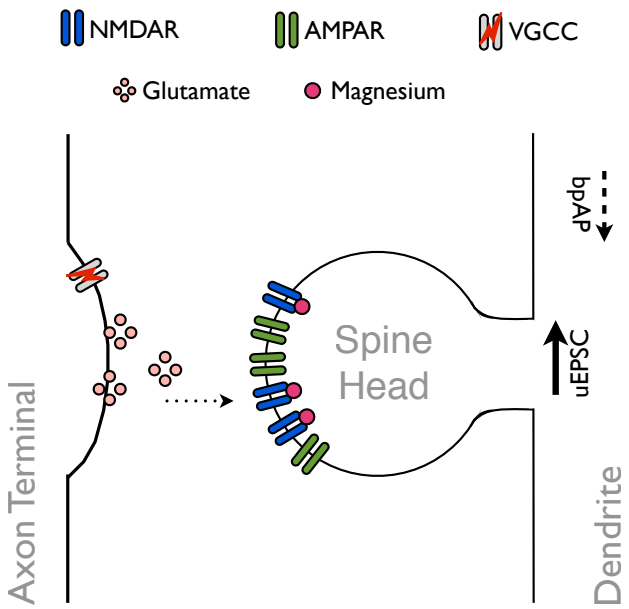

Figure 1.2.1. **An Excitatory Synapse.** Action potentials arriving the axonal terminal activates the voltage-gated Ca^{2+} channels which leads to Ca^{2+} entering the terminal and the release of glutamate. Glutamate binds to AMPA and NMDA receptors. AMPAR requires only glutamate to be activated. NMDAR requires glutamate and electrical depolarization, due to the a Mg^{2+} blocking the channel in a voltage-dependent manner, which makes NMDARs coincident detectors of glutamate binding and depolarization. Upon the depolarization of a neuron, activity back-propagates through dendrites to spines (back-propagating action potential (bpAP)).

tentiation (LTP), whereas prolonged low concentration of Ca^{2+} leads to long-term depression (LTD) (Otmakhov, Griffith, & Lisman, 1997; Lisman & McIntyre, 2001). Hence, Ca^{2+} couples electrical excitation with intracellular signaling pathways (Hestrin, Sah, & Nicoll, 1990). Two main pathways are required for synaptic plasticity and structural remodeling, Ca→CaMK ($Ca^{2+}/Calmodulin$ dependent protein kinase II) pathway

and Ras→MAPK (Mitogen activated protein kinase) pathway (Sheng & Kim, 2002).

The type of LTP mentioned above is called NMDAR-dependent LTP and it has been proposed that there are different temporal phases of this NMDAR-dependent LTP (Bliss, Collingridge, & Morris, 2014), an initial short period lasting about 15-20 min following induction, an early phase often referred of E-LTP that lasts for about an hour, and a third phase, called as late LTP (L-LTP) which persists over a longer period of time and is predominantly characterized by its protein synthesis dependence (Stäubli & Scafidi, 1999; Redondo & Morris, 2011). It has been shown that protein-synthesis inhibitor anisomycin blocks the induction of L-LTP (Fonseca, Nägerl, Morris, & Bonhoeffer, 2004; Govindarajan, Israely, Huang, & Tonegawa, 2011) and long-term memory at 24 h in a novelty exploration task (Wang, Redondo, & Morris, 2010).

It was Donald Hebb who first postulated that *activity* may be the governing factor of synaptic plasticity, which was later supported by experimental evidence (Hebb, 1949; Lowel & Singer, 1992). In his seminal book *The Organization of Behavior: A Neuropsychological Theory*, Hebb famously wrote:

> When an axon of cell A is near enough to excite a cell B and repeatedly or persistently takes part in firing it, some growth process or metabolic change takes place in one or both cells such that A's efficiency, as one of the cells firing B, is increased (Hebb, 1949).

which has later been popularized by Siegrid Löwel's summary:

> Neurons wire together if they fire together (Lowel & Singer, 1992).

Mathematical studies that had been performed around the time that Hebb was developing his ideas (McCulloch & Pitts, 1943; Farley & Clark,

1954), as well as the additional modeling work (Rosenblatt, 1958; Bienenstock, Cooper, & Munro, 1982), suggested that plasticity could be established in two directions: the electro-chemical transmission efficacy between two neurons can either increase or decrease in response to activity. These processes were later experimentally shown to occur across a variety of different synapses (Bliss & Lømo, 1973; Ito & Kano, 1982; Bear & Malenka, 1994), and became known as LTP and LTD, respectively.

Today, it is well established that LTP and LTD are key cellular mechanisms for learning and memory (Sigurdsson, Doyère, Cain, & LeDoux, 2007; Feldman, 2009). Importantly, accompanying these changes in synaptic strength are the structural modifications of dendritic spines, which will be discussed in greater detail below in section 1.4.

1.3 Synaptic Plasticity in the Hippocampus

It has been shown that lesions of the hippocampus (such as in the famous case of HM) led to the inability to form new memories (Scoville & Milner, 1957). Evidently, hippocampus has been the major focus of the studies addressing cellular mechanisms of learning and memory. Bliss and Lømo were the first to show that high frequency electrical stimulation of perforant pathway axons increases the efficacy of synaptic transmission at dentate gyrus-perforant pathway synapses (Figure 1.3.1) of anesthetized rabbit hippocampus (Bliss & Lømo, 1973). This was the first experimental evidence to show the plastic nature of a synapse. Synaptic plasticity has since been characterized at the majority of synapses within the nervous system, from different regions of the hippocampus (Bliss et al., 2014; Huganir & Nicoll, 2013), to the cortex (Froemke, 2015; Friauf, Fischer, & Fuhr, 2015), as well as at subcortical regions such as the amygdala (Mahan & Ressler, 2012) and striatum (Hawes, Gillani, Evans, Benkert, & Blackwell, 2013; Cerovic, dIsa, Tonini, & Brambilla, 2013).

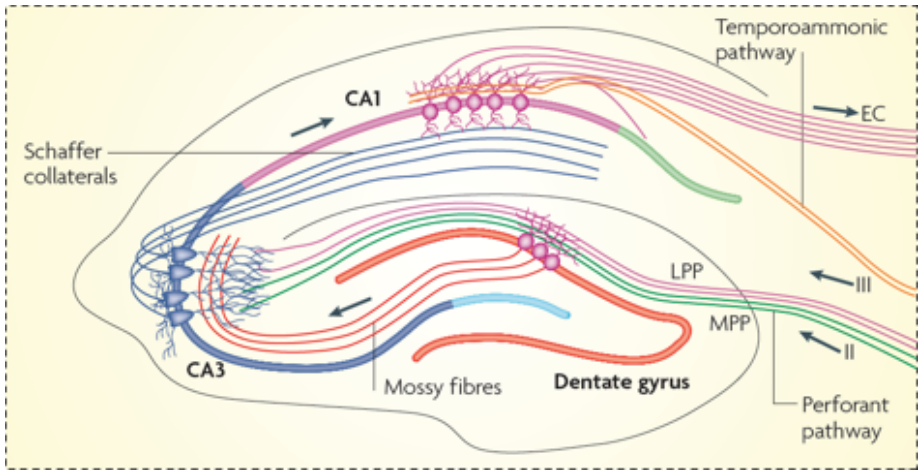

Figure 1.3.1. **Hippocampal Circuitry of a Transverse Slice.** Hippocampus has a very stereotypical structure. Hippocampal slices retain their cytoarchitecture and connections *ex vivo* which facilitates the studies of synaptic plasticity mechanisms. Placing a stimulation electrode at one pathway allows the studies of specific types of synapses. (Image is modified from Deng, Aimone, & Gage, 2010)

The hippocampus is located in the medial temporal lobe and it represents a part of the limbic system (Eichenbaum, 1997). In addition to being the site where synaptic plasticity was first described, is also a structure highly amenable to experimental manipulation. This is due to its highly laminar organization, which allows for the connections within the structure to be maintained when manipulated *ex vivo*. When sliced transversally, tri-synaptic pathway of the hippocampus can be preserved intact. Cortical projections enter the hippocampus via the perforant and the temporoammonic pathways (Figure 1.3.1 (Deng, Aimone, & Gage, 2010)). Perforant pathway starts with dentate gyrus (DG) and DG granular cells send axons to CA3 area via mossy fibers, and the Schaffer collateral axons emerging from CA3 pyramidal neurons form synapses onto the apical dendrites of CA1 pyramidal neurons. On the other hand, temporoammonic pathway

axons form synapses onto the basal dendrites of CA1 pyramidal neurons. In this thesis, Schaffer collateral synapses have been studied.

Behavioral studies showed that CA1 pyramidal neurons fire conditional to the animal's location (hence they are called place cells) (O'Keefe & Dostrovsky, 1971) and the Schaffer collateral synapses were shown to be modified during the formation of this place memory (McHugh, Blum, Tsien, Tonegawa, & Wilson, 1996; Mehta, Quirk, & Wilson, 2000). This long-term modifications on the transmission efficacy of a synapse is a function of the converging activity and the subsequent firing caused by that activity. There has been two ways of studying plasticity electrically, repeated high or low frequency activation of pre-synaptic terminals (Bliss & Lømo, 1973; Bienenstock et al., 1982), and coincident activation of post-synaptic action potentials (APs) and excitatory post-synaptic potentials (EPSPs) (Markram, Lübke, Frotscher, & Sakmann, 1997; Bi & Poo, 1998; Lisman & Spruston, 2010).

Recent advancements in the field of optics in combination with photo-activatable compounds have made it possible to study plasticity at the level of single synapses.

1.4 Dendritic Spines and Structure-Function Coupling

Although focus in Hebbs postulate (see section 1.2) is often placed on the need for coincident activity in order to effect changes in efficacy between synapses, an integral part of the theory is the requirement for *"some growth process or metabolic change"* to accompany the changes in efficacy. Therefore, we will discuss the structural changes that occur during synaptic plasticity below.

Dendritic spines are the post-synaptic structures on which the majority of excitatory synapses of pyramidal neurons in the brain are located.

Their morphology is highly regulated by incoming activity. As described above, the induction of plasticity requires CaMKII and Ras/MAPK signaling pathways. However, the activation pattern and the morphology of the spine determines the level at which these interactions happen. This occurs due to filtering and compartmentalization of electro-chemical interactions within the volume of the spine head (Harris & Stevens, 1989; Tonnesen, Katona, Rózsa, Nagerl, et al., 2014). The post-synaptic density (PSD), the region at the tip of a spine, is the region where the majority of receptors are clustered and interact, and the size of this specialization is strongly correlated with the volume of the spine head (Harris & Stevens, 1989; Arellano, Benavides-Piccione, DeFelipe, & Yuste, 2007). As early as 1975, it was shown that the size of a spine changes immediately following a stimulation (Van Harreveld & Fifkova, 1975) in dentate gyrus granular cells. In a follow up study, this spine enlargement was suppressed when a protein synthesis inhibitor, anisomycin, was applied prior to the stimulation (Fifková, Anderson, Young, & Van Harreveld, 1982). Further evidence supporting the connection between functional and structural coupling was seen when in response to brief bursts of high frequency stimulation of Schaffer collateral-commisural projections, the number of shaft synapses increases and the variability of dendritic spines decreases (Lee, Schottler, Oliver, & Lynch, 1980). More recently, an electron microscopy study showed that when an axon makes more than one synapse with multiple spines, those spines have similar volumes, indicating that activity is critical for determining spine size (Bartol et al., 2015).

A major advance in our understanding of the relationship between spine size and synapse function accompanied the technological development which allowed for precise stimulation of single spines. Technical developments in the field of microscopy enabled researches to monitor structural changes at single-synapse level *in vivo*. Invention of caged compounds in combination with the improved spatial optical targeting

of laser beams advanced the field one step further in terms of the specificity of the targeted synapses (Ellis-Davies, 2007). Caged compounds are light-sensitive precursors of ligands that are inactive in the absence of light. Application of light pulses onto these compounds breaks the cage by a process called photolysis and frees the ligand from the cage, enabling spatio-temporally controlled manipulations of targeted processes. Schiller *et al.* used UV excitable caged glutamate to study NMDA-dependent Ca^{2+} dynamics at single spines (Schiller, Schiller, & Clapham, 1998) and they showed that, when paired with AP firing, uncaging controlled NMDAR activation caused a supralinear increase in Ca^{2+} through these receptors. Patterned two-photon uncaging was used to understand dendritic integration mechanism at cortical (Branco, Clark, & Häusser, 2010) and CA1 pyramidal neurons (Smith, Ellis-Davies, & Magee, 2003; Losonczy & Magee, 2006; Losonczy, Makara, & Magee, 2008). Using two-photon glutamate uncaging in combination with somatic and dendritic patch clamp recordings, significant contributions were made by showing that pseudo-synchroneous multisite glutamate uncaging leads to the non-linear integration of EPSCs at hippocampal CA1 pyramidal neurons (Smith et al., 2003; Losonczy & Magee, 2006; Losonczy et al., 2008) and spatio-temporal properties of the multisite uncaging patterns determine the level of non-linearity of dendritic calcium and somatic EPSC integration (Branco et al., 2010).

This technology allowed for the careful assessment of spine volume in relation to the amount of current that the synapse conducts (Matsuzaki et al., 2004). A tight positive correlation between synaptic current and spine head volume has been demonstrated (Matsuzaki et al., 2004; Asrican et al., 2007; Harvey & Svoboda, 2007). This findings allowed researchers to use spine head volume as a proxy for plasticity.

1.5 Single Spine Plasticity

Matsuzaki *et al.* used two-photon glutamate uncaging and imaging to stimulate single dendritic spines and monitor their structural responses regarding activity (Matsuzaki et al., 2004). They developed a glutamate uncaging protocol by comparing normalized volume responses of dendritic spines to two different electrical stimulation condition. First, they stimulated Schaffer collaterals with 100 Hz, 1 sec electrical stimulation with the presence of 1 mM Mg^{2+} as they imaged a CA1 dendritic branch. Similar spine volume change was also induced by with 2 Hz, 60 sec electrical stimulation without Mg^{2+}. Therefore, this $[Mg^{2+}]$ dependent frequency mapping allowed them to come up with the uncaging pattern they used for the study (60 uncaging pulses (each 0.6 msec) in 1 min, see Table 1.1). Glutamate uncaging induced similar spine enlargement as well, and they also showed that this form of LTP is NMDAR and CaMKII dependent ((Matsuzaki et al., 2004), Figure 1f and Figure 2e, respectively).

In a following study (Harvey & Svoboda, 2007), another regular uncaging pattern was found to evoke similar single-spine volume dynamics using 30 uncaging pulses (each pulse 4 msec, instead of 0.6 msec in the previously described study) for 1 min. Additionally, they showed that the stimulation of multiple spines with two different uncaging protocols (*30 pulses,1 min, 4msec* vs *30 pulses, 1 min, 1msec*), did not lead to the potentiation of spines stimulated with shorter pulse lengths, hence this protocol is referred to as sub-threshold.

Govindarajan *et al.* using the same stimulation protocol in combination with forskolin in order to raise the intracellular levels of cyclic-AMP (cAMP) in the stimulated neurons. cAMP is a second messenger that acts on protein kinase A (PKA) pathway, hence boosting the protein translation in the cell. This study showed that the uncaging induced LTP under

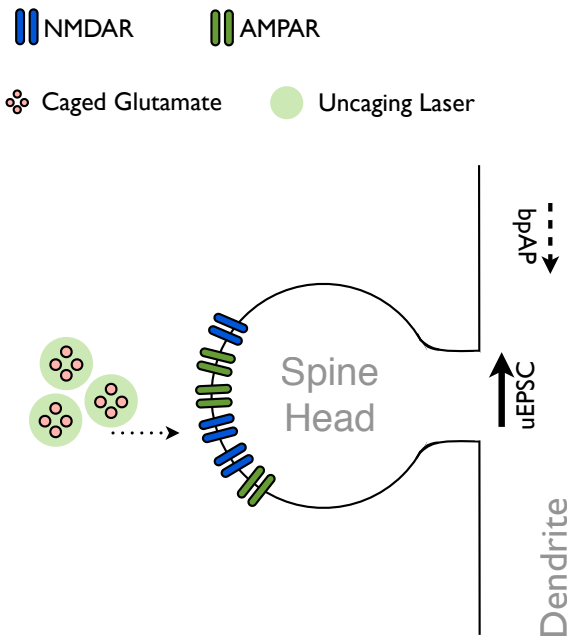

Figure 1.5.1. **Pre-synaptic Neurotransmitter Release can be Mimicked by Glutamate Uncaging.** Two-photon glutamate uncaging allows glutamate to be released in a spatially specific, controlled way, allowing single spines to be studied. Studies addressing NMDA dependent plasticity are performed in the absence of Mg^{2+}

the influence of forskolin extended the longevity of the structural spine plasticity (Govindarajan et al., 2011).

Table 1.1 summarizes the stimulation protocols that has been used to induce LTP at single dendritic spines using electrical and uncaging laser pulses.

Table 1.1. **Requirements of Inducing Plasticity at Single Dendritic Spines.** Plasticity can be induced at single spines using electrical stimulation of glutamate uncaging. Glutamate uncaging under the absence of $[Mg^{2+}]$ induces plasticity that is conditional to the number of uncaging pulses and pulse width.

Study	**Stim. Type**	**Freq. (Hz)**	**Stim. Len. (sec)**	**# of Pulses**	**Mg (mM)**	**Uncaging Pulse Len. (msec)**
Matsuzaki et al. (2004)	Electrical	100	1	100	1	-
	Electrical	2	60	120	**0**	-
	Uncaging	1	60	60	**0**	0.6
Harvey & Svoboda (2007)	Uncaging	0.5	60	30	**0**	4
Israely et al. (2011)	Uncaging	0.5	60	30	**0**	4

1.6 Spike-Timing Dependent Plasticity

It has been shown that relative firing times between a pair of feed-forward connected neurons determines the direction and the level of plasticity at the synapse connecting these neurons. This phenomenon is known as spike-timing dependent plasticity (STDP) (Markram et al., 1997; Bi & Poo, 1998). STDP is proposed to be the mechanism governing the synaptic plasticity *in vivo* (Paulsen & Sejnowski, 2000). However, this proposal is highly debated (Lisman & Spruston, 2005, 2010).

There has been various working models proposed to be the induction mechanism of STDP (Markram, Gerstner, & Sjöström, 2012). Original model was based on the timing difference between one pre-synaptic and one post-synaptic spike. Repeated activation of this pre→post firing order induced LTP at excitatory synapses of pyramidal neurons as long as

timing difference was smaller 50 msec (Bi & Poo, 1998). This finding was in strong agreement with Hebb's original proposal (see section 1.2). Additionally, reversing the order of pre→post firing induced LTD (Markram et al., 1997; Bi & Poo, 1998). This simple two-spike interaction model shown be explaining cortical development and remapping of visual cortical maps through competition (Song, Miller, & Abbott, 2000; Song & Abbott, 2001) and hippocampal receptive fields (Mehta et al., 2000).

Further research showed that this two-spike model is not sufficient to explain a large body of the experimental data which lead to the development of three- and four- spike models (Froemke & Dan, 2002; Froemke, Tsay, Raad, Long, & Dan, 2006; Pfister & Gerstner, 2006). In these models instead of pre→post or post→pre spike interactions, higher order statistical interactions between multiple inter-spike intervals were taken into consideration such as pre→post→pre, post→pre→post (Pfister & Gerstner, 2006), pre→post→pre→post or post→pre→post→pre (Froemke & Dan, 2002). These models were shown to be better at explaining the experimental data which shows the importance of complex spike-timing interactions.

1.7 Naturalistic Patterns, Synaptic Responses and Plasticity

The induction of LTP was discovered by high frequency electrical stimulation (HFS) and variations of HFS trains are used to induce LTP in the hippocampus and other brain regions. Although these constant high frequency protocols are effective at inducing potentiation, they do not represent the breadth of activity patterns that can be observed *in vivo*. The existence of both temporal and rate coding in neural networks has been well established (Ferster & Spruston, 1995; Christopher deCharms & Merzenich, 1996; Prut, Slovin, & Aertsen, 1995; Bienenstock et al., 1982;

Tsodyks & Markram, 1997) yet how such parameters influence plasticity at single inputs has not been addressed yet. A number of computational and experimental studies have been conducted, investigating the effects of naturalistic stimulation patterns on the induction of plasticity. Here, we are going to review these studies briefly and try to summarize how different groups approached this problem.

Migliore and Lanski (Migliore & Lansky, 1999) made a computational model of synaptic transmission to test to what extent the temporal variations at the stimulation train can change the state of a synapse. Their results showed that, even if the mean stimulation frequency is maintained constant, the probability of inducing LTP and LTD can be a function of the temporal variation of the stimulation train. Such temporal variations of the input train has not taken into account in the experiments discussed earlier.

The first study to use naturalistic stimulus patterns (NSP) to study short and long term plasticity showed that NSPs induce LTP in hippocampal slices (Dobrunz & Stevens, 1999), whereas they found no relationship between the instantaneous frequency and the response magnitude for NSPs. The NSPs were taken from the timing of action potentials recorded *in vivo* from hippocampal place cells of awake, freely moving rats. They showed that NSPs show highly variable timing. The interspike intervals measured *in vivo* were multiplied by 3 to account for the temperature difference between the *in vivo* measurements (37 ^{o}C) and slice recordings (24 ^{o}C) (Dobrunz & Stevens, 1999).

This study mostly focused on short term plasticity, such as the response size variations with respect to stimulus number and inter-stimulus intervals (ISI) within the stimulation train. The authors investigated LTP using natural stimulus pattern, and they tested field EPSP slopes for two independent pathways in the same hippocampal slice. A 256-point natural stimulus pattern was applied for 12 min, which caused a long lasting

potentiation (1.5 times more compared with the baseline) of the response to constant frequency (0.17 Hz) stimulation. The control pathway, which was not stimulated with the natural pattern, was not potentiated.

Another study investigated the plasticity concequences of naturalistic patterns in spike-timing dependent plasticity (STDP) setting (Froemke & Dan, 2002). Using the firing patterns of two cortical pyramidal neurons that have overlapping visual fields as pre- and post-synaptic trains, it has been shown that the activity-induced synaptic modifications do not depend only on the relative spike timing between the neurons, but also on the inter-spike intervals within each neuron (Froemke & Dan, 2002).

In neocortical slices, stimulation patterns derived from slow wave sleep (SWS) induced LTP (Rosanova & Ulrich, 2005) or LTD (Czarnecki, Birtoli, & Ulrich, 2007) depending on the pattern of stimulation (Rhythmic burst or spindle-like trains, respectively). deKay *et al.* compared naturalistic patterns with constant frequency stimulation in a comparative study between young adult (P28-P35) and juvenile (P12-P18) rats (deKay, Chang, Mills, Speed, & Dobrunz, 2006). They showed that the average responses to naturalistic stimuli and constant frequency stimulus both showed modest depression in young adults, but juveniles showed facilitation for NSPs but short-term depression after constant frequency stimulation. Tunstall *et al.* (Tunstall, Agnew, Panzeri, & Gigg, 2010) used two different naturalistic stimulus patterns to stimulate neurons in subiculum. First pattern included bursts of activity, whereas second pattern was spaced more evenly. Differences in the short term responses to two different patterns were reported, and they concluded that dynamic interactions between rate and temporal coding exist between input spikes and stimulus response but they have not observed any LTP for either class.

Gundfinger *et al.* used irregular stimulus trains resembling the natural spike statistics from DG neurons to study short and long term plasticity mechanisms at mossy fiber synapses in acute hippocampal slice prepa-

rations (Gundlfinger et al., 2007; Gundlfinger, Breustedt, Sullivan, & Schmitz, 2010). They used *in vitro* electrophysiology and computational modeling to study the interactions between LTP and STP at mossy fiber synapses and showed that LTP occluded the frequency facilitation by reducing the dynamic range of the synapse. They concluded that phenomena such as alterations in the place field size and speed could be explained by mechanism related to experience-dependent changes in the properties of short-term facilitation.

In another study combining electrophysiological recordings with realistic modeling of STP in excitatory hippocampal synapses, Kandaswamy *et al.* showed that STP increases the information transfer in a time and frequency dependent fashion. The study showed that STP in Schaffer collateral synapses increased the information transfer in a wide range of input frequencies from 2 to 40 Hz. Moreover, time dependent analysis of mutual information predicted that in low-release probability synapses, STP acts to maximize information transfer specifically for short high frequency bursts. They concluded that since many types of synapses are not likely to experience extensive periods of high-frequency activity under natural conditions, these synapses do not reach a steady state *in vivo*.

In summary, the studies discussed above found that the short term responses are very sensitive to the temporal variations of the input patterns. Transient bursting patterns are necessary for LTP to occur in the hippocampus (Pike, Meredith, Olding, & Paulsen, 1999) but not sufficient, since not all naturalistic patterns induce LTP. Finally, in the light of these experiments, a biophysical modeling study, Migliore *et al.* concluded that the state of the synapse at the time of plasticity induction is a key factor in determining whether a pattern will lead to the induction of LTP or LTD (Migliore, De Simone, & Migliore, 2015).

1.8 Contribution of this Dissertation

The work in this dissertation investigates the functional and structural consequences of non-regular patterns of activity at single inputs. The aim of the study was to understand how more naturalistic stimulation scenarios encode information at single synapses, and is built around the idea that the transmission of information does not occur through regularly spaced neurotransmitter release *in vivo* (Zador & Dobrunz, 1997).

In chapter 2 we listed the materials that we used in our experiments and explained the methods that have been used.

We introduce a dendritic spine analysis toolbox named SpineS in chapter 3. Studies addressing structural dendritic modifications require the collection of large scale dendritic spine images which requires laborious manual analysis. Manual analysis of vast number of dendritic spines is not only time consuming and tiresome, it also is prone to subjective blunders. Therefore, we developed SpineS for the automatic quantification of dendritic features. SpineS is Matlab based and open-source.

In chapters 4 and 5, we present the investigations of long- and short-term structural spine dynamics comparing regular and Poisson distributed stimulation patterns. This is the first study using naturalistic patterns to understand structural plasticity mechanisms at single dendritic spines.

In chapter 6 we discuss the implications of the findings and consider potential mechanisms underlying the obtained results. Further, we will reflect upon the implications of these findings to the study of synaptic plasticity and how this work may contribute to the understanding of plasticity within neural circuits.

Chapter 2

Materials and Methods

2.1 Materials

2.1.1 Dissection Solution

First, we prepared 10× concentrated Krebs-Ringer solution (Table 2.1) and we kept this stock solution at 4^oC. Later, we prepared 1× solution (Table 2.2) by adding $CaCl_2$ and $MgCl_2$ while the solution was bubbled using 95% O_2 and 5% CO_2 for 30 min. The solution was afforated using distilled water to 250 mL, sterilized with vacuum filter, aliquoted in 40 mL volumes and stored at -20^oC until dissection.

Table 2.1. 10× **Krebs Ringer Dissection Solution.**

10× **Krebs Ringer**	**mM**	**M.W.**	**in 250 mL**
KCl	25	74.55	0.465 g
$NaHCO_3$	260	84.01	5.460 g
NaH_2PO_4	11.5 mM	119.98	0.344 g
$D-Glucose$	110 mM	180.16	4.95 g

Table 2.2. 1× **Krebs-Ringer Dissection Solution.**

1× **Krebs-Ringer**	**mM**	**in 250 mL**
10× **Krebs-Ringer**	100	25 mL
$MiliQWater$	-	300 mL
$Sucrose$	238	20.36 g
$CaCl_2$	1	0.25 mL (1M CaCl2)
$MgCl_2$	5	1.25 mL (1M MgCl2)

2.1.2 Dissection Equipment

Brains were dissected using surgical tools (Figure 2.1.1). During the procedure, the extracted brain and hippocampal slices were kept in ice-cold Krebs-Ringer solution. Following the extraction, hippocampi were placed on a filter paper with Krebs-Ringer solution and fixed on the chopper

(Figure 2.1.2) plate. Afterward, they were sliced 350μm-thick transverse slices and kept in an incubator in six-well plates (Figure 2.1.3).

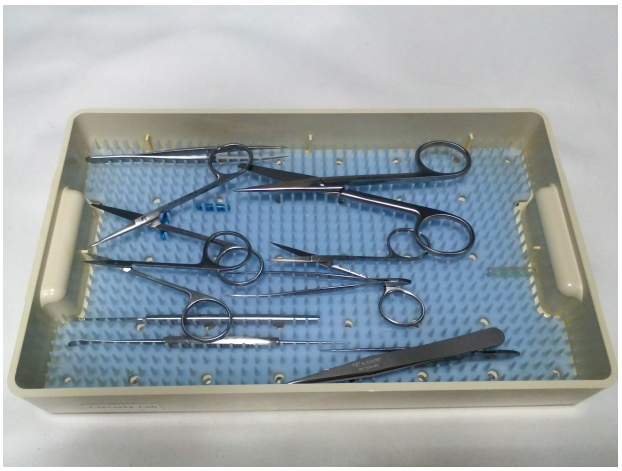

Figure 2.1.1. **Surgical Dissection Set.** Brain is extracted out of skull using the surgical set to be sliced using tissue slicer.

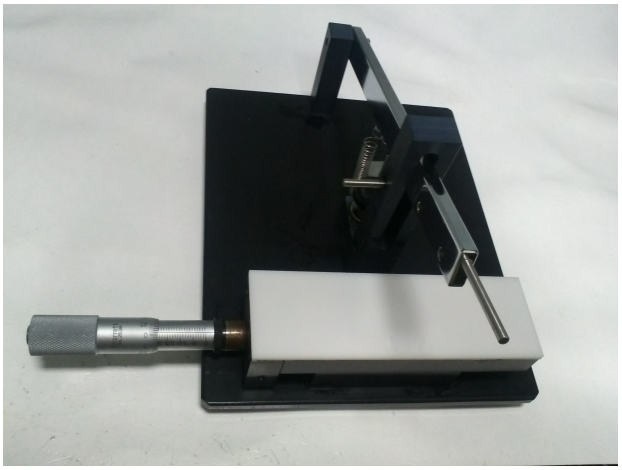

Figure 2.1.2. **Tissue Slicer.** Hippocampi were sliced into 350 μm thick slices for culturing.

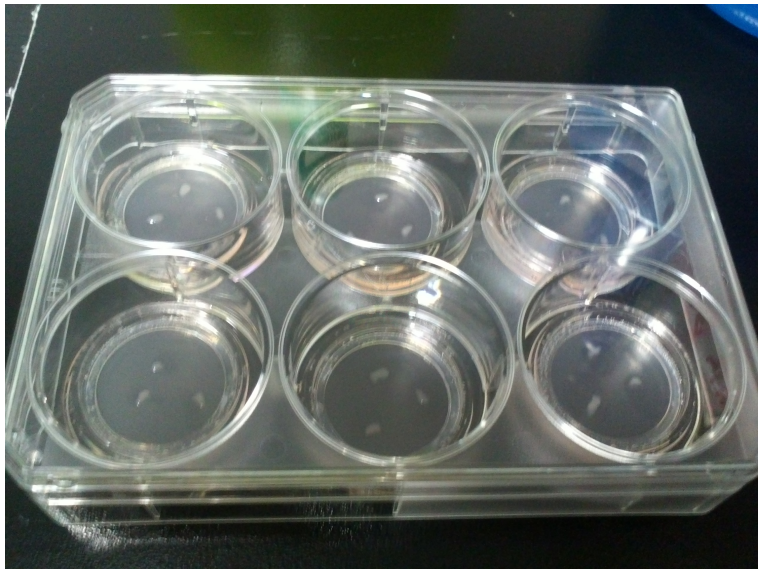

Figure 2.1.3. **Cultures in Six-Well Plate.** Hippocampal slices are incubated in six well plates in the incubator. We placed three to four slices per well sitting on inserts with the culture media underneath them. Medium was changed every two to three days.

2.1.3 Biolistic Gene Transfer

Hippocampal neurons from organotypic slice cultures were transfected using a Helios gene gun (Bio-Rad) after four to seven days *in vitro* (DIV). Gold beads (10 mg, 1.6 μm diameter, Bio-Rad) were coated with 100 μg of pCAGGS-AFP (Fig. 2.1.4) plasmid DNA (Ogawa & Umesono, 1998), according to the Bio-Rad protocol[1], and delivered biolistically into the slices at 180-200 psi (Woods & Zito, 2008).

[1] `http://www.bio-rad.com/LifeScience/pdf/Bulletin_9541.pdf`

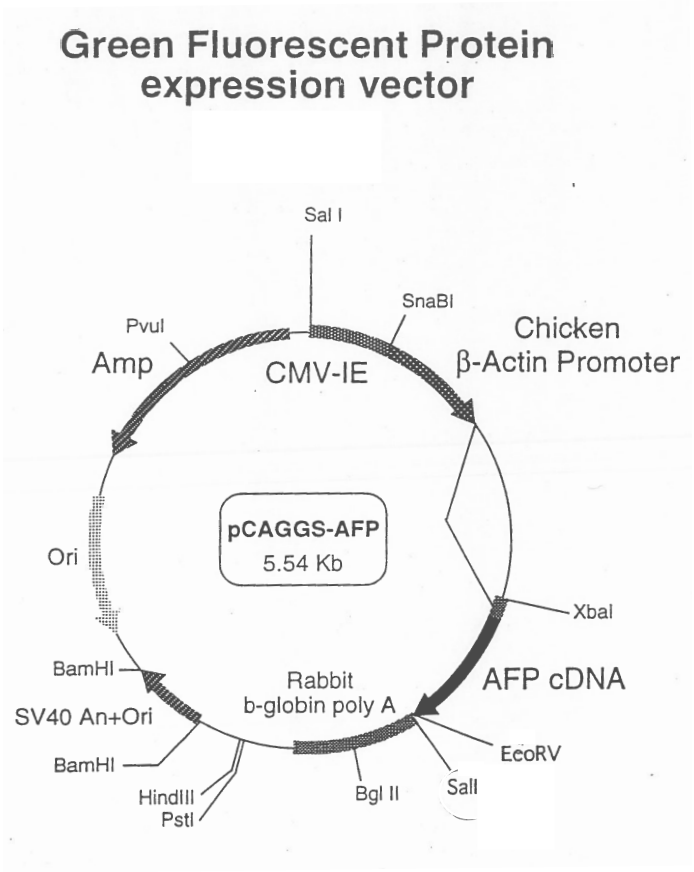

Figure 2.1.4. **pCAGGS-AFP Vector.** pCAGGS-AFP plasmid was used for the sparse transfection of hippocampal neurons. Plasmid size: 5.54 Kb, constructed by Hidesato Ogawa (Ogawa & Umesono, 1998).

2.1.4 Internal Solution for Patch Pipette

Whole cell recordings were performed at room temperature, with glass pipettes (access resistance 6 to 10 MΩ) filled with internal solution con-

Table 2.3. **Artificial Cerebrospinal Fluid (ACSF).**

ACSF (2X)	**mM**	**M.W.**	**in 1 L**
$NaCl$	127	58.44	14.84 g
KCl	2.5	74.55	0.372 g
$NaHCO_3$	25	84.01	4.2 g
NaH_2PO_4	1.25	119.98	0.299 g

taining: 115 mM potassium gluconate, 10 mM HEPES, 20 mM KCl, 4 mM Mg-ATP, 0.3 mM Na-GTP, 10 mM Na-phosphocreatine and 1 μM $CaCl_2$. pH was adjusted to 7.4 using KOH. In some recordings, ALEXA 488 Fluor (30μM, Invitrogen, Germany) was added to the internal solution (Edelmann & Lessmann, 2011).

2.1.5 Artificial Cerebro-Spinal Fluid (ACSF)

During the experiments, the slices were perfused with carbogenated (95% O_2 and 5% CO_2) artificial cerebral spinal fluid (ACSF) containing the following (in mM): 127 $NaCl$, 25 $NaHCO_3$, 25 D-glucose, 2.5 KCl, 1 $MgCl_2$, 2 $CaCl_2$ and 1.25 NaH_2PO_4 and TTX, delivered with a peristaltic pump at 1.5 ml/min (Table 2.3). Uncaging ACSF (uACSF) was the same as ACSF except for 4 mM $CaCl_2$, 0 mM $MgCl_2$, MNI-glutamate and 0 TTX. Anisomycin (50 mM), cycloheximide (60 mM), APV (50 μM) or different $[Mg^{2+}]$ was added to the solution when specified as well (Figure 2.2.2).

Table 2.4. **Organotypic Slice Culture Media.**

	mM	in 500 mL
$NaHCO_3$	6	0.252 g
HEPES	30	3.57 g
D-Glucose	27	2.43 g
1X MEM		394 mL
Horse Serum		100 mL
$CaCl_2$		1 mM
$MgSO_4$		1 mM
Ascorbic Acid	25%	24 μL
Insulin (10 mg/mL)		50 μL
GlutaMax		2.5 mL

2.2 Methods

2.2.1 Organotypic Slice Cultures

Cultured hippocampal slices were prepared from C57BL/6J mice (postnatal day 7 to 10) (Gähwiler, 1981; Stoppini, Buchs, & Muller, 1991). Briefly, 350 μm thick slices were obtained with a chopper in ice-cold ACSF containing 2.5 mM KCl, 26 mM $NaHCO_3$, 1.15 mM NaH_2PO_4, 11 mM D-glucose, 24 mM sucrose, 1 mM $CaCl_2$ and 5 mM $MgCl_2$, and cultured on membranes (Millipore). The slices were maintained in an interface configuration with the following media: 1× MEM (Invitrogen), 20% horse serum (Invitrogen), GlutaMAX 1 mM (Invitrogen), 27 mM D-glucose, 30 mM HEPES, 6 mM $NaHCO_3$, 1 M $CaCl_2$, 1 M $MgSO_4$, 1.2% ascorbic acid, and 1 μg per mL insulin (Table 2.4). The pH was adjusted to 7.3, and osmolarity adjusted to 300-310 mOsm. All chemicals were purchased from Sigma unless otherwise indicated.

2.2.2 Two Photon Laser Scanning Microscopy

Two photon excitation microscopy is an imaging technique that was developed by Winfried Denk as a side project during his doctorate (Denk, Strickler, & Webb, 1990; Svoboda & Yasuda, 2006). This technique uses femto-second laser pulses to excite fluorophores. Femto-second pulses enable pseudo-synchronous excitation of a fluorophore by two-near coincident photons hitting them so that the second photon creates a non-linear jump at the energy level of the excited particles, allowing fluorophores to be imaged using lower laser pulses than in one-photon based techniques.

In our experiments, two-photon imaging and uncaging was performed using a galvanometer-based scanning system (Prairie Technologies, acquired by Bruker recently) on a BX61WI Olympus microscope, using a Ti:sapphire laser (Coherent) controlled by PrairieView software.

Imaging

Slices were perfused with oxygenated ACSF (Section 2.1.5. Imaging was started 15 to 30 min after the initiation of slice incubation. Secondary or tertiary dendrites of CA1 neurons were imaged using a water immersion objective (60×, 0.9 NA, Olympus) with a zoom of 10×. Image stacks (0.3 μm per section) were collected once every 5 min for up to 4 h at a resolution of 1024 × 1024 pixels, resulting in a field of view measuring approximately $19.8\mu m \times 19.8\mu m$. Z-stacks were used to quantify spine volumes (see Chapter 3 for details) in all experimental conditions, and all images in one experiment were acquired under the same imaging conditions maintaining equal laser power and PMT gain settings. We monitored imaging laser power fluctuations throughout experiments using a laser power meter (Thor Labs).

One dendritic segment was analyzed per neuron per experiment.

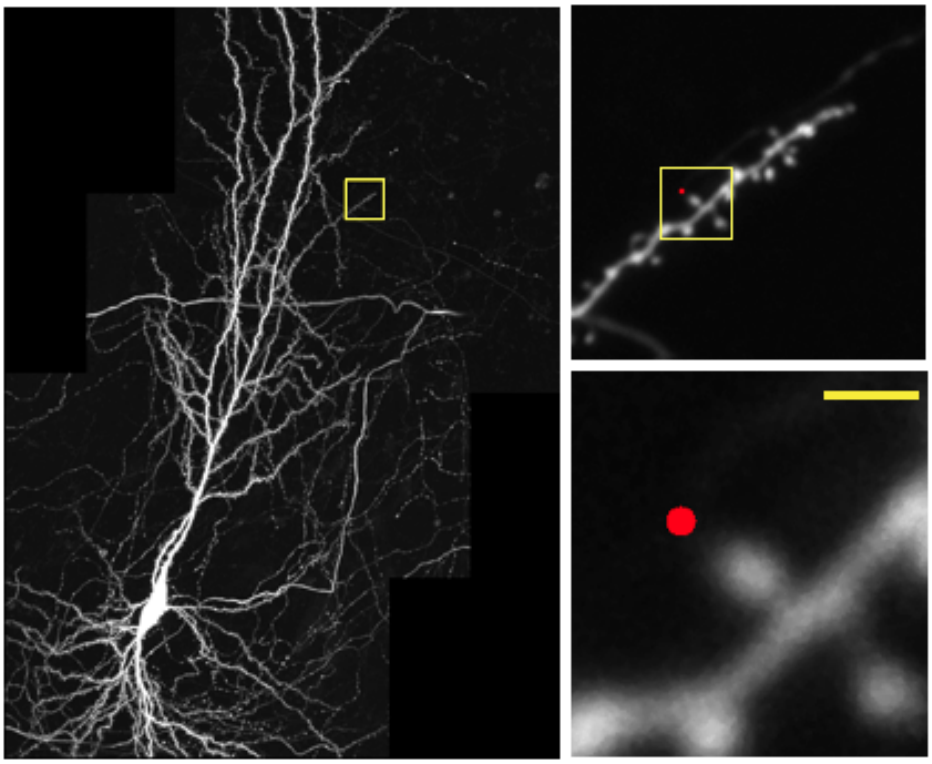

Figure 2.2.1. **Two Photon Imaging and Uncaging of Single Dendritic Spines.** Left: A CA1 pyramidal neuron expression AFP, Right Top: Branch of Interest, Right Bottom: Stimulated Spine. Scale Bar: $1\mu m$

Glutamate Uncaging

Glutamate is the major neurotransmitter operating at excitatory synapses. MNI-caged-L-glutamate (4-methoxy-7-nitroindolinyl-caged-L-glutamate) is a compound that is inert in cells in the initial form. Two photon laser pulses at 720 nm wavelength are able to break the cage hence enabling spatio-temporally controlled simulation patterns for the mimicry of synaptic activation.

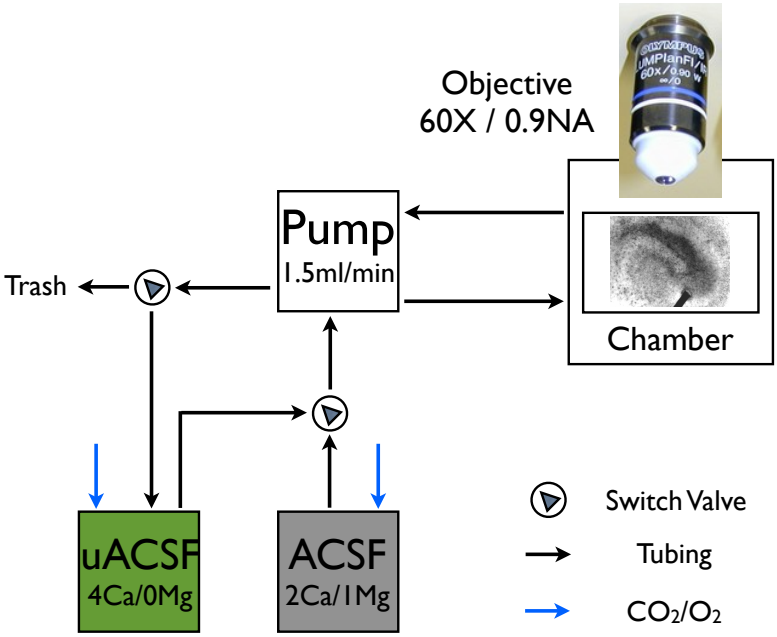

Figure 2.2.2. **ACSF Circulation.** During imaging and uncaging, slices were perfused using artificial cerebro-spinal fluid (ACSF). Two different ACSFs were used with different concentrations of Ca^{2+}, Mg^{2+} and MNI-L-Glutamate. Normal ACSF was used during incubation, baseline, and post-stimulus periods, whereas uncaging-ACSF (uACSF) was used only during the stimulation period which starts with the completion of the last baseline image stack and ends with stimulus delivery (6 min in total).

Before using a new batch of MNI-L-glutamate (Tocris), we performed whole-cell patch-clamp recordings of pyramidal neurons to monitor uncaging-evoked mini EPSCs (mEPCSs). We located the laser pulse approximately 0.5 μm away from the spine head perimeter (Figure 2.2.1). First, we recorded spontaneous mEPSCs for 5 to 10 min and attempted the application of different laser power values under physiological Ca and

Mg concentrations (2 mM $CaCl_2$, 1 mM $MgCl_2$) to obtain an uncaging-evoked mEPSC similar in size to the spontaneously occurring mEPSCs on average.

Experimental Design

We incubated slices 20 to 30 min as they are perfused with ACSF ($0.5\mu M$ TTX, 2 mM Ca, 1 mM Mg) at room temperature before the beginning of the experiment. Experiments are initiated with baseline Z-stack imaging of a secondary or tertiary dendritic branch of a CA1 neuron (Figure 2.2.1). The dendritic branch was imaged every 5 min for 15 to 30 min before glutamate uncaging. After the collection of baseline images, we switched to uncaging-ACSF (uACSF), containing 2.5 mM MNI-Glutamate, 0 mM Mg and 4 mM Ca. Uncaging Pattern (Figure 2.2.3) delivered $0.5\mu m$ away from the tip of the spine.

We switched back to the use of normal ACSF after uncaging, and take the first image was obtained 2 min after the stimulation and, afterward, every 5 min during the following 4 h.

2.2.3 Pulse Train Modeling using a Poisson Process

We designed uncaging pulse trains using a homogeneous Poisson process to generate irregular uncaging patterns that we call **naturalistic trains** to stimulate single dendritic spines.

There are two ways of generating homogeneous Poisson spike trains. The first approach is based on subdividing total spike train length into a series of non-overlapping time intervals, each of duration δt. Afterward, a sequence of uniformly distributed random numbers between 0 and 1 can be used to generate a spike for each interval as long as the random number $x \leq r\delta t$. Here r is the instantaneous firing rate, which is constant over time for homogeneous Poisson train. This means that the probability

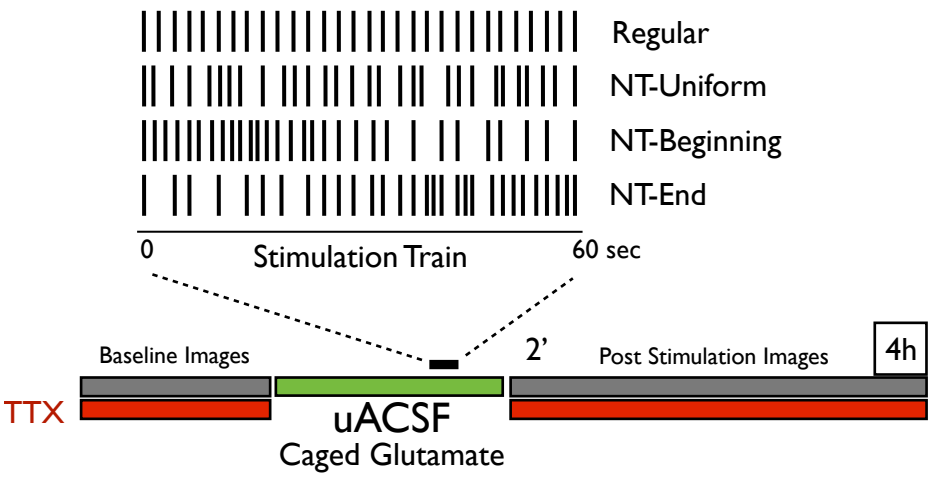

Figure 2.2.3. **Schematic Illustration of the Experiment.** Following the incubation, baseline images were collected. uACSF circulation started immediately after the acquisition of last baseline image stack. At the 5^{th} min of uACSF circulation, one of four uncaging patterns was delivered for 1 min and structural imaging was continued up to 4 h post-stimulation in order to follow uncaging-evoked spine volume changes.

of a spike occurring during a time interval δt is equal to the value of the instantaneous firing rate during that interval times the length of the interval (Equation 2.1).

$$\mathrm{P}\{1 \text{ spike during } (t - \delta t, t + \delta t)\} = r\delta t \tag{2.1}$$

In the second approach exponential distribution is used to derive interspike intervals for a Poisson spike train. Poisson process provides a description of the number of events in a given time period (Equation 2.2).

$$\mathrm{P}(\text{n spikes during } \Delta\mathrm{t}) = \frac{e^{-r\Delta t}(r\Delta t)^n}{n!} \tag{2.2}$$

The exponential distribution, which can be obtained by taking the derivative of the cumulative distribution function of the Poisson distribution, will provide the length of time between events (Equation 2.3).

$$\mathrm{f}(\Delta \mathrm{t}) = r\Delta t e^{-r\Delta t} \tag{2.3}$$

Once the exponentially distributed random spike times are generated, successive spike times can be obtained by adding the previous spike time with the randomly drawn interspike interval.

2.2.4 Statistical Analysis

All statistical analyses were performed using custom code written in Matlab. Permutation (Shuffle) test was used for the analysis presented in Figure 5.3.7. Nonparametric MannWhitney-U test was used to compare spine volumes at any time bin versus baseline or different condition. Time series were compared using repeated-measures ANOVA.

In order to compare the error between different volume estimation methods and volume differences that might introduced due to fluorescence fluctuations over time, we used a symmetric mean absolute percentage error (sMAPE) based similarity score (SS). The sMAPE is a common measure for trend comparisons between time series data (Makridakis, 1993).

$$sMAPE^{spine}_{method^1-method^2} = 100 \times \frac{1}{n}\sum_{i=1}^{n}\frac{|method_i^1 - method_i^2|}{|method_i^1 + method_i^2|} \tag{2.4}$$

Here, n is the number of time points for the analyzed spine. sMAPE is used in sections 3.3 and 3.7.

Chapter 3

Spines: A Tool for Automatic Dendritic Spine Analysis

Contributions: Ali Özgür Argunşah, Devrim Ünay and Inbal Israely conceived the study. Ali Özgür Argunşah, Ertunç Erdil, Muhammad Usman Ghani, Arif Murat Yağcı, Sümeyra Demir Kanık and Devrim Ünay wrote the code. Ali Özgür Argunşah, Anna Felicity Hobbiss and Yazmín Ramiro Cortés provided experimental data.

Affiliations:
[1]Champalimaud Neuroscience Programme, Lisbon, Portugal.
[2]Sabancı University, Istanbul, Turkey.
[3]Bahceşehir University, Istanbul, Turkey.
[4]Boğaziçi University, Istanbul, Turkey.
[5]Universidad Nacional Autonoma de Mexico, Mexico City, Mexico.
[6]Izmir University of Economics, Izmir, Turkey.

Support: This work is supported by Fundação para a Ciência e a Techologia (FCT), Fundação Champalimaud (FC) and Instituto Gulbenkian de Ciência (IGC) and The Scientific and Technological Research Council of Turkey (TÜBiTAK).

3.1 Abstract

Two photon-imaging experiments have begun to elucidate the dynamic nature of dendritic spines, showing that they undergo changes in shape both during development and in response to synaptic stimulation. The experiments which track such changes require the collection of multi-dimensional data over prolonged periods of time, generating large amounts of information which requires tedious manual labor in order to be analyzed. In addition to involving lengthy analysis periods, manual analysis may introduce operant bias which may alter the accuracy of quantification. Therefore, we developed an open source image-processing toolbox called SpineS for the automatic quantification of dendritic features such as spine head volume, spine neck length, and inter spine distances, from imaging data collected with confocal and two-photon fluorescence microscopy. This toolbox allows for the rapid quantification of many spines within the field of view, as it increases estimation precision and eliminates inter-operant estimation differences.

3.2 Introduction

The efficacy of excitatory synapses changes with activity (Bliss & Lømo, 1973) as well as during learning (Whitlock et al., 2006), and these changes correlate with the morphological alterations of dendritic spines (Asrican et al., 2007; Matsuzaki et al., 2004). In particular, the linear relationship between spine volume and current amplitude of a spine (as discussed in section 1.4), and bidirectional changes in spine volume correspond to the induced plasticity (Asrican et al., 2007; Matsuzaki et al., 2004; Ramiro-Cortés & Israely, 2013; Tonnesen et al., 2014). These changes in efficacy and structure reflect activity at a synapse, and can impact subsequent information transmission between inputs across the dendritic arbor (Magee,

2000; London & Häusser, 2005; Bartol et al., 2015). Understanding how such changes are physically maintained in the cell is key to elucidating the mechanisms whereby information is stored in the brain. Activity-dependent structural changes at spines can last from several minutes to hours, and are visualized through multi time point sampling of Z-stack images, often collected for many hours. For example, in an experiment that addresses structural LTP or LTD mechanisms at a single dendritic spine using two photon glutamate uncaging and imaging, researchers image a dendritic branch every 5 min up to 4 h (48 Z-stacks). Given the image acquisition conditions and the type of neuron that dendritic segment images are collected from, one branch may have up to 50 spines. Analyzing 2400 spines is not only laborious and time-consuming but also prone to operant subjectivity.

Therefore, we developed a Matlab based toolbox called SpineS for rapid and robust quantification of spine head volumes and neck lengths. Z-stacks from multiple time points can be analyzed using SpineS. The process starts with importing Z-stacks and registering them over time. Maximum intensity projections (MIPs) of Z-stacks are computed after the registration and filtered using a median filter. Filtering is followed by segmentation of head of dendritic spines and spine volumes are estimated using integrated fluorescence intensity (IFI) method. Afterward, neck paths are computed using a fast-marching algorithm for the estimation of spine neck lengths. Detailed description of these steps is presented below.

The first step performed by the SpineS package is to load data. Since each lab uses a different imaging system, and data formats and specification can be very different, we used bio-formats library provided by *Open Microscopy Environment (OME) Project* (Goldberg et al., 2005). Bio-formats library provides tools for importing various image formats. The algorithm computes maximum intensity projected (MIP) images (Figures 3.2.1 and 3.2.3), for each time point as it loads image stacks and performs

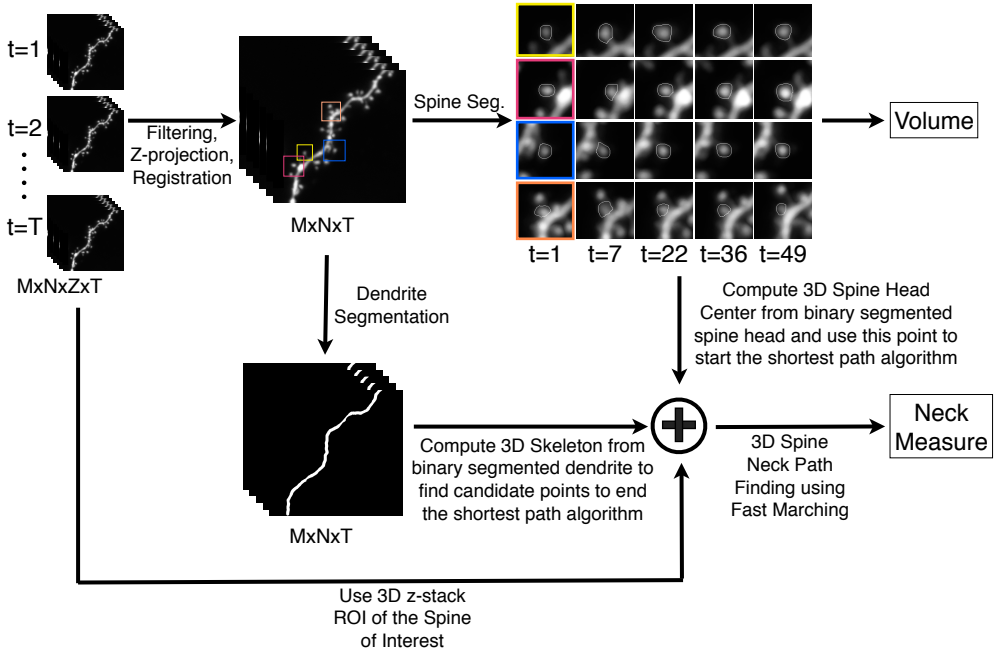

Figure 3.2.1. **Workflow of SpineS.** Z-stack from multiple time points are analyzed. Each Z-stack is imported and registered after Z-projections computed and filtered using median filtering. Dendritic spines are segmented using a watershed based algorithm and each spine volume is estimated using IFI method and normalized with the median fluorescence intensity of the dendrite at the corresponding time point. Neck paths are computed using a fast-marching algorithm from spine head center to the closest geodesic point on the dendrite by imposing some constraints.

an initial translation correction (Figure 3.4.1). Users select the spines to be analyzed by clicking on the center of the spine head at the first time point (Figure 3.2.2). Next, the registered MIP images are filtered using a simple median filter during the segmentation process. The median filter has just one parameter in order to determine the number of neighboring pixels that are used for the calculations of the median value,

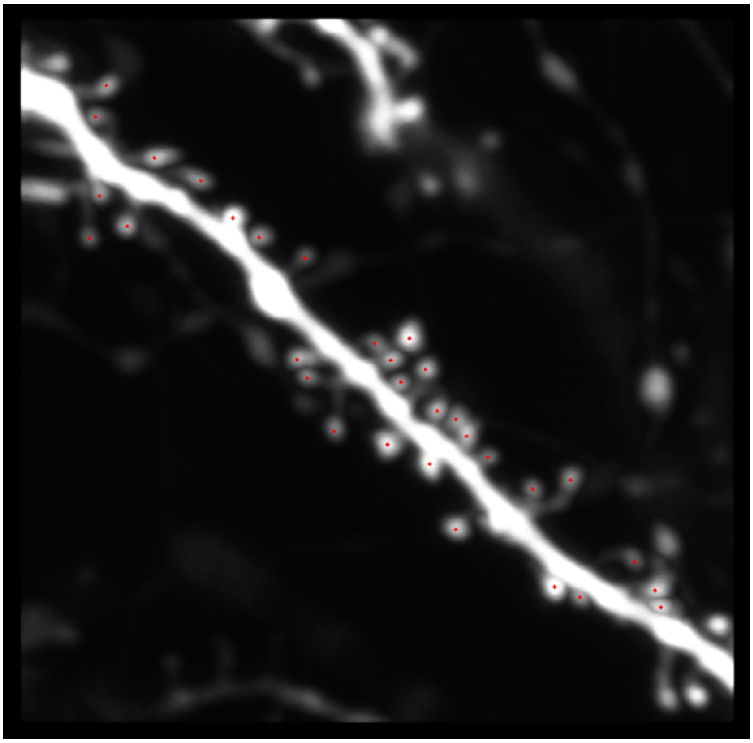

Figure 3.2.2. **Spine Selection for Analysis.** User clicks at the center of every spine at the first time point. These spines will be tracked in the next time points by the algorithm.

which is set by the user. The filtered image is then binarized using Otsu thresholding (Otsu, 1975), which results in a rough segmentation of the dendritic branch including spines. Further, the medial axis of the dendrite is computed by applying a fast marching distance transform (Kimmel & Sethian, 1996) on the dendritic segment, then we apply a locally adaptive sized disk-shaped structuring element around the medial axis of the dendrite to remove spines for dendrite segmentation. To further refine the segmentation, we use the assumption that the dendrite diameter remains consistent in the local field of view after the initial registration. We com-

pute the diameter of the dendrite at all locations and consider the median value to be the true dendrite diameter and remove all pixels beyond the diameter. This gives us a clear segmentation of the dendrite.

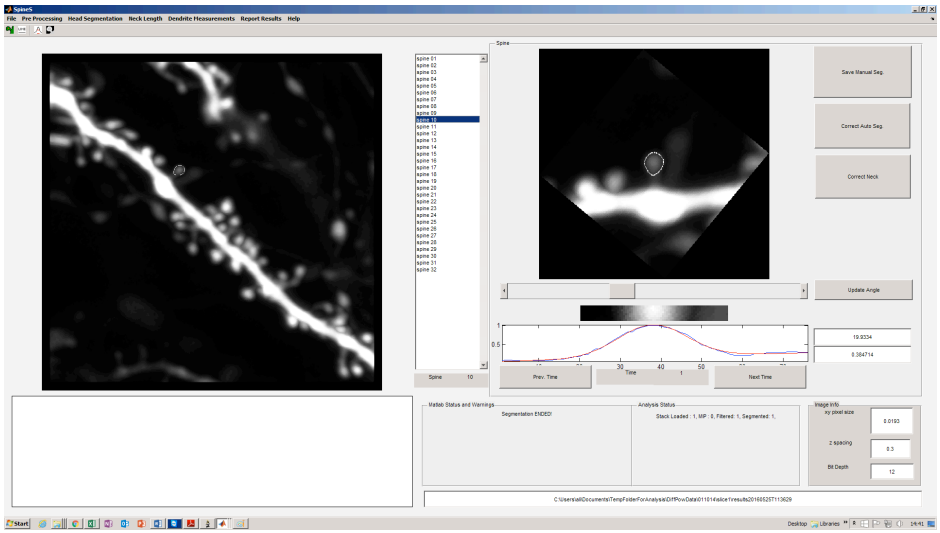

Figure 3.2.3. **SpineS Graphical User Interface (GUI).** GUI provides filtering, automatic segmentation, segmentation correction, manual segmentation and manual FWHM estimation tools. The big plot on the left is the MIP image of the analyzed dendrite. Smaller plot on the right show one of the 32 spines that are analyzed in this example.

In order to define the spine head, we use a multilevel segmentation algorithm. First, we obtain a coarse segmentation of the spine-head using a watershed-based technique. Since the spine head boundaries found in this step are generally larger than the expected boundaries, we segment the interior of this region for refinement. A graph-based image segmentation algorithm followed by hierarchical agglomerative clustering is applied to obtain refined spine head segmentation (Figure 3.5.1). Spine volumes can be computed using IFI of the segmented spine head image. Once the spine of interest has been segmented, a fast marching algorithm computes the

spine neck path in 3D from the centre of the head of the segmented spine to some candidate neck base points that are found using morphological operations. Further, we apply three constraints to select the neck path from these candidate paths. These constraints are neck path length, path complexity (L1-norm of path derivatives), and path smoothness (L1-norm of image intensities along the path). We select the neck path that has collectively lowest value for these three constraints.

In order to compute inter-spine distance, the nearest point from the neck base point to the dendrite medial axis is found for each spine in 3D. The distance between these points computed through dendrite medial axis is called the inter-spine distance.

3.3 Spine Head Volume Estimation Methods

The main focus of structural studies of dendritic spines has thus far been centered on estimating the volume of the spine head through one of two predominant methods: 1) integrated fluorescence intensity (IFI) and 2) full-width at half maximum (FWHM) (Figure 3.3.1). IFI is based on summing all of the fluorescence values in a z-stack within a region of interest (ROI) drawn around the spine head of interest (Nimchinsky, Yasuda, Oertner, & Svoboda, 2004; Holtmaat et al., 2005) (Figure 3.3.1a). In the second method, an intensity profile over a line passing through the spine head center is used to fit a Gaussian (Figure 3.3.1b-3.3.1d and 3.3.2). The maximum FWHM value is used as an approximation of the diameter of a sphere representing the spine head, which is insensitive to fluorescence fluctuations. Each of these methods has certain limitations. IFI is sensitive to the dramatic fluctuations of intensity that could be caused by the imaging system (Figure 3.3.3e), whereas FWHM suffers from over or under estimations of volume as the spine head deviates from a perfectly spherical shape, which can be quite often (Harris & Stevens, 1989). We

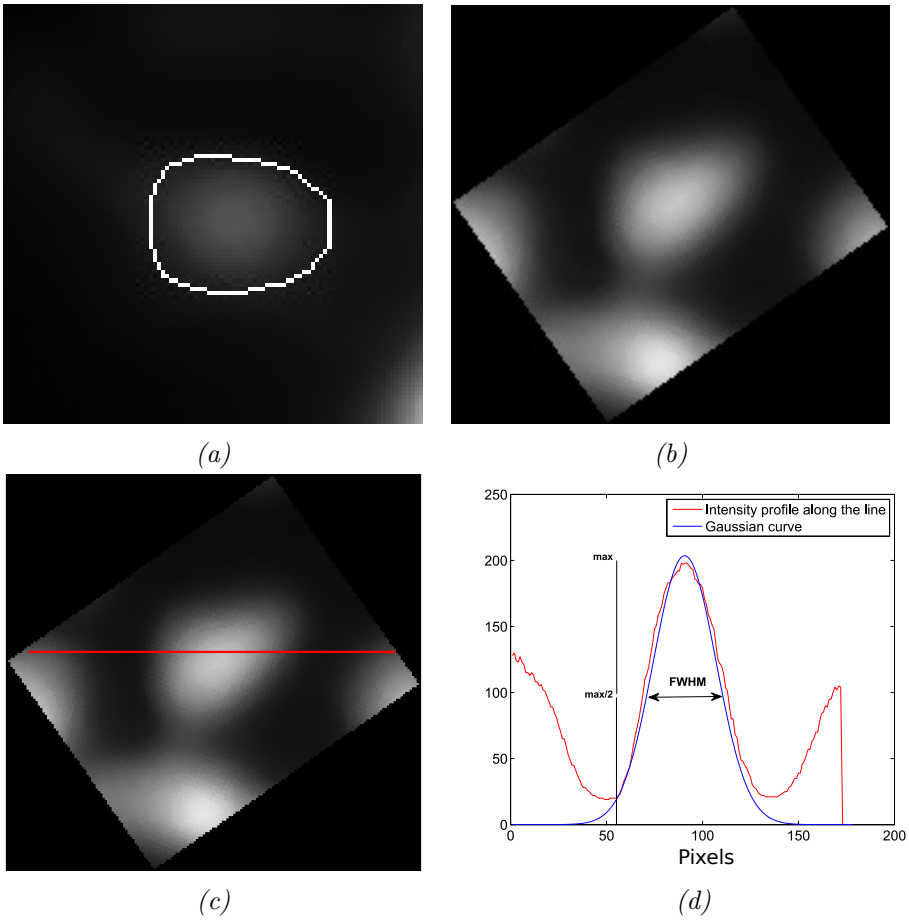

Figure 3.3.1. **Integrated Fluorescence Intensity (IFI) and Full-Width at Half Maximum (FWHM) Volume Estimation Methods. a)** A segmented spine. IFI is calculated within the segmentation boundary after background subtraction and normalization to dendrite fluorescence. **b)** ROI of a dendritic spine, **c)** A line passing through the spine head center, **d)** Intensity profile of the line in c and the fitted Gaussian. FWHM is estimated using the Gaussian Fit (in blue). One pixel is 0.0198 μm

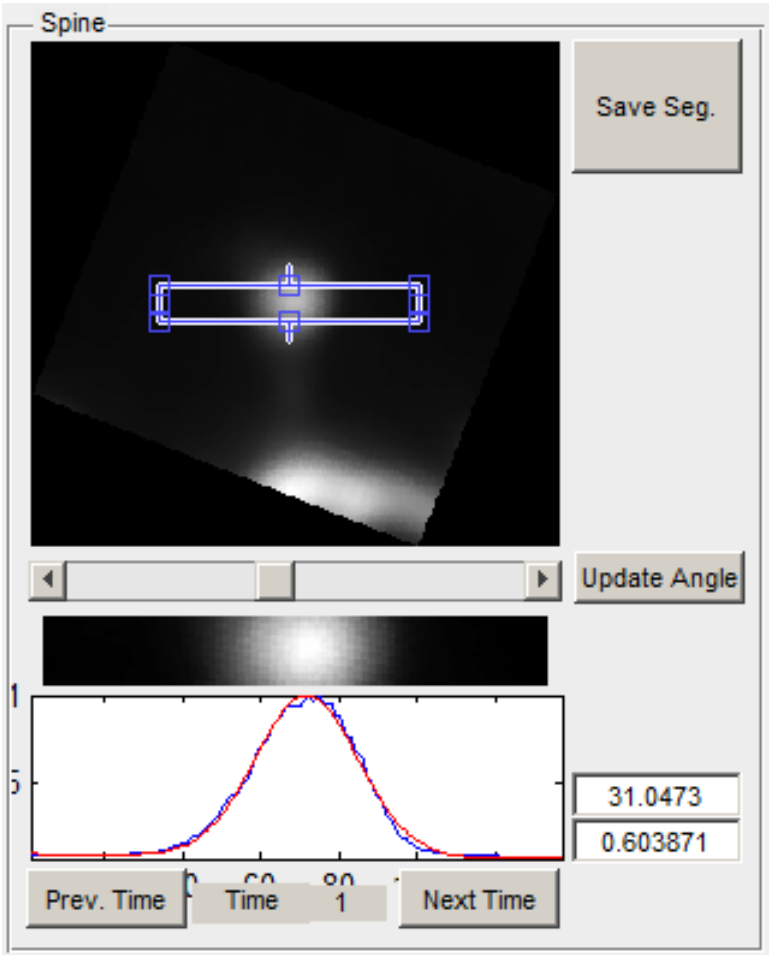

Figure 3.3.2. **Manual FWHM Quantification.** An intensity profile over a line passing through the spine head center is used to fit a Gaussian. FWHM value of the estimated Gaussian fit is used as the diameter of a hypothetical sphere representing the spine head. Numbers on the right represent spine diameter in pixels (top) and micrometers (bottom).

imaged a dendritic branch by fixing photo-multiplier tube (PMT) gain and imaging laser dwell times and systematically changing laser power under physiological Ca and Mg concentrations as well as adding 1 μM

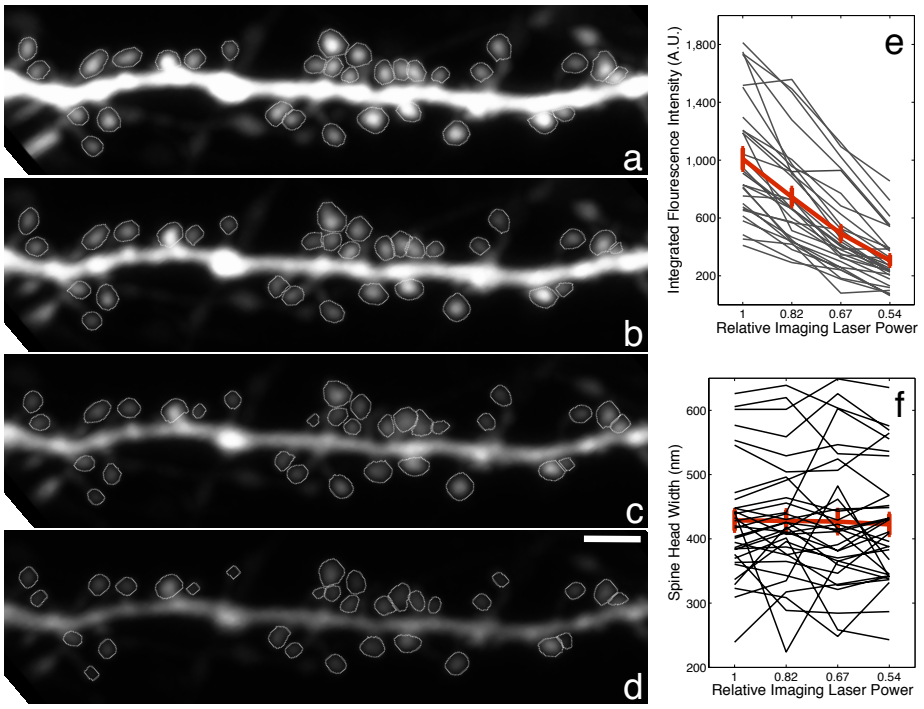

Figure 3.3.3. **Fluorescence Sensitivity of Spine Head Volume Estimation Methods. a-d)** Two photon images of a dendritic segment collected using four different laser powers (relative power normalized to the power at (a): 1, 0.82, 0.67, 0.54) under 2 mM Ca, 1 mM Mg and $1\mu M$ TTX conditions. Photomultiplier tube (PMT) gain and dwell time are fixed. **e)** Spine head segmentations were not affected by laser power drop but IFI drop as power drops. **f)** FWHM values do not represent a function of imaging laser power. Scale bar in (d) is $2\mu m$

TTX. Under these conditions, spine volumes should not change due to the lack of activity. Therefore the only reason of the change in fluorescence should be due to imaging laser power alterations (see Figure 3.3.3a-d). In order to overcome this intensity variations that might happen during image acquisition, IFI volume estimations can be corrected by normalizing with the intensity of the nearby dendrite after background subtraction

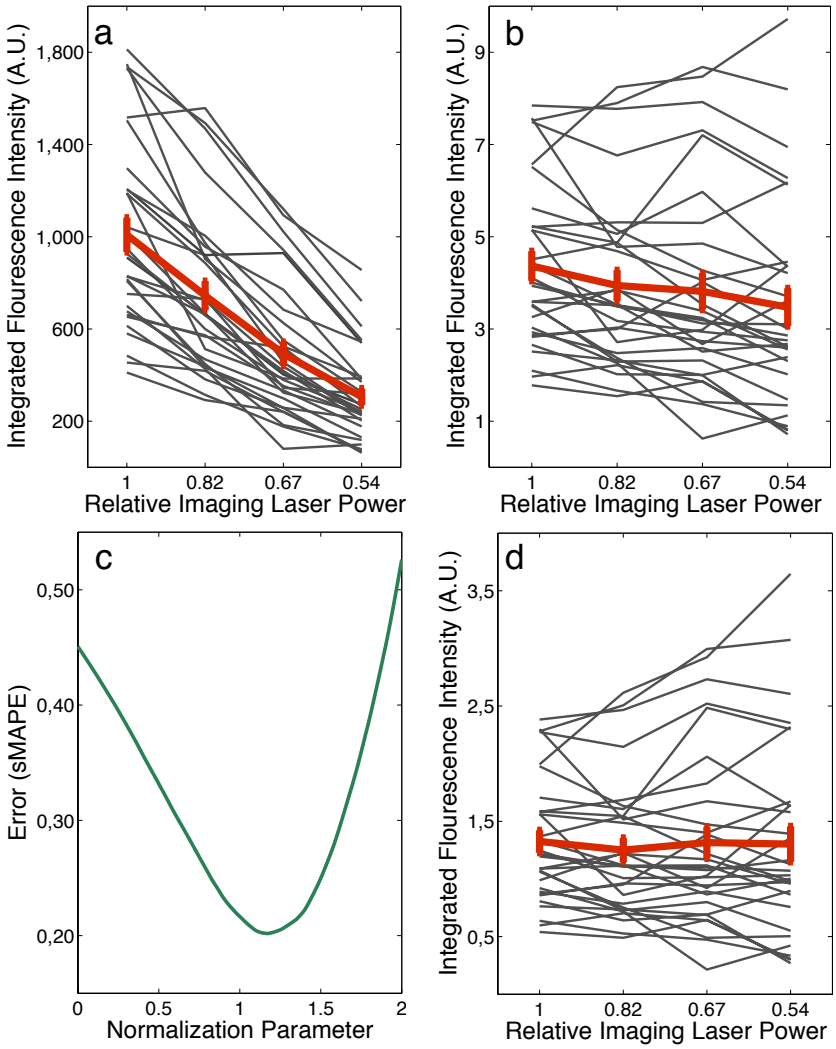

Figure 3.3.4. **IFI Volume Normalization.** Two photon images of a dendritic segment collected using four different laser powers (relatively: 1, 0.82, 0.67, 0.54) under 2 mM Ca, 1 mM Mg and $1\mu M$ TTX conditions (as in figure 3.3.3 but without segmentations). **a)** IFI based volume before normalization, **b)** IFI based volume after linear normalization, **c)** Normalization error vs parameter, **d)** IFI based volume after non-linear normalization.

(Nimchinsky et al., 2004; Holtmaat et al., 2005) (Figure 3.3.4a-b). Since the over or under estimation of spine head volumes with FWHM are unbiased, this limitation becomes less problematic when large numbers of spines are analyzed. However, our analysis revealed that volume estimation errors increase non-linearly as the acquisition fluorescence levels change, and linear normalization to the dendrite intensity under-estimates the spine head volume (Figure 3.3.4).

Below, we will present the algorithmic details of the analysis steps.

3.4 Dendritic Segment Registration

Input: A set of time-series images, $\{f_{t_0}, f_{t_1}, \ldots, f_{t_{N-1}}\}$
1 movingImage = f_{t_0} ;
`// Pick each region (spine) of interest (ROI) manually`
2 setOfROI = SelectROI(movingImage) ;
3 Segment(movingImage, setOfROI) ;
4 **foreach** $t_j = t_{j-1} + \triangle t$ **do**
5 fixedImage = f_{t_j} ;
6 transformation = Register(fixedImage, movingImage) ;
7 setOfROI = transform(setOfROI, transformation) ;
`// Segment fixed image with new setOfROI`
8 Segment(fixedImage, setOfROI) ;
9 movingImage = fixedImage ;
10 **end**

Algorithm 1: Dendritic Spine Tracking in Image Time-Series.

The imaged sample is fixed in a chamber which is constantly perfused with ACSF at a rate of 1.5 mL/min. Due to this fluidic current (mechanical movement), every image is slightly off-registered from each other. We propose a solution for the spine registration problem in Algorithm 1. We apply an image registration approach together with the segmentation of

local regions of interest. Details of registration are given in this section, while those of the segmentation are provided in the next section.

Once a spine is marked at time, t_0, its location can be registered automatically through time and reported with $\triangle t$ intervals.

The registration function takes two dendrite images, f_{t_j} and $f_{t_j+\triangle t}$, as inputs and finds a transformation to align the two images (Figure 3.4.1). We call these images *moving image* and *fixed image*, respectively. At time t_0, a set of ROIs is initiated. Once the automatic segmentation is performed on the moving image, it is registered to the fixed image, *i.e.*, the next image in time-series. The transformation vector is applied to the set of ROIs automatically to find their locations in the fixed image. The algorithm iterates until all time-series images are processed.

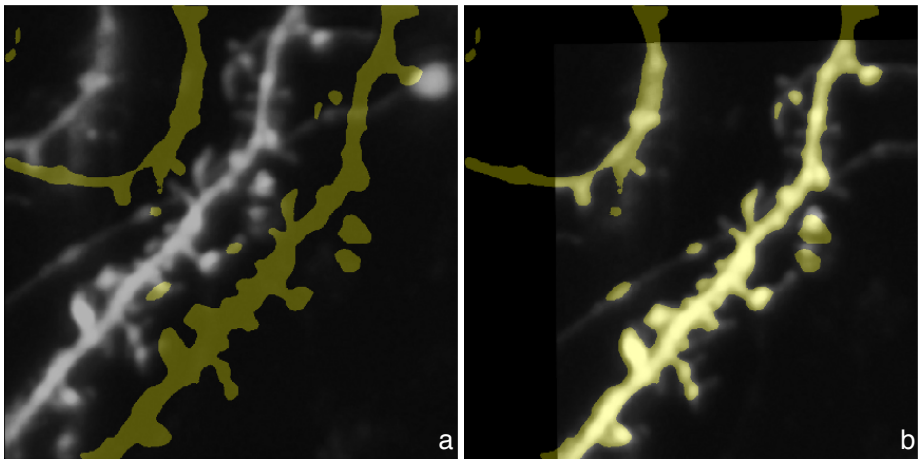

Figure 3.4.1. **Dendritic Segment Registration.** Due to the mechanical movement cause by ACSF perfusion process, images from different time points might be slightly off registered. Translational registration of dendritic segments over time is a necessary step for spine identity tracking. White and yellow are two MIP images of a dendrite at two different times points. **a)** Before registration. **b)** After registration. Due to spine motility, registration is not perfect.

After studying the image time-series, we find it sufficient to use rigid transformation in 2D, i.e. translation and rotation as degrees of freedom.

The registration algorithm optimizes a cost function to find the best alignment between fixed and moving images. In our approach, we implemented functions based on correlation, F-score, and information-theoretic mutual information (MI). The best results were obtained using MI as the cost function. An interpretation of MI can be stated as *finding as much of the complexity in the two subsequent images preserving their own specific information by maximizing sum of marginal entropies such that at the same time they explain each other well by minimizing joint entropy* (see equation 3.1). This formulation is somewhat tolerant to changes in spine morphologies in successive images as the images approach to alignment. MI is maximized at optimal alignment. All of the values needed to calculate MI, can be obtained from the normalized joint histogram of the intensity images which simply represents the joint probability density function (PDF) of the intensities of two images as random variables. We implemented a normalized version of MI (NMI) which facilitates comparison of different values.

$$MI(X,Y) = H(X) + H(Y) - H(X,Y) \tag{3.1}$$

We usually observed tight translation and rotation limits in the image time-series. Therefore, it is possible to design a brute force registration algorithm to check every possible transformation within these limits and choose the best with respect to the metric. Although this approach is more computationally overwhelming, it is more robust compared to an approximate algorithm like (Wells, Viola, Atsumi, Nakajima, & Kikinis, 1996). We designed a 2-pass registration algorithm where in the first pass, a coarser alignment is achieved by keeping the step sizes in translational dimensions large. This is compensated in the second pass with 1-pixel iterations in both dimensions and appropriate rotational increments.

3.5 Dendritic Spine Head Segmentation

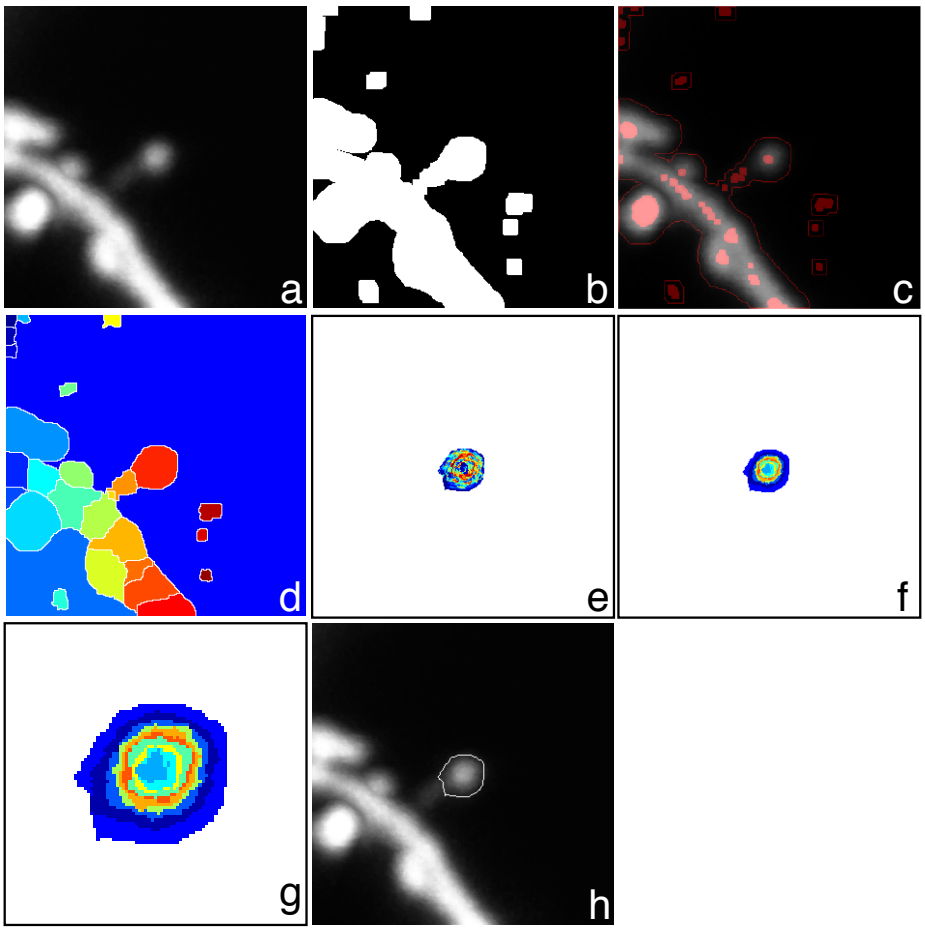

Figure 3.5.1. **Automatic Spine Head Segmentation Steps. a)** Spine ROI, **b)** Binarization using Otsu thresholding, **c)** EMT detects local maxima regions, **d)** Watershed segmentation of EMT regions, **e)** Graph-based intensity clustering, **f)** Hierarchical clustering merges over segmented regions, **g)** Magnified version of f, **h)** Final segmentation.

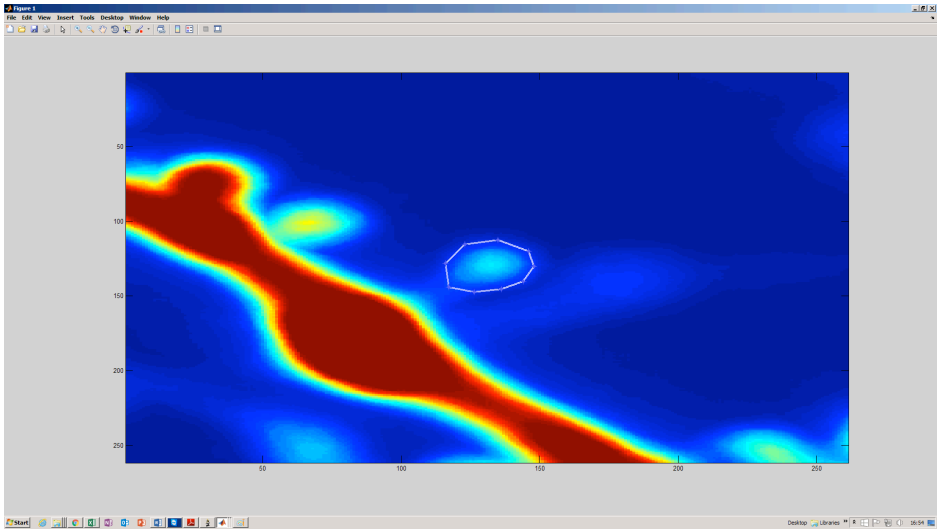

Figure 3.5.2. **Manual Segmentation of Spine Head.** If the final spine segmentation is erroneous, it is possible to segment a spine manually by clicking spine head borders in SpineS GUI, either for the purpose of correction or just for the purpose of manual quantification.

User clicks in the centre of every spine to be analyzed at the first time point to start the analysis. We hold the assumption that dendritic spine head includes a maxima region. Morphological image processing (Soille, 2013) provides a powerful reconstruction algorithm called extended maxima transform (EMT) to extract such regions with a versatile contrast criterion, h. Red blobs in feature image given in figure 3.5.1c shows maxima regions found by extended maxima transform (HMAX, see equation 3.2). Finding maxima regions provides a perfect basis to run watershed algorithm as an initial spine segmentation process.

$$HMAX_h(f) = R_f(f - h) \tag{3.2}$$

Here f is the image function, h is a contrast criterion and the transformation R suppresses all maxima whose depth is lower than or equal to h.

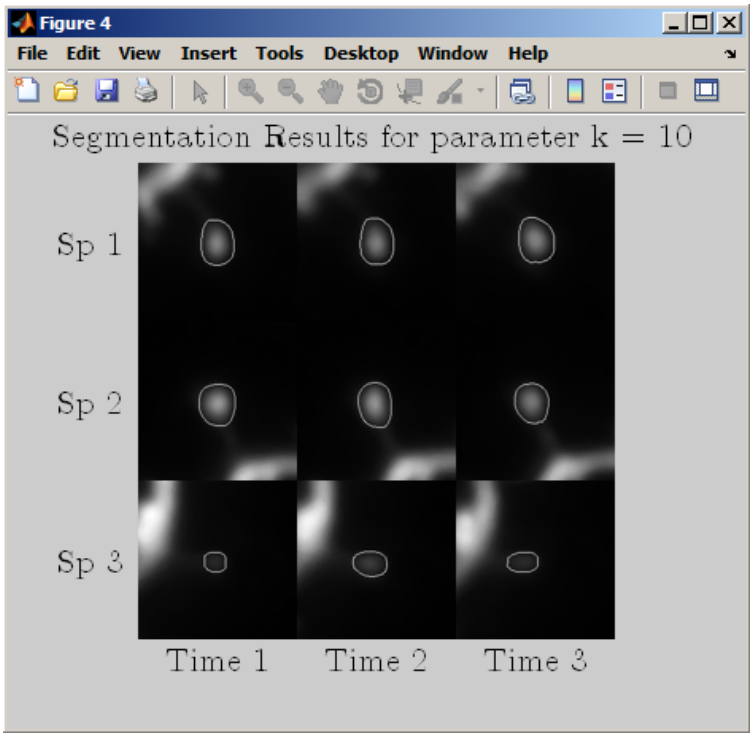

Figure 3.5.3. **Reviewing Spine Head Segmentation.** Segmentation results for three spines for three time points. After the segmentation ends, user can go through all segmentations to check if they look good. If they do not appear good, users clicks the center of the spines to be corrected and segmentations runs with the new spine center coordinates. This procedure often corrects problematic segmentations. If problem persist, it is possible to correct segmentation manually.

We invert the cropped region of interest and then impose all the detected maxima regions as well as the image background as minima. Here, image background refers to the region outside the detected dendrite seg-

ment boundary. We defined the boundary as difference of binarized region of interest from its eroded version where binarization is achieved using Otsu's method (Otsu, 1975). The outside of the borderlines shown in Figure 3.5.1c shows the estimated background. Eventually, all minima regions become the deep regions of all possible basins in the image so that watershed algorithm can start filling them. Dams are constructed at the object boundaries. As is, watershed algorithm usually finds larger boundaries than the expert results show, as presented in Figure 3.5.1d. Therefore, a second level of segmentation is necessary to further refine the results of watershed segmentation. The second level of segmentation takes each previously found component in the ROI and refines it using a modified version of a graph theoretic algorithm for arbitrary shape detection (Mimaroglu & Erdil, 2011) together with hierarchical clustering, in order to improve segmentation results.

Each component C in figure 3.5.1e can be represented as a graph using K-neighborhood where similarity between two pixels is defined as;

$$s(p_i, p_j) = exp(\frac{-(f(p_i) - f(p_j))^2}{\sigma_c^2}) \tag{3.3}$$

Here, σ_c^2 refers to the variance of intensity levels within the component. This definition produces a good transient similarity function. An undirected graph, $G = (V; E)$, is constructed so that its vertices correspond with pixels in C and edges represent the abovementioned similarities between vertices. The original algorithm (Mimaroglu & Erdil, 2011) defines a property called attachment. An unlabeled vertex with the highest attachment is considered a good starting point (seed) for region growing, since it may be the center of a homogeneous region. Starting with the seed vertex, the algorithm automatically finds regions in a breadth-first search fashion. A vertex is included in the region if it has no stronger connection to another vertex than its neighboring vertex in the region. Furthermore,

if a region cannot be enlarged further, then the next unlabeled vertex with the highest attachment is selected as a seed to start a new region. The segmentation process terminates when all pixels are labelled. As is, this graph-theoretic algorithm creates over-segmentation, which can be tackled with to some level, by using a relaxation criterion (Erdil et al., 2012). Since the relaxation factor is very sensitive and proved hard to tune in our experiments, we instead used hierarchical clustering (Mimaroglu & Erdil, 2011) to merge over-segmented regions by defining an inter-cluster similarity measure. We define the cluster similarity as absolute differences of average intensities in the clusters. Hierarchical clustering merges over-segmented regions until an expected number of clusters, k, is obtained.

Hierarchical clustering facilitates the elimination of over-segmentation by forming quasi-concentric connected components. In most cases, the intuitive idea of providing $k = 2$ and separating the region as foreground and background does not work well and creates under-segmentations. Instead, choosing larger k values provides the algorithm with the ability to slowly shrink the region into a more refined segmentation. We formed final segmentation by assigning the outermost component to background and the other components to the foreground. Once the components are found and refined, the spine is automatically detected among them using the assumption that the spine lies at the center of the ROI. Figure 3.5.1h shows the resulting segmentation of the spine of interest.

Spine segmentations can manually be checked (Figure 3.5.3) or corrected (Figure 3.5.2) following the automatic segmentation.

3.6 Spine Neck Path and Length

Further studies revealed that spine neck features such as neck width and neck length are also important structural modifications correlated with activity (Kasai, Fukuda, Watanabe, Hayashi-Takagi, & Noguchi, 2010).

It has been shown that spine neck gets shorter and thicker as spine head gets bigger following LTP(Tonnesen et al., 2014).

Neck length computation is a challenging task due to spine shape variations and neck motility. We begin with partial segmentation of spine head by applying watershed segmentation using $k = 1$. This is further used to compute the center of spine head by finding its center of mass. Further, dendrite skeleton and segmentation is computed in 2D. In order to map the dendrite on z-axis, we construct a vector with intensity values for all slices on z-axis at each skeleton point and fit a Gaussian. The mean value of fitted Gaussian corresponds to coordinate of dendrite in z-direction. These observations are noisy due to the fact that often there are spines on dendrites (along z-direction). To cope with this noise, median of all z-coordinate values is computed. Although this assumption is not always true globally (for entire dendritic branch), however, this approximation holds locally (in the region of interest). Similar approach is used to map center of spine head on z-axis.

Each slice of dendritic branch image is eroded with a disk-structuring element to reduce the spurious paths. Multi stencil fast marching (MSFM) method (Hassouna & Farag, 2007) is applied to compute the 3D distance map using spine head center as source point. The Runge-Kutta algorithm is applied on 3D distance map to compute the shortest paths (geodesic) from N point on dendrite perimeter to the spine head center. These N points are selected by finding N nearest points from spine head center to dendrite perimeter (using Euclidean distance as metric).

$$L_P = \int_P dS \tag{3.4}$$

$$C_P = \left\| \frac{\delta P}{\delta x} \right\|_1 + \left\| \frac{\delta P}{\delta y} \right\|_1 + \left\| \frac{\delta P}{\delta z} \right\|_1 \tag{3.5}$$

$$S_P = \left\| \frac{dV(x_P, y_P, z_P)}{dI} \right\|_1 \tag{3.6}$$

$$NeckPath = \underset{P}{\operatorname{argmin}} \left(\frac{L_P}{max(L_P)} + \frac{C_P}{max(C_P)} + \frac{S_P}{max(S_P)} \right) \tag{3.7}$$

$$NeckLength = L_p - SpineNeckPortionInHead \tag{3.8}$$

Finally, selection of the correct neck path is the crucial step. A simple approach would be to select the path with minimum length (Equation 3.4), but it would fail in this scenario because of motile nature of spine necks. Therefore, path length constraint alone is not sufficient. We introduced two additional constraints to select the path with best geodesic approxi-

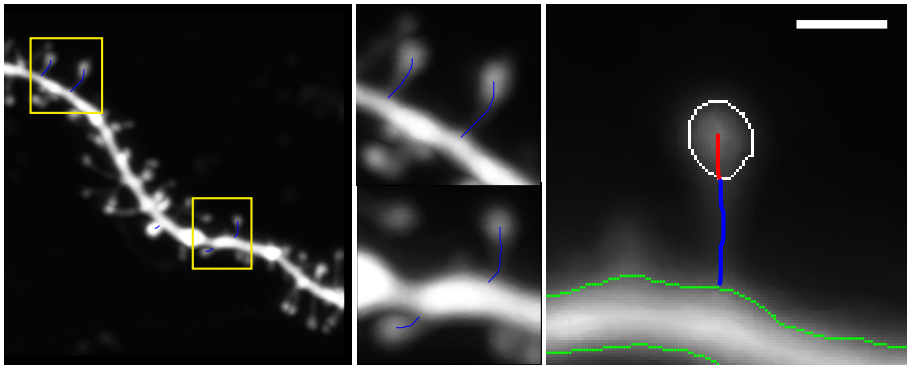

Figure 3.6.1. **Spine Neck Length Calculation.** A dendritic branch with five spine neck paths in blue (left). Closer look at four of those spines (middle). After the spine neck path from the center of the spine to dendrite perimeter (green) found, spine neck length is computed using equation 3.8, by subtracting full neck length (blue+red) from neck portion in spine head perimeter (red). Scale bar is $1\mu m$.

mation. The first additional constraint is path complexity (Equation 3.5), i.e. path should be as simple as possible. Other constraint is smoothness of image intensities on the path (Equation 3.6), i.e. intensity changes on the path should be as minimal as possible. Equation 3.7 is applied to find the correct neck path (Figure 3.6.1).

Equation 3.5 corresponds to the path length from the dendrite surface to spine head center. To compute neck length, we first compute the radius of spine head by fitting a circle using Hough Circle Transform on watershed segmented spine head with $k = 10$ and then use Equation 3.8.

3.7 Results and Conclusions

In order to compare the quality of the proposed automatic analysis with expert's results, we used a symmetric mean absolute percentage error (sMAPE) based similarity score (SS) (Makridakis, 1993) (see Section 2.2.4).

$$SS^{spine}_{method^1-method^2} = 100 - sMAPE^{spine}_{method^1-method^2} \tag{3.9}$$

Here, n is the number of time points for the analyzed spine. Comparisons of our results produced by SpineS with expert's manual computations (manual segmentation based IFI and manual FWHM) are given in table 3.1 for 27 spines from 9 different dendrites.

Similarity scores of estimated intensity based volumes from manually segmented spine heads and SpineS output suggest automatic segmentation yields very similar ($\mu = 87.75\%; \sigma = 8.15\%$) spine head segmentations with the expert's since both used intensity-based volume estimation method. We also compared our results with manual FWHM volume estimation results to see how much overlap we get between two volume estimation methods used in the field. **SpineS**: IFI based volume using automatic segmentations; **M-I**: IFI based volume using manual segmen-

tations by an expert; **M-FWHM**: FWHM based volume quantified by a different expert.

In figure 3.7.2, we present a comparative analysis for a single spine over time along with corresponding spine ROI images for seven time points. Normalized spine volume changes over time seems to agree with visual inspection for all three methods. As one would expect, SpineS and M-I (blue and yellow lines) seem to correlate more which indicates the proximity between automatic and manual segmentations.

Figure 3.7.1 shows that on average, all three methods converged to the same statistical distribution (all pairwise t-tests, $p > 0.99$).

SpineS reports similar spine head volume results compared to volume quantification based on manually segmented spine heads and on average

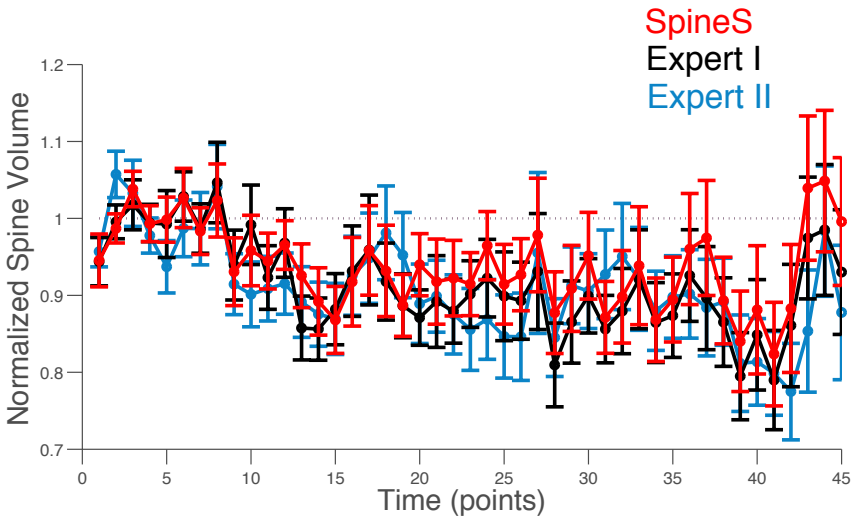

Figure 3.7.1. **Performance of SpineS Compared to Manual Segmentation based IFI and FWHM.** Here is the average of 27 spines from 9 dendrites from 9 chemical LTD experiments. First six points are baseline. DHPG applied after baseline for 5 min. Red: IFI using SpineS, Black: IFI based on manual segmentations, Blue: manual FWHM

Table 3.1. **Performance of SpineS Compared to Manual Segmentation based IFI and FWHM.**

Similarity Scores (%)				
Dendrite	**Spine**	**SpineS vs M-I**	**SpineS vs M-FWHM**	**M-I vs FWHM**
1	1	94.3589	77.4508	77.8126
	2	91.7690	67.0097	69.2701
	3	89.9466	87.1170	87.8953
	4	94.6821	78.2715	78.5801
2	5	91.1221	77.4064	79.3692
	6	89.4878	79.8868	82.8800
	7	82.3776	55.5188	55.8325
3	8	94.7981	80.7409	77.5585
	9	93.3184	84.1880	86.3130
	10	93.4738	73.7198	78.6996
	11	84.6000	76.8546	81.7697
	12	93.9778	81.8241	80.3675
	13	94.2463	84.8752	84.7990
4	14	92.0029	88.5253	88.3591
	15	75.6294	78.8051	84.9315
5	16	87.2726	73.0195	75.7853
	17	84.7986	57.1934	59.2845
6	18	86.0672	82.1992	78.9639
	19	62.7521	62.4207	62.7810
	20	73.5343	58.1966	73.1153
7	21	93.0215	92.8845	91.4917
	22	73.0984	69.2588	94.1526
8	23	89.3805	91.7864	91.1700
	24	95.1736	78.8624	78.3193
9	25	83.4779	33.2023	34.3038
	26	93.5946	55.8149	58.0175
	27	91.2172	78.6321	78.9491
Mean	**All**	**87.75**	**74.28**	**76.70**
StdDev	**All**	**8.15**	**13.42**	**13.12**

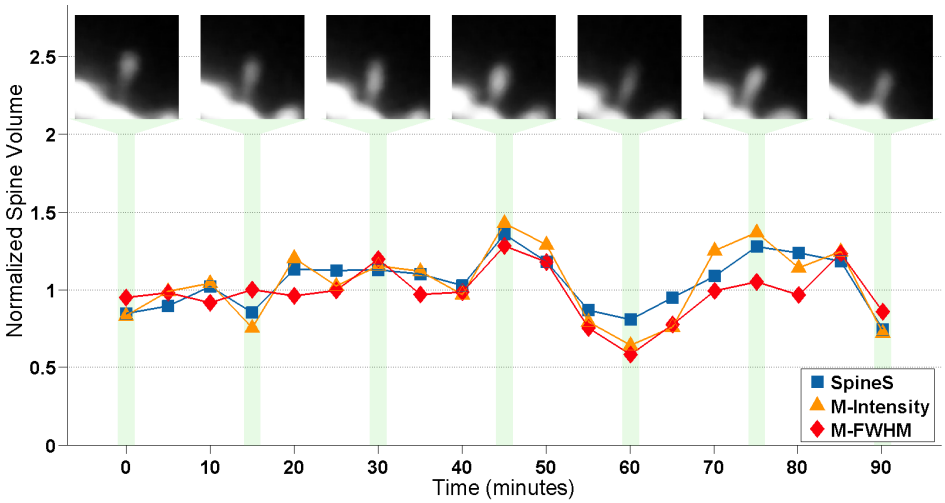

Figure 3.7.2. **Comparison of Volume Quantification Methods for a Spine.** This spine fluctuated between $\times 0.5 - \times 1.5$ during the course of the experiment. All methods seem to capture the change.

Table 3.2. **Image Analysis Speed Comparison.** Here we compare manual and automatic processing times between previous tools developed for manual analysis of dendritic spines and manual and automatic analysis tools in SpineS toolbox for the analysis of 1000 dendritic spines. Tools provided by SpineS makes the analysis faster for both manual and automatic assesment of the data (Computer used for these analysis has 3.4 GHz Intel Quad-core processor, 16GB RAM, Windows 7 OS and Matlab version 2011a).

ImageJ		**SpineS**		
Manual Segmentation	**Manual FWHM**	**Manual FWHM Tool**	**Manual Segmentation Tool**	**Automatic Segmentation**
5h	30h	3.4h	2.7h	1.2h

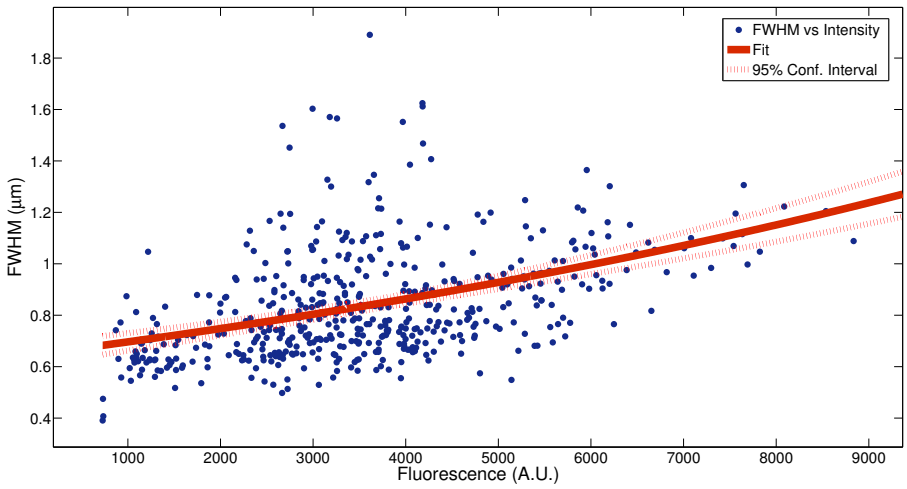

Figure 3.7.3. **Volume Conversion: Arbitrary to mm^3.**

IFI and FWHM based volume results (Figure 3.7.1). It is possible to convert arbitrary IFI units into absolute units (μm^3). User can either estimate the diameter of a spherical-looking spine using FWHM and find a conversion factor using IFI and FWHM-based volume result by simple division (Figure 3.7.3) or estimate the volume of the PSF of the imaging system using fluorescence beads, and IFI multiplied by this value will give spine volume in μm^3 (Nimchinsky et al., 2004; Holtmaat et al., 2005).

We developed an image-processing tool for the segmentation of dendritic spines. The proposed tool yields good results in terms of accuracy and run times for spine segmentation. Results suggest that the proposed tool can be a reasonable choice over manual segmentation-based volume estimation, due to good similarity scores in comparison to the field experts, faster processing (see Table 3.2), and objectivity. Furthermore, the obtained results suggest that the intensity-based and FWHM-based methods can be used interchangeably for individual volume trend assessment, given that the spine keeps its circular-like shape at every time point or can

be used interchangeably when pooled data is the key to research. SpineS does not provide good segmentation results when the spine of interest has very similar neck and head intensities, however, the tool provides interactive segmented spine head boundaries and spine neck paths for post quality assessment, which gives users the flexibility to manually reject or correct segmentations and neck paths at any particular time point.

Chapter 4

Single Spine Structural Plasticity Induced by Naturalistic-like Trains

Contributions: Ali Özgür Argunşah and Inbal Israely conceived the study and designed the experiments. Ali Özgür Argunşah conducted the experiments and analyzed the data.

Affiliations: Champalimaud Neuroscience Programme, Lisbon, Portugal.

Support: This work was supported by Fundação para a Ciência e a Techologia (FCT), Fundação Champalimaud (FC) and Instituto Gulbenkian de Ciência (IGC).

4.1 Abstract

Synaptic plasticity has predominantly been studied through the application of either high or low frequency regularly spaced stimulations, patterns which do not occur commonly in the brain. In order to understand how the diverse activity patterns more frequently observed in the brain encode information at single inputs, we designed single spine stimulation protocols sampled from a Poisson process, in order to mimic the firing patterns that are observed *in vivo*. Using two-photon glutamate uncaging and fluorescence imaging, we were able to precisely deliver various patterns of activity to individual dendritic spines located on CA1 pyramidal neurons in the mouse hippocampus, and observe the resulting structural plasticity. We selected representative patterns in which the stimulations were either homogeneously distributed across the stimulation period, or in which their distribution was skewed towards either the beginning or the end of the activity period. We found that the timing structure of the uncaging patterns leads to diverse long-term structural plasticity outcomes. During naturalistic stimulations, which contain a more or less uniformly distributed number of stimuli, long lasting potentiation is achieved, as measured by the sustained structural growth of spines over the course of many hours. We showed that this form of plasticity is NMDAR and protein-synthesis dependent. In contrast to this, patterns in which the majority of the stimulation events occur either early or late during the train are less competent at inducing long lasting plasticity at individual spines. Interestingly, while the structure of the delivered stimulations varied, the overall length of the activity period and the total amount of glutamate that was delivered remained constant. Therefore, our experiments demonstrate that diverse forms of activity can have significantly different plasticity consequences for individual inputs.

4.2 Introduction

Synaptic plasticity is considered the basis for learning and memory formation in the brain. Therefore, the characterization of how plasticity is induced by different patterns of activity is necessary in order to understand how information is encoded at synapses. In general, the types of stimuli used in synaptic plasticity studies have been very stereotypical; in other words, the pattern of activity that is delivered usually follows a repetitive, regular pattern. Examples of commonly used stimulation paradigms are a 100 Hz stimulation delivered for 1 min or a theta burst stimulation which consists of short bursts at 100 Hz repeated at 5 Hz in order to induce LTP, while a 15 min long 1 Hz stimulation protocol is commonly applied for the induction of LTD (Figurov et al., 1996; Staubli & Lynch, 1987; Mulkey, Endo, Shenolikar, Malenka, et al., 1994; Malenka & Bear, 2004).

When a bundle of axons are stimulated using an electrode as it occurs during high frequency stimulation during field recordings, synchronous activation of many synapses depolarizes the neuron. In order to study synaptic plasticity at the single synapse level, two-photon glutamate uncaging has been utilized to stimulate single dendritic spines because of the high spatial resolution of this approach (Matsuzaki et al., 2004). However, in order to induce plasticity at single synapses, it is necessary to activate the receptors which in turn allow for the appropriate downstream signaling to occur. In order to depolarize the neuron to high enough levels to remove the Mg block from the NMDAR, glutamate uncaging at single spines is performed is he absence of Mg, a manipulation which produces similar levels of plasticity compared to what is observed with a 100 Hz electrical stimulation paradigm (for example, 60 pulses of 0.6 msec length delivered in 60 sec, see Figure 4.2.1a). By applying this uncaging protocol, significant spine growth was observed which strongly correlated with the increased electrophysiologically recorded EPSC sizes, thus demonstrating

for the first time that potentiation of a single input leads to the growth of the associated spine (Matsuzaki et al., 2004). Importantly, the observed structural plasticity was restricted to the stimulated spines, and immediately adjacent neighbors remained stable in size, highlighting the specificity of this methodology.

Following this, additional protocols were characterized, in which LTP could be induced at single spines, such as by applying fewer pulses of longer glutamate uncaging duration (30 pulses of 4 msec length, Figure 4.2.1b) (Harvey & Svoboda, 2007). This method has subsequently become a widely used paradigm for the induction of single spine plasticity (Harvey, Yasuda, Zhong, & Svoboda, 2008; Hill & Zito, 2013; Govindarajan et al., 2011). One adaptation of this protocol involves the strengthening of the stimulation, for example by applying a pharmacological agent to activate the cAMP pathway, which leading to a longer lasting form of plasticity at single spines (Govindarajan et al., 2011). Importantly, this study demonstrated that structural plasticity at single spines can be either short lasting or long lasting, depending on the presence of the cAMP agonist, matching what has been observed in electrophysiological studies in which functional plasticity can be either short or long lasting, the latter being protein synthesis dependent and maintained for many hours (Govindarajan et al., 2011). Therefore, in our studies, we take advantage of this well characterized protocol in which 30 pulses of glutamate are uncaged at 0.5 Hz in order to robustly induce LTP at single dendritic spines over 1 min, and we will refer to this protocol as the "regular train", and this form of LTP is protein synthesis-dependent.

We aimed to determine whether irregular patterns of activity induce plasticity at single dendritic spines, and if so, how this plasticity compares to the one that results from the regular stimulation train described above. In order to address this question, we aimed to identify a means by which to stimulate single inputs in a manner that more closely mimics the activ-

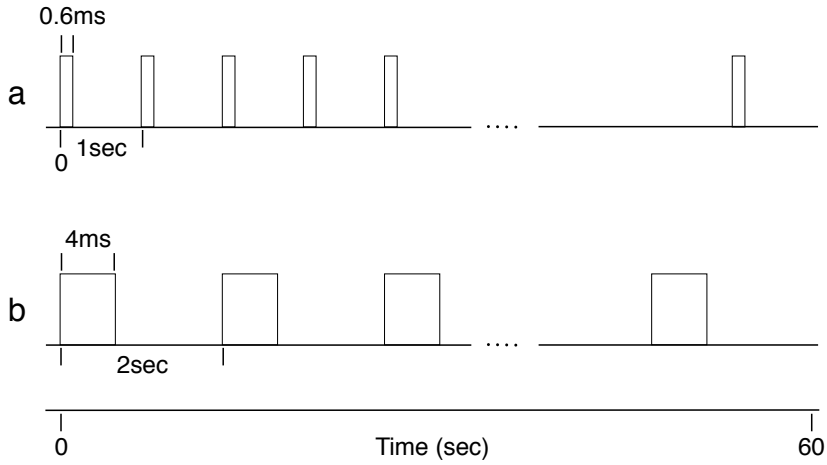

Figure 4.2.1. **Regular Glutamate Uncaging Protocols for the Induction of LTP. a)** 60 evenly-spaced pulses in 60 s, **b)** 30 evenly-spaced pulses in 60 s.

ity structures observed endogenously. Many studies have concluded that spiking statistics of neurons are compatible with Poisson or Poisson-like processes. A Poisson process is a random process in which the events occur independently from each other over time with some probability and the intervals between these events are shown to follow an exponential distribution. The Poisson process does not characterize neural spike trains completely, however it is proven to be a good approximation (Leon-Garcia, 2008; Wallisch et al., 2014). Spiking patterns of CA3 neurons revealed the irregular nature of inter-spike intervals (ISIs) of these neurons (Dobrunz & Stevens, 1999). Although ISIs of individual CA3 cells are highly heterogeneous, on average they fit exponential distributions (Frerking, Schulte, Wiebe, & Stäubli, 2005). In the case of retinal ganglion cells, the interval statistics of spike trains within these neurons are accurately modeled with gamma-distributed intervals (Troy & Robson, 1992), which corre-

spond to the non-homogeneous Poisson distributed firing patterns. Bair *et al.* found that one-third of the neurons are compatible with a Poisson process, and that the rest of the neurons fire in bursts, which are then spaced in a Poisson fashion, with a burst-dependent refractory period (Bair, Koch, Newsome, & Britten, 1994). Given these data, we decided to test the plasticity consequences of Poisson structured forms of activity at single spines, hypothesizing that stimulation patterns which follow such distribution more accurately reflect the nature of endogenous activity. In order to achieve this, it was important to derive pulse trains that could be compared to known paradigms for inducing plasticity, in particular, the previously described regular protocol.

4.3 Generation of Naturalistic-like Trains

We wanted to identify the types of activity generated endogenously at CA3 pyramidal neurons in the mouse hippocampus, as these are the inputs to the synapses that we were studying on CA1 pyramidal neurons. In particular, we wanted to examine patterns correlated with the encoding of information, and thus we performed simultaneous recordings from CA3 and CA1 during a behavioral task where mice explored a linear track back and forth[1] (Figure 4.3.1). As animals explore the linear track, refinement of place fields has been proposed to occur at Schaffer collateral synapses through LTP (Mehta et al., 2000).

We used a homogeneous Poisson process to generate irregular patterns that we call naturalistic-like trains. Homogeneous in this application refers to the instantaneous firing rate which is constant over time, while the inter spike intervals (ISIs) of homogeneous Poisson processes are exponentially distributed. We chose homogeneous over non-homogeneous because this

[1]Data is collected at Circuit and Behavioral Physiology Lab. of Thomas J. McHugh in Riken BSI and extended information can be found in (Middleton & McHugh, 2016)

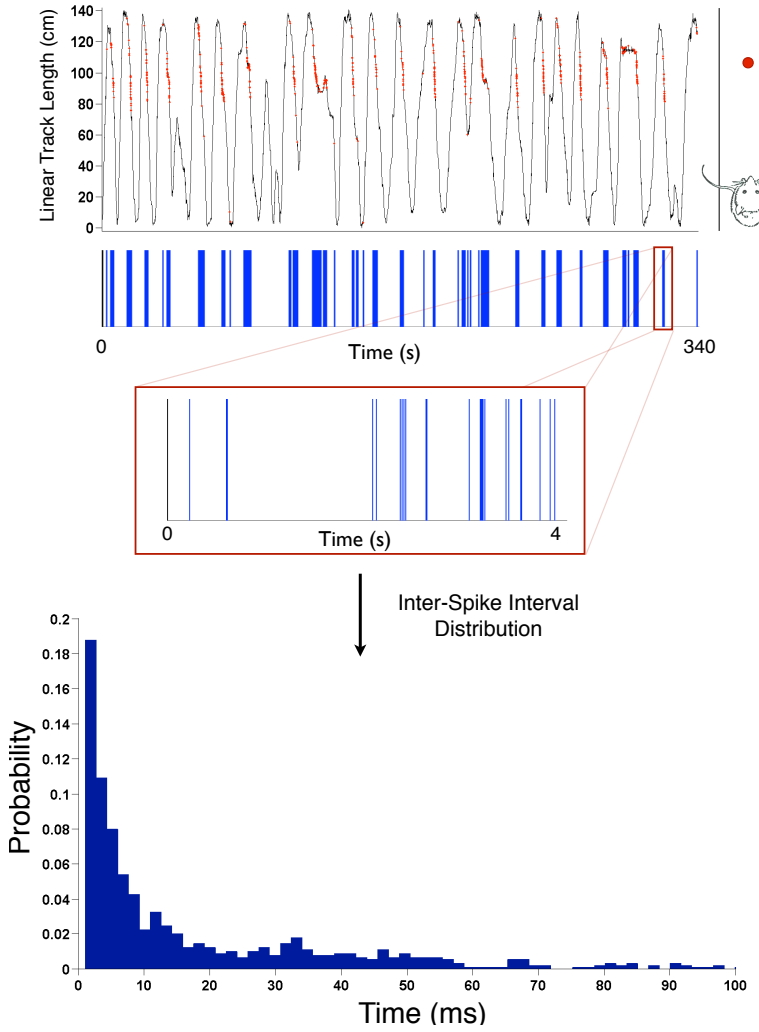

Figure 4.3.1. **Inter Spike Intervals (ISIs) of CA3 Neurons are Exponentially Distributed.** Here we plotted an example CA3 place cell firing pattern over the course of an experiment. Recordings were made using tetrode drives. Spike trains were obtained after spike sorting and velocity filtering ($> 5cm/s$)

matched the ISI distributions that we obtained in our recordings from CA3 neurons (Figure 4.3.1 and Figure 4.3.3a).

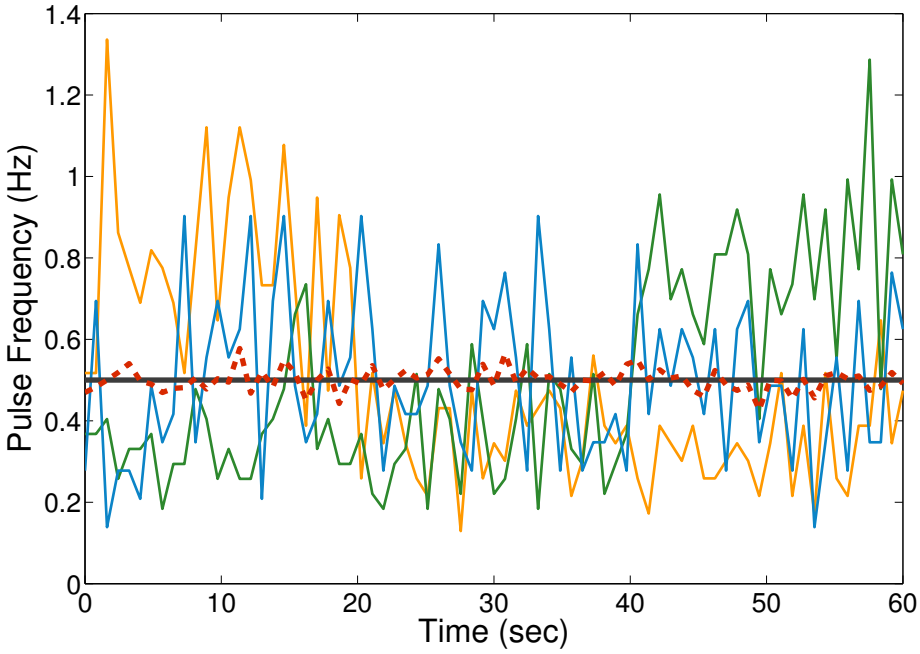

Figure 4.3.2. **Instantaneous Pulse Frequencies of Generated Naturalistic-like Trains.** Regular train has a constant frequency which is 0.5 Hz (gray), NT-Uniform trains have instantaneous frequencies fluctuating around 0.5 Hz (blue), NT-Beginning trains have higher instantaneous frequencies in the first 20 sec (yellow), NT-End trains have higher instantaneous frequencies in the last 20 sec (green). Red represent the instantaneous frequencies of all generated Naturalistic-like trains combined.

We chose the instantaneous frequency (IF) of 0.5 Hz for our homogeneous Poisson trains in order to compare it with the previously established regular train paradigm (Figure 4.3.2 and Figure 4.3.3a). We first generated 10000 naturalistic-like trains using the equation 2.3, as explained in section 2.2.3. Of the10000 generated patterns, only 780 of them had ex-

actly 30 pulses (Figure 4.3.4). As explained earlier, the plasticity inducing regular train delivers 30 pulses in 60 sec, and therefore IF is 0.5 Hz (Figure 4.3.2). In contrast to this, a Poisson distribution with a rate of 0.5 Hz does not necessarily contain exactly 30 pulses in 60 sec (Figure 4.3.3b). Since we wanted to keep the number of pulses fixed to 30 in 60 sec in order to reduce variability and equate the amount of glutamate that would be released at a given synapse between between protocols, we selected the subset of Poisson patterns with this same number of events. Afterward, we selected three representative patterns in which the stimulations were either pseudo-uniformly distributed across the stimulation period, or in which the timing structure was skewed to occur either towards the beginning or the end of the activity period. We named these patterns NT-Uniform (NT-UNI) (Figure 4.3.3c), NT-Beginning (NT-BEG) (Figure 4.3.3d) and NT-End (NT-END) (Figure 4.3.3e), respectively, where NT stands for naturalistic-like train. For each of these patterns, 30 pulses are differentially distributed over the 60 sec stimulation period. In the case of the NT-UNI pattern, there are 10 pulses per 20 sec bin. In the case of both the NT-BEG and NT-END patterns, each have half of the total pulses occurring either at the beginning or in the last 20 s bin, respectively, while the remaining 15 pulses are distributed across the remaining 40 sec. Although the distribution of events within these trains varies, the total number and the total time in which they are delivered is constant. Thus, the amount of glutamate that is delivered to the synapse is equal in all conditions.

As the vast majority of electrophysiological studies addressed LTP using high frequency regular stimulation trains, glutamate uncaging based studies as well used regularly spaced uncaging laser pulse trains to induce LTP (Figure 4.3.4). It has been reported that regular glutamate uncaging stimulation at single dendritic spines induces LTP (Matsuzaki et al., 2004; Harvey & Svoboda, 2007; Govindarajan et al., 2011) and the

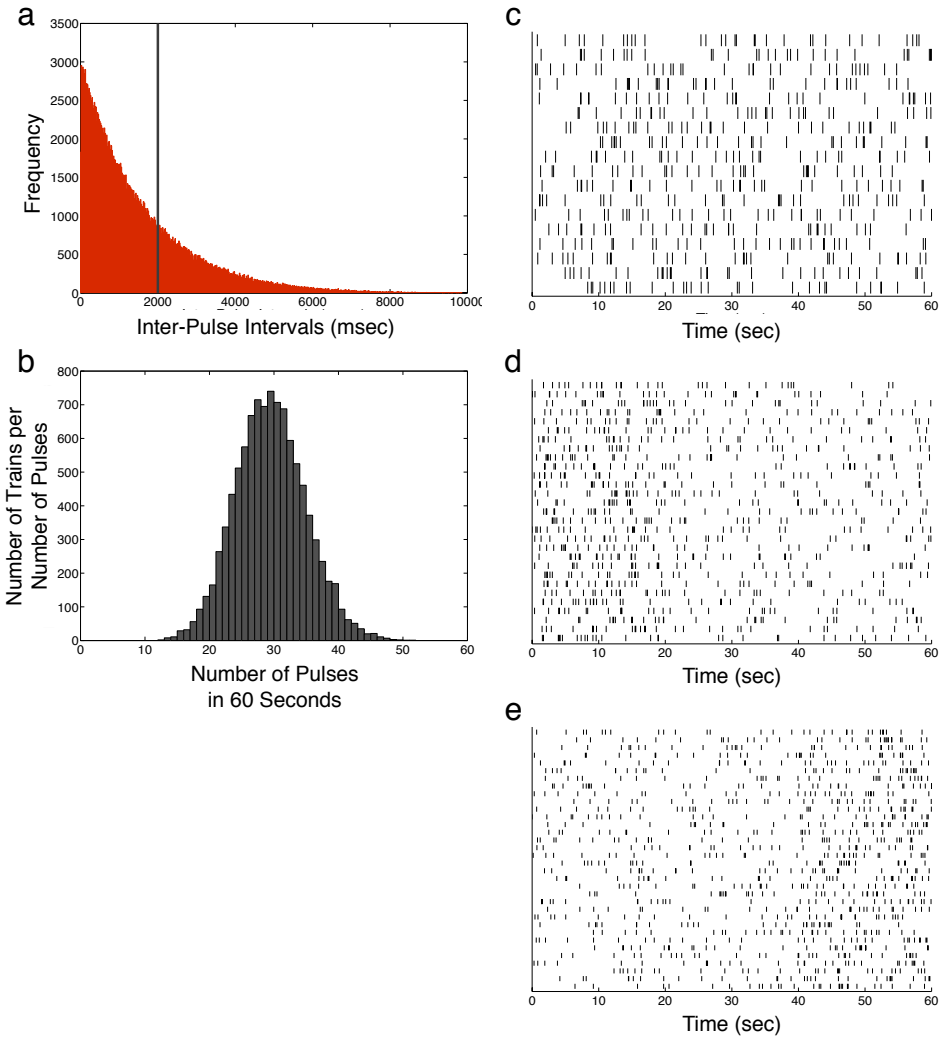

Figure 4.3.3. **Naturalistic-like Trains and Inter Pulse Intervals.** **a)** Inter pulse intervals (IPI) of Poisson distributed trains exponentially distributed (red), gray line represents deterministic IPI interval value of Regular Train, **b)** Out of all 10000 generated NTs only 740 of them had exactly 30 pulses. Number of pulse distribution is Gaussian, **c)** NT-Uniform trains **d)** NT-BEG trains **e)** NT-END trains.

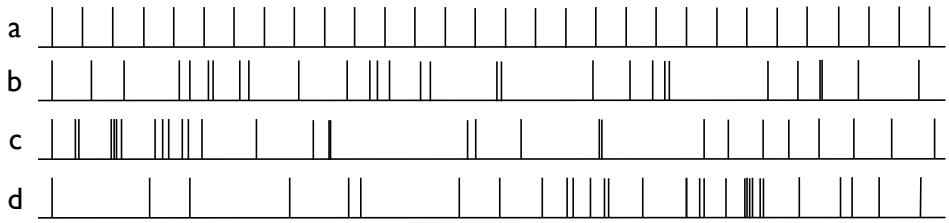

	1	2	3	4	5	6	7	8	9	10	11	12	13	14	15	16	17	18	19	20	21	22	23	24	25	26	27	28	29	30
REG	0	2000	2000	2000	2000	2000	2000	2000	2000	2000	2000	2000	2000	2000	2000	2000	2000	2000	2000	2000	2000	2000	2000	2000	2000	2000	2000	2000	2000	2000
NTU	0	2589	2014	3596	711	862	515	1880	543	3306	3157	1564	430	683	1504	1050	4373	281	2003	5996	2532	1504	813	240	4519	2098	1531	80	2424	4001
NTB	0	1544	166	2221	116	155	335	2221	579	585	352	821	476	848	3603	3723	1120	34	9043	632	3029	5171	176	6803	1692	2302	1778	1968	2371	2571
NTE	0	6444	2749	6630	3917	805	6557	2529	3065	1400	472	1266	1152	375	1955	2930	816	236	1438	1293	76	246	199	719	118	1306	2689	920	1687	2683

Figure 4.3.4. **Visual Comparison of Uncaging Patterns.** We compared plasticity consequences of previously described Regular pattern in (a) with three different NTs: NT-Uniform in (b), NT-BEG in (c) and NT-END in (d). Table shows the inter-pulse-intervals (in msec) for each interval[2].

late-phase of this regular-train induced LTP is protein synthesis dependent (Govindarajan et al., 2011).

4.4 Results

We first wanted to establish a baseline level of plasticity through glutamate uncaging at single spines using the Regular (REG) protocol of 30 uncaging pulses that are 4msec-long at 0.5 Hz, with a laser power of 30 mW as measured at the back aperture, described above in section 2.2.2. This serves to validate that structural plasticity at single inputs can be expressed in our system, given the uncertainty of the stimulation with the naturalistic based paradigm results. Consistent with the published work, we found that glutamate uncaging with the Regular pattern of activity leads to robust growth of the stimulated spine compared with the baseline ($\Delta V_{REG} = 157 \pm 10.3\%$, $P = 2.39^{-12}$, last 60 min, $mean \pm s.e.m.$), while unstimulated neighbors remained unchanged ($\Delta V_{REG_{neigh}} = 107 \pm 4.7\%$, $P = 0.16$, last 60 min) (Figure 4.4.2). In all time series plots, we report IFI-based spine volumes of stimulated and un-stimulated neighboring spines (Figure 4.4.1) over time.

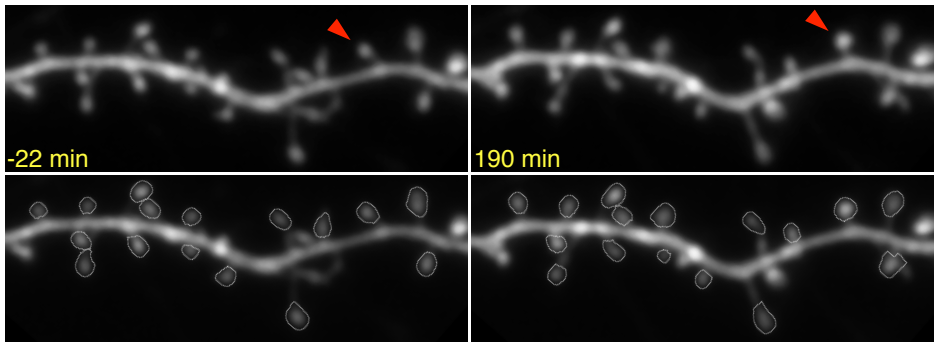

Figure 4.4.1. **Representative Two-Photon Microscopy Images of a Dendritic Branch Before and After Uncaging Stimulation.** Red triangle indicates the stimulated spine. Upper panel shows spines before segmentation. Lower panel shows segmentations used for volume quantification. Spine is stimulated at time 0.

We found that such stimulation led to the induction of long lasting potentiation and growth of the spine for up to 225 min post-stimulation, which was significantly greater than the initial size of that spine ($\Delta V_{REG} = 189 \pm 22.4\%$, $P = 3.16^{-9}$, 0-15 min; $\Delta V_{REG} = 135 \pm 8.4\%$, $P = 4.38^{-8}$, 45-75 min; $\Delta V_{REG} = 160 \pm 9.8\%$, $P = 6.66^{-9}$, last 30 min) (Figure 4.4.2).

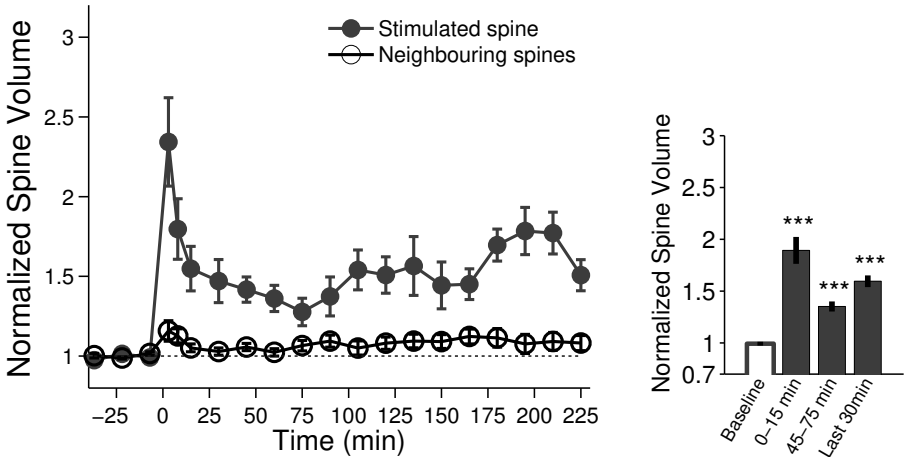

Figure 4.4.2. **Regular Pattern Induces Long-Lasting Spine Growth.** Regular train induced LTP that lasts 4 h. ($n_{stim} = 17$, $n_{neigh} = 200$)

4.4.1 Timing Structure of the Naturalistic-like Train Determines the Longevity of the Plasticity

We next tested whether the homogeneously distributed Poisson train, NT-UNI, was capable of inducing plasticity at a single input. Stimulation with the NT-UNI activity pattern led to the long-lasting induction of potentiation at single inputs ($\Delta V_{NT-UNI} = 158 \pm 21.6\%$, $P = 1.92^{-9}$, last 60 min) which was similar to the plasticity induced with the REG train ($P_{REG-NTUNI} = 0.75$, 0-15 min; $P_{REG-NTUNI} = 0.97$, 45-75

min; $P_{REG-NTUNI} = 0.123$, last 30 min) (Figures 4.4.3b and 4.4.4b). In stark contrast to this finding, while stimulations with either the NT-BEG or the NT-END patterns elicited short term potentiation during the first 15 min which was similar to that seen with the REG stimulation

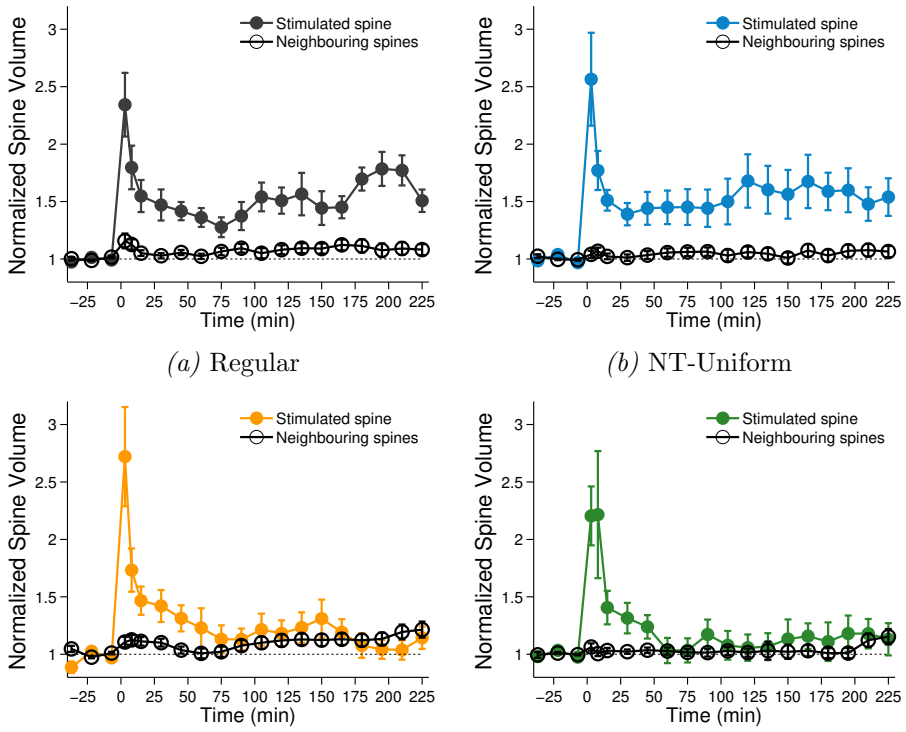

(a) Regular *(b)* NT-Uniform

(c) NT-Beginning *(d)* NT-End

Figure 4.4.3. **Activity Dynamics Determine the Structure of the Induced LTP. a)** Evenly-spaced (regular train) 30 pulses in 60 sec induced LTP that lasted 4 h. ($n_{stim} = 17$, $n_{neigh} = 200$) **b)** NT-UNI train induced long lasting LTP. ($n_{stim} = 16$, $n_{neigh} = 200$) **c)** NT-BEG train induced short lasting LTP. ($n_{stim} = 16$, $n_{neigh} = 192$) **d)** NT-END train induced short lasting LTP with an upward trend towards the end. ($n_{stim} = 18$, $n_{neigh} = 264$)

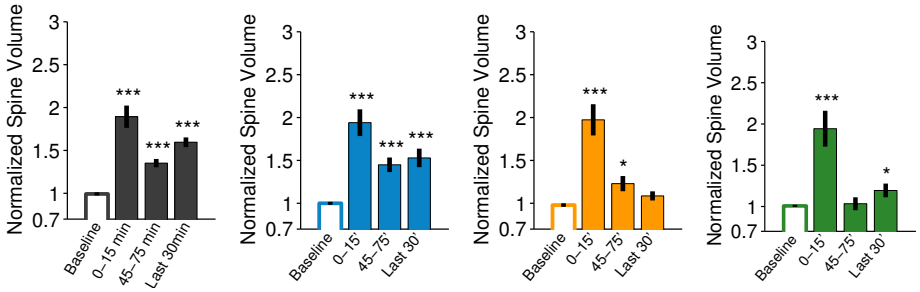

Figure 4.4.4. **Temporal Dynamics of Uncaging Stimulus Determines the Longevity of Single Spine Plasticity.** In the first 15 min after the stimulation, all protocols were shown to induce statistically similar plasticity. However, this initial induction did not lead to the long-lasting plasticity for every case. While NT-UNI train induced long-lasting LTP similar to the Regular train, NT-BEG and NT-END trains did not maintain the initial plasticity. Normalized spine volumes at 3 time bins $(0' - 15', 45' - 75', 195' - 225')$ were compared to baseline. (mean + s.e.m, statistical comparisons were done with Mann-Whitney-U test,*<0.05, **<0.01, ***<0.001).

paradigm ($\Delta V_{NT-BEG} = 197 \pm 31.5\%$, $P = 1.45^{-9}$; $\Delta V_{NT-END} = 194 \pm 37.6\%$, $P = 1.4^{-9}$; $P_{REG-NTBEG} = 0.986$; $P_{REG-NTEND} = 0.584$), this plasticity was short lived, returning to baseline levels after less than two hours post stimulation ($\Delta V_{NT-BEG} = 123 \pm 15.2\%$, $P = 0.11$, 45-75 min; $\Delta V_{NT-BEG} = 108 \pm 9.4\%$, $P = 0.54$, 195-225 min; $\Delta V_{NT-END} = 103 \pm 11.7\%$, $P = 0.08$, 45-75 min; $\Delta V_{NT-END} = 119 \pm 14.4\%$, $P = 0.12$, 195-225 min) (Figures 4.4.3c-d, 4.4.3c-d).

4.4.2 NT-Uniform Induced Plasticity is NMDAR-Dependent

We wanted to characterize the plasticity elicited by the NT-UNI uncaging paradigm. Previous studies had showed that the REG stimulation induces NMDAR-dependent LTP (Matsuzaki et al., 2004; Govindarajan et al., 2011). In order to determine whether the plasticity induced by the NT-UNI train is also NMDAR-dependent, we used a selective NMDAR antagonist (2R)-amino-5-phosphonopentanoate (APV) in the ACSF during the uncaging stimulation.

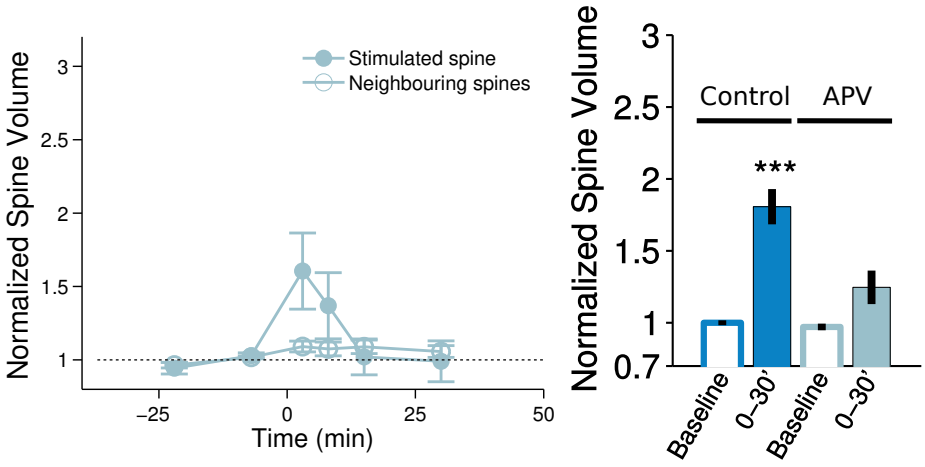

Figure 4.4.5. **NT-Uniform LTP Requires NMDA Receptors.** APV blocks NT-UNI induced LTP ($n_{stim} = 5$, $n_{neigh} = 73$) Mann-Whitney-U test, ***<0.001).

We found that this manipulation blocked the induction of plasticity, eliciting only a transient potentiation in the presence of APV which was not significantly different from baseline 30 min after the stimulation ($\Delta V_{APV} = 99 \pm 15.6\%$, $P = 0.43$, 20-30 min)(Figure 4.4.5).

To further validate the requirement for NMDA receptor activation by the NT-UNI train, we stimulated individual spines in the presence of 0.25 mM Mg^{2+} (Figure 4.4.6). As the induction of plasticity through

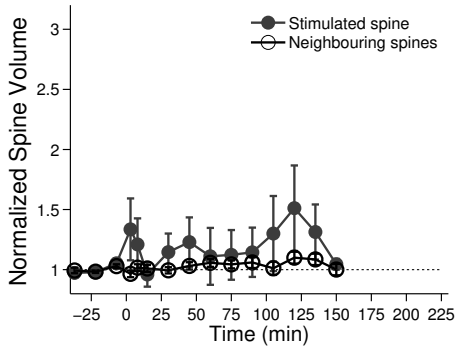

(a) Regular Train, 0.25mM Mg^{2+}, $n_{stim} = 7, n_{neigh} = 82$

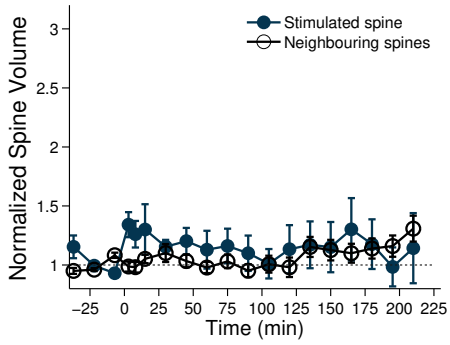

(b) NT-Uniform, 0.25mM Mg^{2+}, $n_{stim} = 4, n_{neigh} = 44$

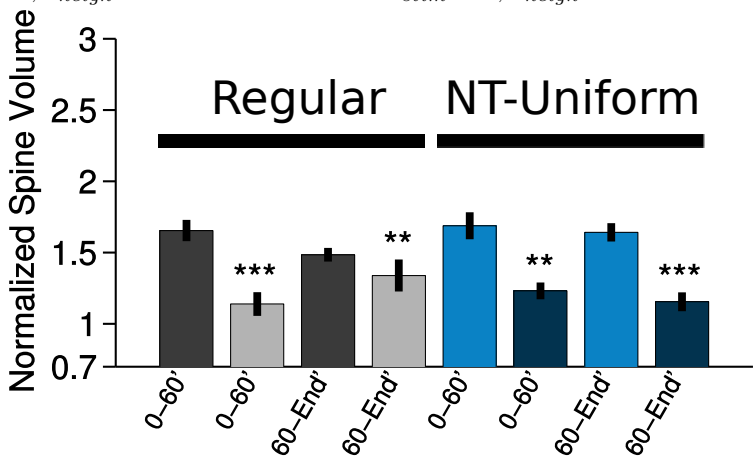

(c) Black: Regular Train, 0 and 0.25 mM Mg^{2+}, respectively, Blue: NT-Uniform Train, 0 and 0.25 mM Mg^{2+}, respectively.

Figure 4.4.6. **NT-Uniform LTP Requires the Removal of Mg Blockade.** Partial blockage of NMDARs using 0.25 mM Mg^{2+} in ACSF during uncaging delivery significantly reduces the LTP induced by Regular and NT-UNI trains.

the NMDA receptor requires removing magnesium blockade, glutamate uncaging mediated plasticity at single spines is carried out in the presence of 0 mM Mg^{2+} in the uncaging ACSF. We tested both REG and

NT-UNI train in the presence of 0.25 mM Mg^{2+} and found that delivery of the NT-UNI stimulation to single inputs in the presence of 0.25 mM Mg^{2+} significantly reduced the induction of plasticity similarly to the case following REG stimulation ($\Delta V_{REG_{Mg}} = 114 \pm 20.4\%$, $P = 1.6^{-5}$; $\Delta V_{REG_{Mg}} = 133 \pm 29.7\%$, $P = 0.0022$; $\Delta V_{NT-UNI_{Mg}} = 123 \pm 14.5\%$, $P = 0.0051$; $\Delta V_{NT-UNI_{Mg}} = 115 \pm 21\%$, $P = 2.62^{-4}$, compared to 0 Mg, 60-150 or 60-210 min for REG and NT-UNI, respectively)(Figure 4.4.6).

4.4.3 Longevity of the NT-Uniform Induced Plasticity is Protein-Synthesis Dependent

As described previously, long lasting functional plasticity that recruits new protein synthesis also leads to long lasting structural changes (Govindarajan et al., 2011). As we observed that the plasticity elicited at single spines leads to structural changes that last for many hours, we hypothesized that the induced plasticity requires new protein synthesis. Therefore, we performed both the REG and NT-UNI stimulations in the presence of the protein synthesis inhibitors anisomycin or cycloheximide (Figure 4.4.7a-c), and observed that this manipulation blocked the late-phase of uncaging induced LTP ($\Delta V_{REG_{Aniso}} = 103 \pm 13.91\%$, $P = 0.49$, 60-90 min, compared with the baseline; $\Delta V_{REG_{Cyclo}} = 120 \pm 26.5\%$, $P = 0.89$, 60-90 min, compared with the baseline) as reported for the regular train (Govindarajan et al., 2011). We have seen a similar blockage for NT-UNI induced LTP ($\Delta V_{NT-UNI_{Aniso}} = 108 \pm 10.34\%$, $P = 0.06$, 60-90 min, compared with the baseline; $\Delta V_{NT-UNI_{Cyclo}} = 115 \pm 7.4\%$, $P = 0.02$, 60-90 min, compared with the baseline) (Figure 4.4.7d-4.4.7f).

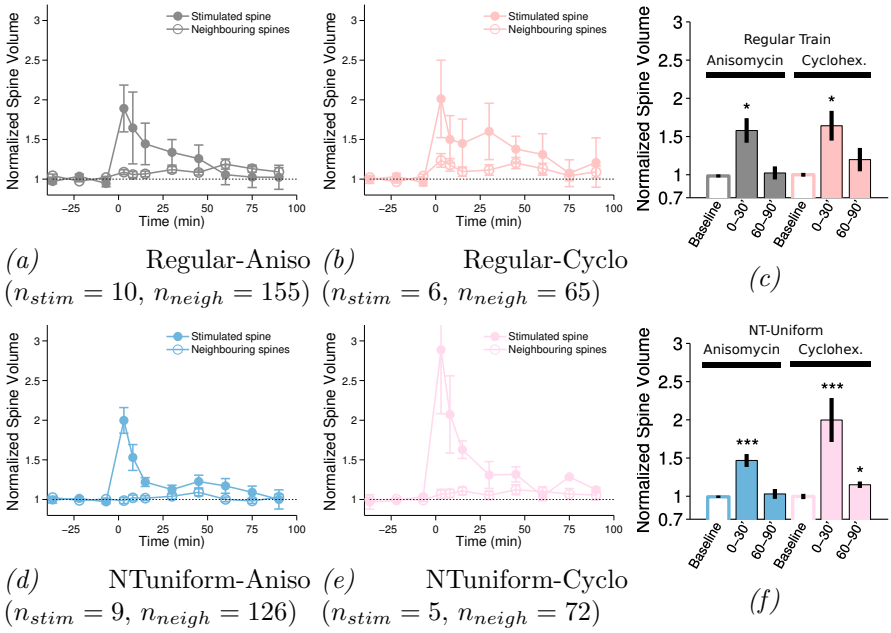

(a) Regular-Aniso ($n_{stim} = 10$, $n_{neigh} = 155$) *(b)* Regular-Cyclo ($n_{stim} = 6$, $n_{neigh} = 65$) *(c)*

(d) NTuniform-Aniso ($n_{stim} = 9$, $n_{neigh} = 126$) *(e)* NTuniform-Cyclo ($n_{stim} = 5$, $n_{neigh} = 72$) *(f)*

Figure 4.4.7. **Late Phase of the Plasticity is Protein Synthesis Dependent.** Protein synthesis blockers anisomycin and cycloheximide blocks the late phase of REG and NT-UNI induced plasticity. Mann-Whitney-U test,*<0.05, **<0.01, ***<0.001).

4.4.4 Plasticity Levels do not Depend on the Initial Spine Size

Matsuzaki *et al.* showed that spines that are larger than 0.1 μm^3 exhibit only the transient structural LTP that goes back to baseline after 40 min (Matsuzaki et al., 2004). Although we did not stimulate any spines that are bigger than 0.1 μm^3 (a post-hoc realization, $\mu_{spineVolume} = 0.0515 \mu m^3, \sigma_{spineVolume} = 0.0136 \mu m^3$, Figure 4.4.9), we attempted to determine the existence of a volume difference conditional to the initial spine size. We grouped spines depending on their initial baseline sizes into two groups using k-means clustering. We did not see any statis-

tically significant differences between the amount of plasticity expressed at small or large spines ($P_{REG} = 0.79$, $P_{NT-UNI} = 0.54$, $P_{NT-BEG} = 0.41$, $P_{NT-END} = 0.44$, all big vs small comparisons, repeated-measures ANOVA from 0 to 225 min). Big and Small cluster averages are given in Figure 4.4.8 legend for comparison.

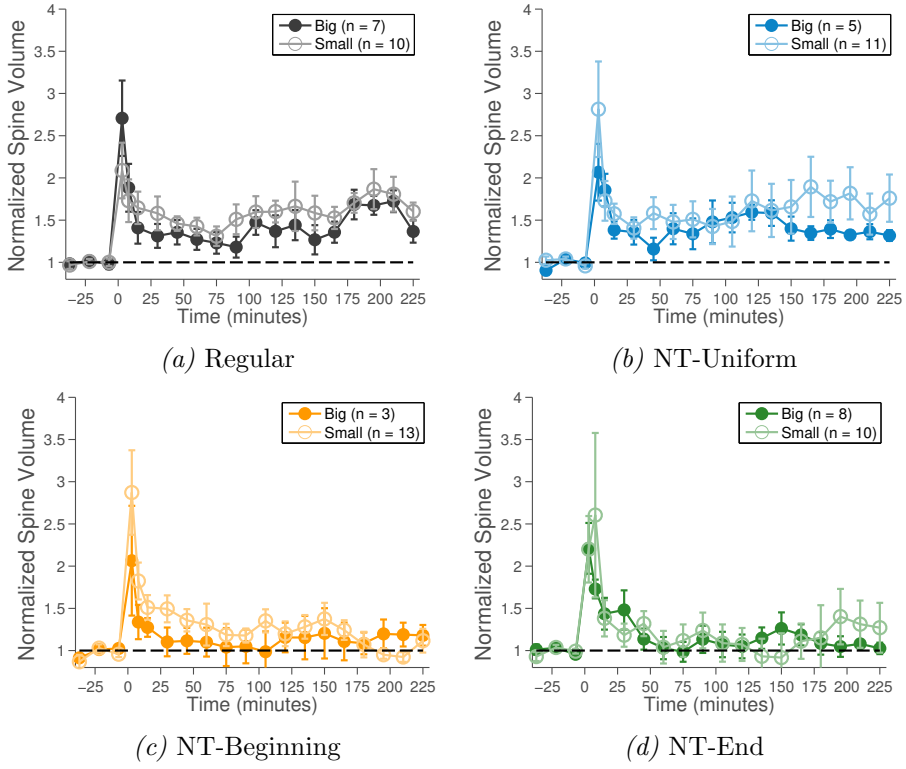

(a) Regular

(b) NT-Uniform

(c) NT-Beginning

(d) NT-End

Figure 4.4.8. **Initial Spine Size does not Correlate with the Amount of Structural Plasticity Expressed.** Average initial sizes (in μm) for big and small spines after k-means clustering for each condition are as follows: **a)** $\mu_{big} = 0.70, \mu_{small} = 0.47$, **b)** $\mu_{big} = 0.67, \mu_{small} = 0.42$, **c)** $\mu_{big} = 0.77, \mu_{small} = 0.42$, **d)** $\mu_{big} = 0.59, \mu_{small} = 0.42$

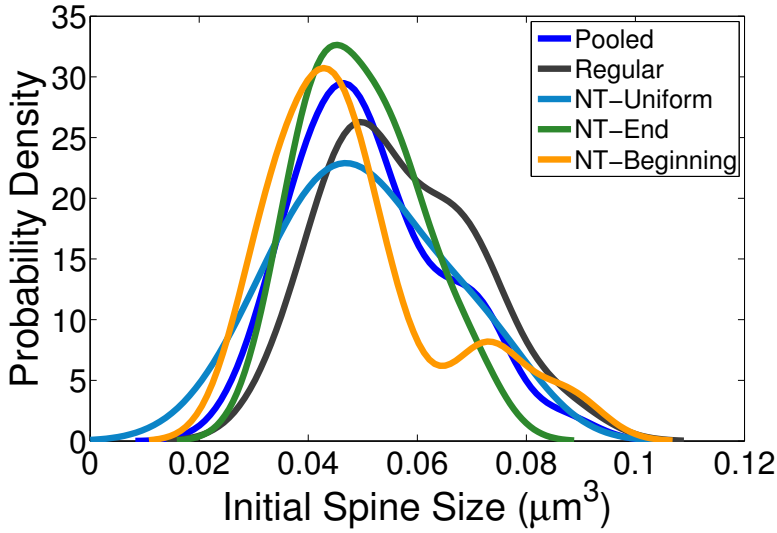

Figure 4.4.9. **Initial Spine Size Distributionss.** Distribution density for each group estimated using a Gaussian smoothing kernel. (Bishop, 2007)

4.5 Conclusions

Here, using two-photon fluorescence imaging and glutamate uncaging, we studied single spine plasticity of CA1 pyramidal neurons using stimulation trains sampled from a Poisson process resembling firing patterns of CA3 neurons.

We found that the late phase of LTP, but not the early phase, is determined by the timing structure of the uncaging train. It should be re-emphasized that all three NTs are composed of 30 pulses in 60 sec, just like the REG train which induced long lasting LTP. Out of the three NTs we tested, the NT-UNI train was the only one that induced long-lasting LTP that was protein synthesis-dependent. This result may not be too surprising, due to its relatively closer proximity to the regular train,

compared to NT-BEG and NT-END. This suggests that the regularity or stationarity of the stimulation train plays a role in the induction of long-lasting LTP. However, previous studies showed that when regular 30-pulse protocol were used with 1 msec long uncaging laser pulse-widths instead of 4 msec (subthreshold protocol), stimulated spines did not express long lasting LTP (Harvey & Svoboda, 2007; Govindarajan et al., 2011) (see Section 1.5). Shorter uncaging laser pulses leads less glutamate to be uncaged. Hence, given the total amount of uncaged glutamate is fixed, regularity seems to be necessary for the induction of long-lasting LTP but it is not sufficient, and the level of irregularity (here represented by instantaneous pulse frequency fluctuations over time (see Figure 4.3.2)) is apparently responsible for the determination of the threshold for LTP induction.

In conclusion, we suggest that given that the number of stimulation pulses and total stimulation time are fixed, stationarity is necessary but not sufficient for a train to induce long-lasting LTP at single dendritic spines.

Chapter 5

Rapid Structural Spine Dynamics and Long-Term Consequences

Contributions: Ali Özgür Argunşah and Inbal Israely conceived the study and designed the experiments. Ali Özgür Argunşah performed the experiments and analyzed the data.

Affiliations: Champalimaud Neuroscience Programme, Lisbon, Portugal.

Support: This work is supported by Fundação para a Ciência e a Techologia (FCT), Fundação Champalimaud (FC) and Instituto Gulbenkian de Ciência (IGC).

5.1 Abstract

Structural changes of dendritic spines can be used as a proxy for synaptic plasticity. Studies that address single-spine plasticity have often been conducted by structural imaging before and after the induction of plasticity. Here we extended this approach by imaging the stimulated spines during the course of uncaging delivery. We found that the timing structure of the uncaging patterns did not lead to significant structural differences. However, using correlation and clustering analysis, we showed that these rapid structural spine growth dynamics have differential predictive powers in terms of explaining the longevity of the induced plasticity for regular and naturalistic-like trains. While rapid structural spine growth during the course of 60 sec-long regular train delivery did not show any correlation with the longevity of the induced plasticity, spines that were stimulated using naturalistic-like trains were positively correlated to various degrees. Thus, these experiments suggest that dendritic spines have the capacity of translating the timing structure of the stimulus differentially.

5.2 Introduction

The time delay between the stimulation and structural spine changes has been debated in the field. It has been argued that there is a 2 to 3 sec delay between the electrical stimulation and the initiation of NMDA dependent LTP, while the additional 20 to 30 sec are needed for the potentiation to reach peak levels (Gustafsson & Wigström, 1990). The potentiation subsequently decays to a degree which depends primarily on tetanus length. Matsuzaki *et al.* interpreted these results as an evidence of a time delay between spine enlargement and synaptic stimulation (Matsuzaki et al., 2004). In contrast, conflicting evidence suggested that filopodium or spine formation requires at least 20 min following the induction of LTP

and hence cannot explain the rapid onset of LTP (Engert & Bonhoeffer, 1999; Maletic-Savatic, Malinow, & Svoboda, 1999). All three of studies used electrical stimulation for the induction of plasticity, and therefore, the results are not very clear from the perspective of single spines.

In another set of studies that used an uncaging stimulation approach, the spatiotemporal dynamics of various fluorescence tagged proteins, such as Ras (Harvey et al., 2008), CaMKII (Lee, Escobedo-Lozoya, Szatmari, & Yasuda, 2009) and actin (Bosch et al., 2014) have been investigated. They all concluded that structural changes are instantaneous rather than time delayed.

In this section, we will present the results of the rapid structural dynamics of dendritic spines conditional to regular and naturalistic-like trains, as well as the results showing how these rapid structural changes affect the longevity of the induced plasticity.

5.3 Results

During our experiments, we realized that the spine structure begins to change already during the course of stimulation. In order to capture structural spine dynamics during uncaging stimulus, we made time-lapse images (videos) of the region of interest of the stimulated spine (Figure 5.3.1) in XY-plane starting before the onset of the stimulation until up to 5 sec after the delivery of the last uncaging pulse.

5.3.1 Stimulation Pattern does not Cause Significant Spine Growth Differences During the Course of Stimulation

First, we wanted to determine if there are significant differences in the rapid structural growth of individual spines that are stimulated using different stimulation trains. The stimulated spine, presented in Figure 5.3.1 grew to almost four times its initial size during the course of stimulation.

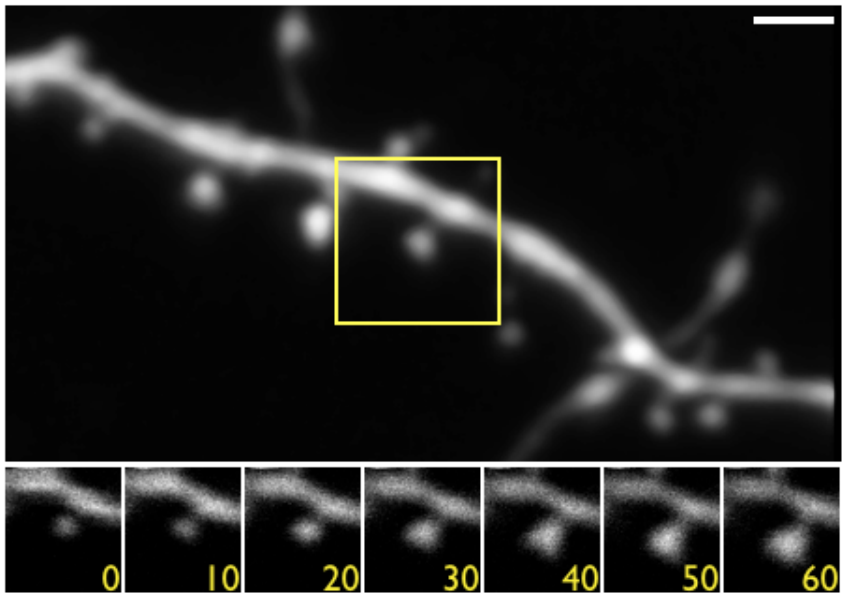

Figure 5.3.1. **Rapid Structural Growth During Stimulation.** Upper panel shows the dendrite of interest and the stimulated spine is indicated in the yellow box. Lower panel shows how the spine structure changes during the course of stimulation (in seconds). Scale bar is $2\mu m$.

So, for each stimulated spine, we quantified the IFI of the spine head fluorescence over time from the two-photon time lapse images we collected during the uncaging delivery. Figures 5.3.2A shows the normalized spine volume changes during the course of stimulation with four different stimulation trains. Each line represents a different spine.

We found that on average all four stimulation conditions induced similar levels of structural plasticity during the course of uncaging delivery ($\Delta V_{REG} = 226 \pm 37\%$; $\Delta V_{NT-UNI} = 190 \pm 19\%$; $\Delta V_{NT-BEG} = 195 \pm 19.8\%$; $\Delta V_{REG} = 236 \pm 37\%$, at 60 sec, normalized to baseline), and we have not observed any statistically significant differences between different conditions (p>0.5, repeated-measures ANOVA) (Figure 5.3.2B).

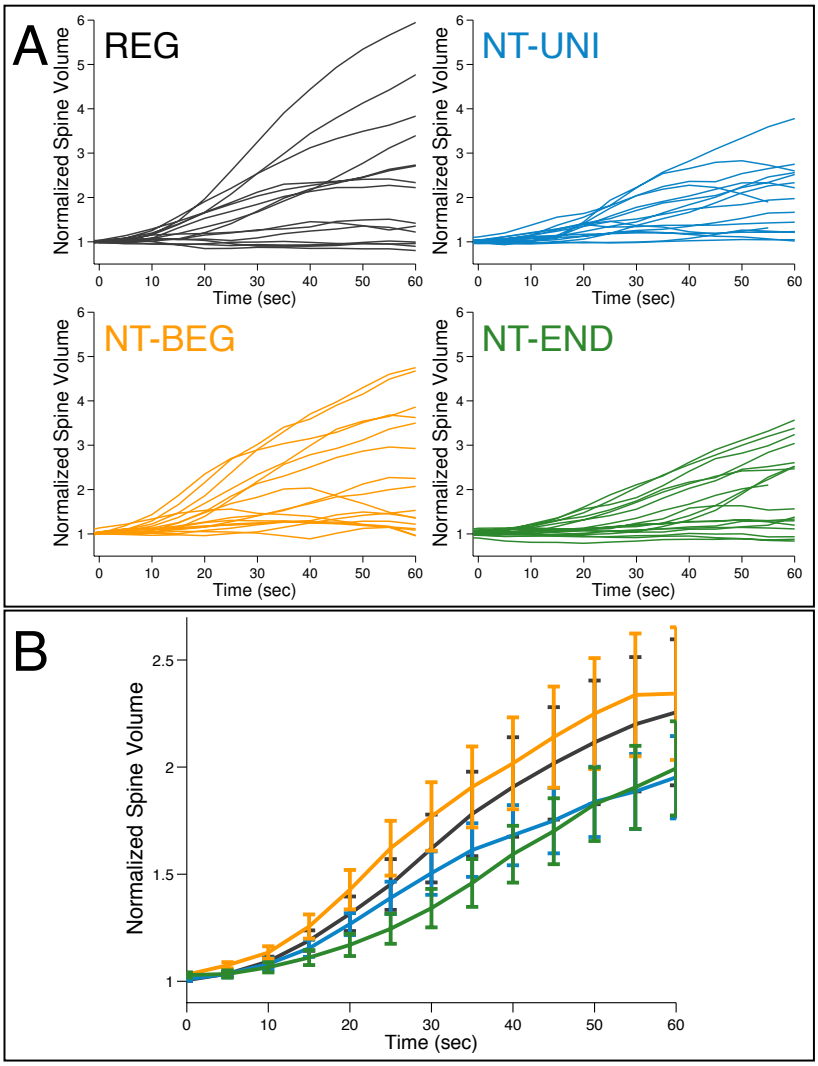

Figure 5.3.2. **Rapid Normalized Spine Growth for All Conditions. A)** Individual rapid structural dynamics for each condition, **B)** Statistical comparison of rapid growth data for different condition reveals that there is no statistical differences between these growth curves in [0,60] sec interval. The only observed difference is between NT-BEG and NT-END in [0,40] sec interval ($p = 0.033$, repeated measures-ANOVA).

5.3.2 Rapid Spine Growth During the Course of Stimulation Signals Longevity

Following this, we aimed to determine if there are any relationship between the rapid structural changes occurring during the course of stimulation and long-term structural dynamics. In order to do that, we computed the correlation coefficient (Leon-Garcia, 2008) between the area under each growth curve (integral) and the long-term normalized volume for every time bin (Figure 5.3.3).

$$\rho(I_{Rapid}, V_L(t)) = \frac{COV(I_{Rapid}, V_L(t))}{\sigma(I_{Rapid})\sigma(V_L(t))} \tag{5.1}$$

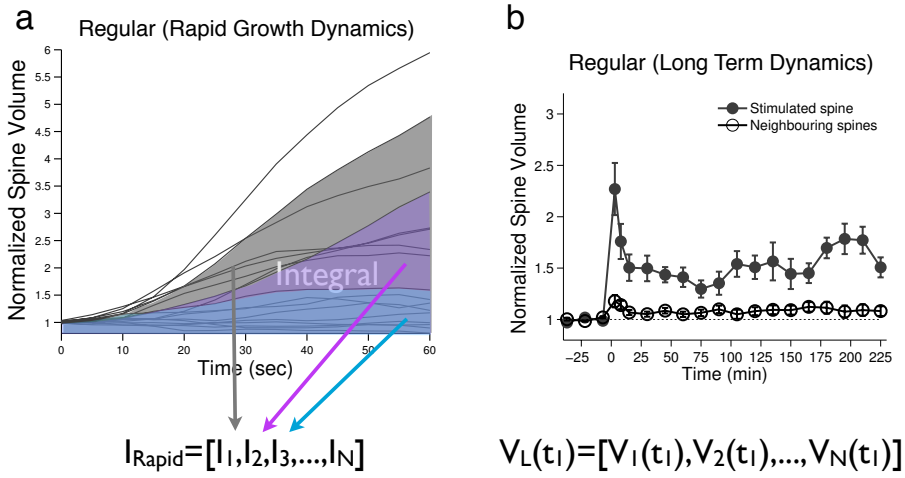

Figure 5.3.3. **Correlating Short Term Growth with Long-Term Dynamics.** In order to correlate rapid short term volume dynamics with long-term volume dynamics (post-uncaging delivery imaging), we computed the area under each growth curve during the course of stimulation as shown in **a**, and correlated this vector with post-stim volumes for every time bin in **b**, which gave us time series progression of correlations.

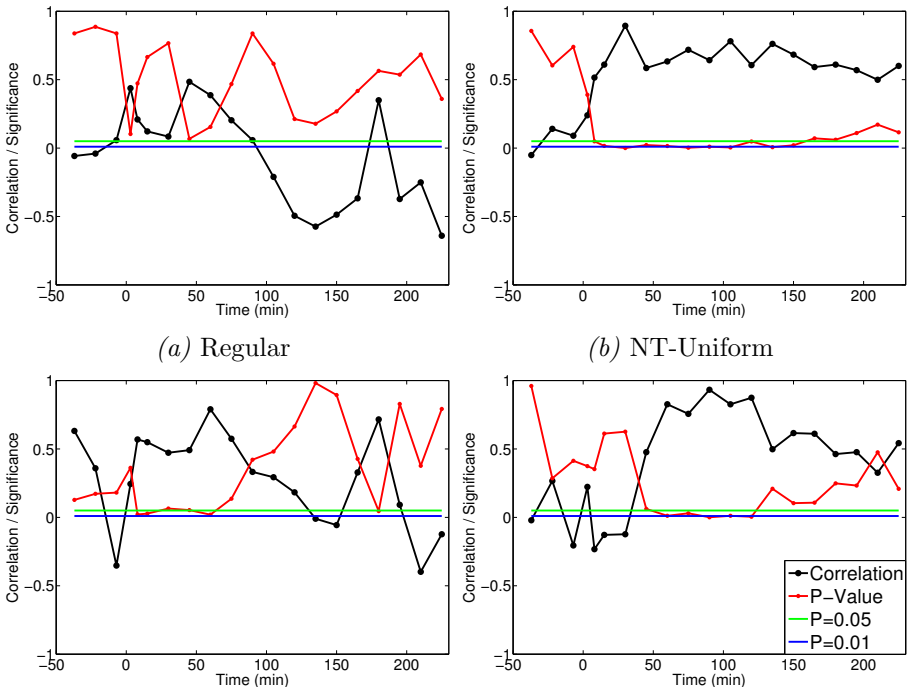

(a) Regular

(b) NT-Uniform

(c) NT-Beginning

(d) NT-End

Figure 5.3.4. **Correlations Between Short-Term Growth with Long-Term Dynamics Shows Stimulus Dependency.** In order to check the relationship between the rapid spine growth during the course of stimulation and the post-stimulus spine volume over time, we computed the correlation between the area under each rapid growth curve for a given stimulus pattern and the normalized spine volume at ay time point after the stimulation. Black lines represent the correlation for each time bin. Red lines are the significance of that correlation estimated using permutation (shuffle) test. Green represents p=0.05, Blue represents p=0.01.

Correlation analysis revealed very interesting differences between spines that are stimulated using the Regular and Naturalistic-like trains. Although both of these uncaging trains have 30 pulses spread over 60 sec and both are NMDAR and protein-synthesis dependent, while no significant correlations were observed between the rapid dynamics and

long-term changes for spines that are stimulated using REG train (Figure 5.3.4a), we have obtained strong and significant correlations for the spines stimulated using NT-UNI (Figure 5.3.4b). Significant correlations were obtained for NT-BEG and NT-END trains as well, but to a lesser extent. Additionally, when we pooled all the naturalistic-like trains together, correlation structure held up (Figure 5.3.5).

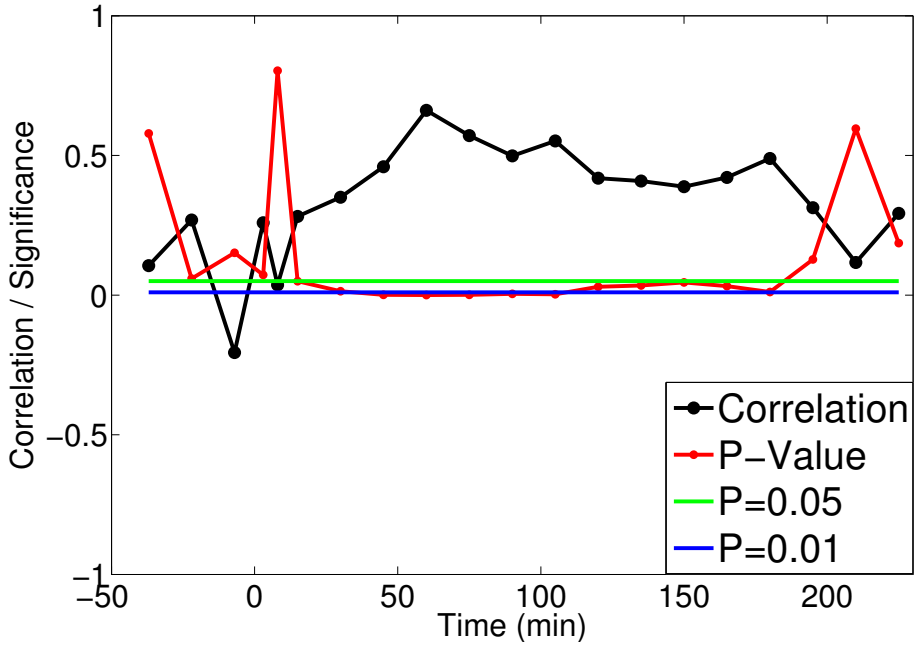

Figure 5.3.5. **Correlations Between Short-Term Growth with Long-Term Dynamics for All Naturalistic Trains Combined.** Correlations are computed using the same methods described previously. Black represent the correlation for each time bin. Red is the significance of that correlation estimated using shuffle test. Green represents p=0.05, Blue represents p=0.01.

To further test the short-term vs long-term relationship, we performed a second analysis. We clustered rapid structural growth dynamics for each

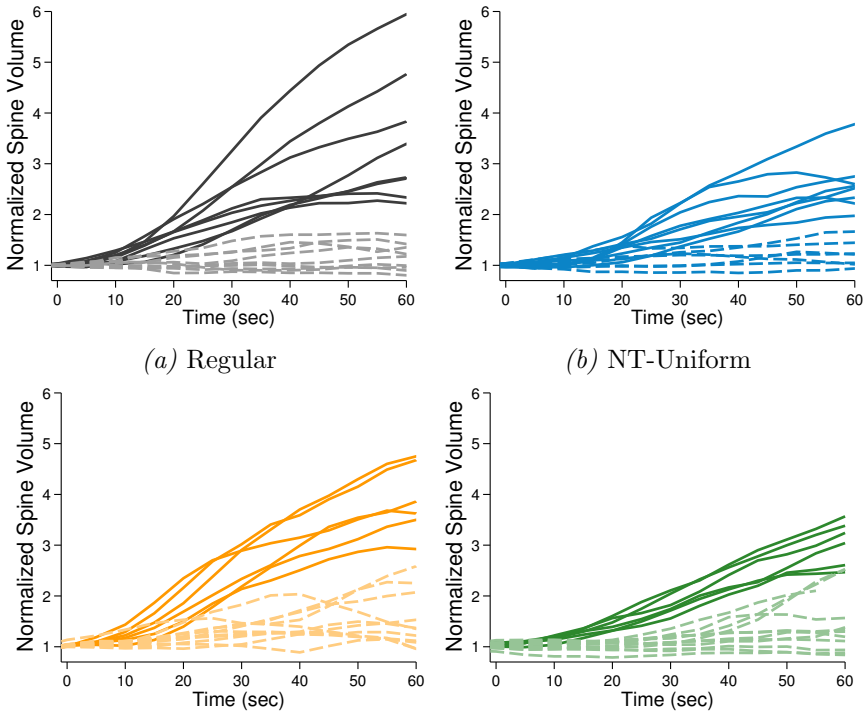

(a) Regular *(b)* NT-Uniform

(c) NT-Beginning *(d)* NT-End

Figure 5.3.6. **Clustering Rapid Dynamics.** As a secondary confirmation, we divided rapid growth curves into two classes using k-means algorithm and grouped the corresponding long-term dynamics according to the classes. Those that grow more were designated, **High class**, while those that grew less were **Low class**.

condition into two clusters using the k-means algorithm (Figure 5.3.6). K-means partitions the data into k groups so that the sum of squares from points to the assigned cluster centers is minimized (Bishop, 2007). Briefly, the k-means algorithm is described as follows:

1. Start with initial guesses for cluster centers (randomly assign two cluster centers known as centroids).

2. For each data point, find closest cluster center (partitioning step).

3. Replace each centroid by average of data points in its partition.

4. Iterate step-1 and step-2 until convergence.

We named the obtained clusters *high* and *low*. Afterward, we grouped the long-term results into two with respect to the cluster they belong to. Figure 5.3.7 shows long term normalized spine volume change for high and low clusters for all tested conditions.

As the correlation analysis showed, spines that were stimulated using REG train did not show any significant plasticity differences conditional to clustered rapid structural dynamics (Figure 5.3.7a). In contrast to this, all naturalistic-like train stimulated spines showed differences conditional to rapid dynamics clusters to a certain extent.

Clustering analysis supported the correlation analysis, which can be seen in Figures 5.3.7 and 5.3.8. Spines that fell under **high**- or **low**-clusters according to their rapid-growth curves did not exhibit significant volume differences in long-term ($P_{REG_{high-low}} = 0.56$, repeated-measures ANOVA)(Figure5.3.7a-5.3.7c). However, all NT induced rapid growth had some predictive value in term of long-term plasticity levels (Figure 5.3.7d-5.3.7l).

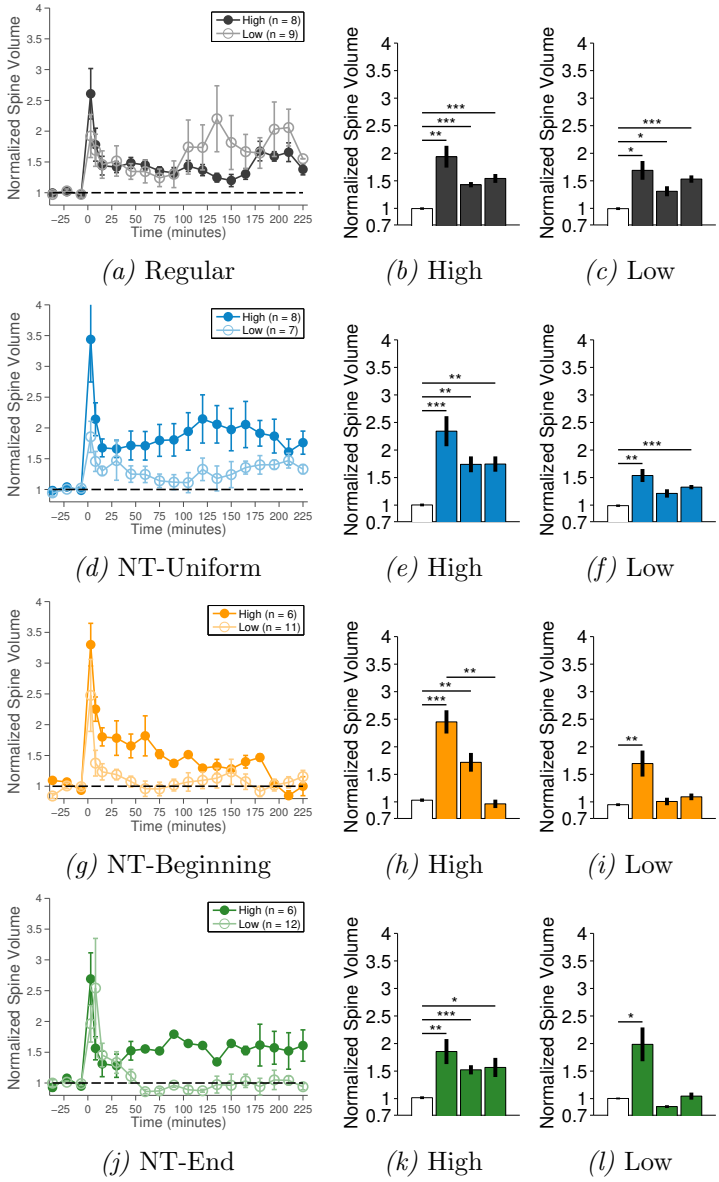

Figure 5.3.7. **Cluster-Dependent Long-Term Dynamics.** Naturalistic trains exhibit rapid growth-dependent long-term dynamics, whereas the regular train does not. ($* < 0.05, ** < 0.01, *** < 0.001$) Time bins for boxplots are as follows (ordered left to right): Baseline / 0-15 min / 45-75 min / Last 30 min.

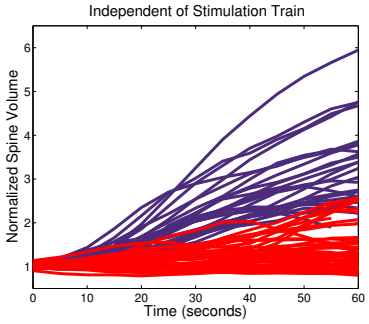

(a) All naturalistic-train induced rapid changes

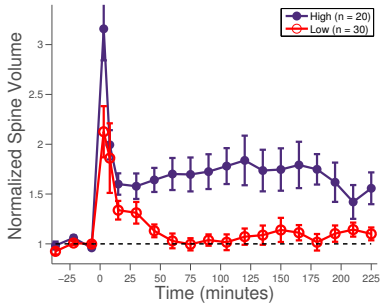

(b) Post K-means long term dynamics.

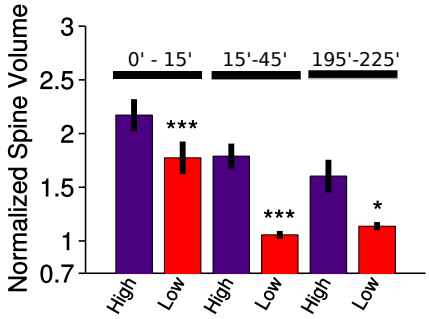

(c) Statistical comparisons of High and Low for indicated time bins.

Figure 5.3.8. **Naturalistic Train Induced Rapid Growth Predicts the Longevity of the Plasticity. a)** We pooled all rapid structural growth dynamics for Naturalistic-like trains and separate into 2 clusters using the k-means algorithm,**b)** Two distinct long-term dynamics emerged from these clusters ($P_{NT_{High-Low}} < 0.001$, repeated-measures ANOVA), **c)** Post-clustering long-term dynamics have statistically different plasticity levels over time.

5.4 Conclusions

As two-photon time lapse imaging of dendritic spines during glutamate uncaging stimulation showed, spine structure can change on the timescale of seconds. Although it seems that for all conditions the stimulated spines exhibit similar growth dynamics, it appears that there is a slight difference between NT-BEG and NT-END induced spine growth in the first 40 sec from the onset of the first pulse of the corresponding train delivered (Figure 5.3.2B). This difference can be interpreted as the instantaneous rate of the stimulation train that affects the rapid spine growth (Figure 5.3.2).

Correlation (Figure 5.3.5) and k-means clustering (Figure 5.3.8) analyses showed that the rapid structural changes caused by naturalistic trains signal the longevity of induced LTP. This is not the case for LTP that is induced by Regular train, which shows that dendritic spines have the capacity to interpret instantaneous rate changes within 60 sec differentially for deterministic (regular) and random (naturalistic) trains. This may mean that plasticity induced by regular trains is fundamentally different than plasticity induced by naturalistic trains.

As demonstrated in Sections 1.7 and 4.3, naturalistic stimulation trains studied by electrophysiological and computational techniques elicit STP dynamics that have different properties than tetanic stimulation. These studies concluded that the state of a synapse at the time of stimulation is crucial for the induction of plasticity, and that the tetanic stimulation may be driving synapses to a steady-state regime, making synapses unable to respond to stimulation within a dynamic range. In Chapter 4.3, we showed that, on average, only NT-UNI train stimulated spines expressed long-lasting LTP. However, post k-means analysis showed that 6 out 17 NT-BEG train stimulated and 6 out of 18 NT-END train stimulated spines

showed relatively longer lasting LTP compared to group averages. There results may reflect state dependency.

Chapter 6

Discussion

Synaptic plasticity is traditionally studied using high or low frequency, regularly spaced stimulation trains. However, although activity seen by a particular dendritic spine can have varying frequencies over time *in vivo*, inter-spike intervals of this incoming activity is not regularly spaced (Zador & Dobrunz, 1997; Dobrunz & Stevens, 1999; Paulsen & Sejnowski, 2000). In order to study plasticity in a relatively more naturalistic setting, we generated pulse trains resembling *in vivo* spiking activity of CA3 neurons. We used these generated naturalistic-like activation patterns to study short- and long-term structural plasticity at single dendritic spines using two-photon fluorescence imaging and glutamate uncaging. We found that the longevity of induced plasticity is activation pattern dependent and the structural changes that are induced by naturalistic-like trains during stimulations correlates with the long-term plasticity levels of the stimulated spine.

As we concluded earlier, stationarity seems to be necessary for a train to induce long-lasting LTP in single dendritic spines. However, previous studies had showed that regularity itself is not sufficient to induce long-lasting LTP (Harvey & Svoboda, 2007; Govindarajan et al., 2011) (see

Section 1.5). When researchers used a regular uncaging protocol with a 1 msec pulse- width instead of a 4 msec one, stimulated single spines did not express LTP. Therefore, stationarity is necessary but not sufficient to induce long-lasting plasticity in single spines. We know that the shorter the uncaging laser pulse is, the smaller the amount of glutamate that is released during uncaging. This difference between glutamate levels will affect the number of NMDARs that are activated. Ca^{2+} entry through NMDARs is necessary for the induction of plasticity and the level and duration of this Ca^{2+} entry determines the direction of the induced plasticity. Where high concentration of Ca^{2+} entering into the cell in a short time frame induces LTP, low concentration of Ca^{2+} entering over prolonged periods of time induces LTD (Lisman & McIntyre, 2001; Lisman & Spruston, 2005). This differential level of $[Ca^{2+}]$ leads to activation of different kinase/phosphatase pathways and the kinase/phosphatase balance determine the direction of plasticity (Otmakhov et al., 1997; Asrican et al., 2007; Cooper & Bear, 2012). Hence, stimulation pattern structure and the micro-domains within the pattern should be dynamically modulating the kinase/phosphatase balance over time and determining the type of plasticity.

In our experiments, NT-UNI was the only naturalistic-like stimulation pattern that induced long-lasting structural changes and we have shown that this plasticity is NMDAR-dependent. Therefore, the Ca^{2+} should be the main player for the induction of the observed plasticity. Moreover, we have shown that the longevity of this plasticity is protein-synthesis dependent. These results imply that downstream processes following Ca^{2+} entry through NMDARs triggered a cascade of protein-protein interactions that ended up in pushing the kinase/phosphatase balance in favor kinases that eventually ended up activating translation machinery that provided proteins that are necessary for the long-lasting structural modifications. Although sampled from the same Poisson distribution, other

two naturalistic-like patterns NT-BEG and NT-END did not induce long-lasting plasticity. As we pointed out earlier, the main difference between NT-UNI with NT-BEG and NT-END is the instantaneous frequencies of these patterns over time. Therefore, we believe that the stationary nature of NT-UNI is the reason for the long-lasting changes. As shown previously, REG pattern has a similar stationary structure and this pattern leads to protein-synthesis dependent long-lasting potentiation (Govindarajan et al., 2011). If we assume that kinases are more active during the high-frequency portion of the stimulation pattern and phosphatases are more during the lower-frequency portion, this might explain why NT-UNI is inducing a different form of plasticity than NT-BEG and NT-END. NT-UNI pattern has a 0.5 Hz stationary glutamate delivery during the course of 60 sec stimulation, while NT-BEG has approximately 0.75 Hz for first 20 sec and 0.375 Hz for following 40 sec and NT-END has 0.375 Hz for first 40 sec and 0.75 Hz for the following 20 sec. These time-frequency structures should be determining the Ca^{2+} dynamics, hence governing the dynamic kinase-phosphatase interactions. A good follow up study would be Ca^{2+} imaging of single spines during the delivery of different naturalistic-like trains to see to what extend stimulation pattern timing structure affecting the Ca dynamics. Additionally, kinases such as CaMKII and phospatases like calcineurin could be tagged with fluorescence proteins and imaged during the stimulus delivery. If our hypothesis is true, one should see a difference in cumulative CaMKII/calcineurin ratios over time for stationary and non-stationary portions of the stimulation patterns.

Following the analysis of the effects of different uncaging stimulation patterns on the long-lasting structural plasticity of single dendritic spines, we focused on effects or these trains on the structure during the stimulus delivery. It has previously being shown that dendritic spine structure can change rapidly upon activation (Van Harreveld & Fifkova, 1975; Fifková et al., 1982; Harvey et al., 2008; Lee et al., 2009). So, we wanted to test if

stimulation pattern structure is evoking different structural changes during the course of stimulation and if so, if there is any relationship between short- and long-term structural modifications.

We haven't seen any differences between four different conditions when we compared the stimulation induced structural changes during the coarse of stimulation. However, when we investigated individual structural growth traces, we noticed variability within conditions. In order to test if this variability has any long-term consequences, we performed two separate analyses: correlation-based and clustering-based.

Correlation analysis showed that the relationship between short- and long-term dynamics is stimulation pattern dependent for naturalistic-like patterns. While when pooled, naturalistic-like trains exhibit a positive correlation between short- and long- dynamics on average, correlation holds longer for NT-UNI in comparison to NT-BEG and NT-END. Moreover, although on average NT-BEG and NT-ENG induced plasticity has very similar structural plasticity dynamics over time, the correlation structures are very different. NT-BEG induced spines show positive correlation between short- and long- term structure starting from the first point after the stimulation until the 60th min when the correlation structure disappears, whereas NT-END induced spines do not exhibit any correlations until the 45th min and this correlation lasts following 80 mins. It appears that correlation structure over time has some commonalities with the instantaneous pulse frequencies (IPF) within naturalistic-like stimulation patterns. NT-BEG starts with relatively higher IPF at the beginning and correlations between short- and long- term dynamics are positive at the beginning, as starting point being the end of stimulation. NT-END does not show significant correlations at the beginning as it has lower IPF at the beginning of its pattern.

Interestingly, while all naturalistic-like trains showed significant positive correlations between short- and long-term dynamics to a degree,

REG pattern did not show any significant correlations, positive or negative. Since the closest pattern to REG in terms of temporal structure is NT-UNI which showed the longest correlation structure, the difference between these two results should be introduced due to the respective levels of irregularities. REG pattern is completely regular with fixed IPI of 0.5 Hz. This level of saliency might either be too extreme to be experienced by dendritic spine *in vivo* or very high saliency might have some sort of physiological meaning like emergency or high-priority information to be stored. Both cases might be forcing a type of plasticity into a spine that activates a separate pathway for plasticity compared to naturalistic-like patterns. Similar imaging studies we proposed earlier might be helpful for understanding these differences.

Clustering analysis supported the results we found using correlation analysis. Additionally, it has revealed that although on average they did not, both NT-BEG and NT-END have the capacity to induce long-lasting plasticity but to a lesser extend, if these patterns induced strong short-term structural changes during stimulation. This might mean that all naturalistic-like pattern can potentially induce long-lasting LTP but the probability of this induction is pattern structure dependent, most probably due to the stationarity over time as we discussed earlier.

Additionally, previous studies revealed that the activity of neurons in single cells (Mainen & Sejnowski, 1995) and local circuits (Vinje & Gallant, 2002; Herikstad, Baker, Lachaux, Gray, & Yen, 2011) are fundamentally different for regularly spaced stimuli compared to naturalistic - or noisier - stimuli ((Faisal, Selen, & Wolpert, 2008). Mainen and Sejnowski showed that noisy current injection into a single pyramidal neuron evokes temporally precise spiking responses whereas non-noisy constant current injections evokes strong, but temporally variable, neuronal responses (Mainen & Sejnowski, 1995). Circuit level studies in the primary visual cortex have revealed similar characteristics, where artificial stimuli evoke strong

but temporally variable neuronal responses, while responses to natural stimuli are weak but temporally precise. It has been suggested that the precise interplay of excitatory and inhibitory synaptic inputs in the receptive fields of neurons in the visual cortex might play a significant role in modulating these responses (Kremkow et al., 2016). It is hypothesized that the stochastic nature of receptor activation kinetics is responsible for regulating firing at the level of single neurons. In addition to this electrically coupled parameter, biochemical interactions, such as the balance between protein phosphatases and kinases, are believed to regulate the direction and longevity of synaptic plasticity (Wang & Kelly, 1996; Otmakhov et al., 1997; Winder, Mansuy, Osman, Moallem, & Kandel, 1998). Moreover, information theory suggest that a train with a completely deterministic inter-spike/pulse intervals carries less information compared with a random counterpart (Touretzky, 1996; Stevens & Zador, 1996). This may speak to a sort of information content depending encoding at single spines.

Our results seem to combine components from both electrical and biophysical interactions. During the stimulation period, receptor activation dynamics are determined by the ionic interactions within the various subunits of the receptors, and therefore it is likely that electro-chemical processes govern the rapid structural growth dynamics. These are believed to be effected by the remodeling of the actin cytoskeleton (Okamoto, Nagai, Miyawaki, & Hayashi, 2004; Fonseca, 2012). The late phase of LTP has been shown to be maintained by newly synthesized proteins (Otmakhova & Lisman, 1996; Sutton & Schuman, 2006), and our results support the finding that this also holds true for long lasting structural plasticity (Govindarajan et al., 2011). What we do not know is how the short-term temporal dynamics determine the engagement of downstream processes such as the protein synthesis machinery of the neuron.

Many studies attempted to determine the relationship between time and frequency dependence of pre-synaptic activity, post-synaptic firing and induced plasticity (Bienenstock et al., 1982; Markram et al., 1997; Bi & Poo, 1998; Froemke & Dan, 2002; Izhikevich & Desai, 2003; Pfister & Gerstner, 2006). While they were able to describe some rules by which synaptic plasticity is induced, none of them hypothesized potential mechanisms for how the longevity of plasticity is maintained once it is induced. Our results suggest that *in vivo* activity patterns that are received by a particular spine might contribute to that spines future structural reorganization. This may be particularly interesting in terms of predicting *in vivo*long-term structural dynamics of a synapse, based on short-term structural imaging observations.

These results show how different patterns of activity can elicit plasticity processes at synapses, presenting a window into understanding how neural activity patterns *in vivo* might have long-term consequences for synaptic strength and circuit organization.

Our results also showed that, on contrary to previous research (Matsuzaki et al., 2004), initial spine sizes do not modulate the plasticity levels for different stimulation conditions. Matsuzaki *et al.* reported that dendritic spines that are larger than $1\mu m^3$ did not show long-lasting enlargement following a regular glutamate uncaging stimulation which induced long-lasting enlargement in smaller spines (Matsuzaki et al., 2004). However, axonal bouton volumes and active zone areas of hippocampal CA3 neurons are highly heterogeneous and this heterogeneity reflects the probability and amount of glutamate that is released by those terminals (Holderith et al., 2012). These results suggest that the smaller the axonal terminal, the harder is to induce LTP at the corresponding spine. Furthermore, axonal bouton- and dendritic spine- volumes are shown to be positively correlated (Holderith et al., 2012; Meyer, Bonhoeffer, & Scheuss, 2014). Hence, evidence supported by previously conducted

research in combination with our results suggest that dendritic spine sizes should not present neither an advantage or disadvantage for the spine in terms of ease of potentiation. Therefore, the idea of spine size dependency for potentiation should be revisited.

Appendix I:

	1	2	3	4	5	6	7	8	9	10	11	12	13	14	15	16	17	18	19	20	21	22	23	24	25	26	27	28	29	30
REG	0	2000	2000	2000	2000	2000	2000	2000	2000	2000	2000	2000	2000	2000	2000	2000	2000	2000	2000	2000	2000	2000	2000	2000	2000	2000	2000	2000	2000	2000
NTU	0	2589	2014	3596	711	862	515	1880	543	3306	3157	1564	430	683	1504	1050	4373	281	2003	5996	2532	1504	813	240	4519	2098	1531	80	2424	4001
NTB	0	1544	166	2221	116	155	335	2221	579	585	352	821	476	848	3603	3723	1120	34	9043	632	3029	5171	176	6803	1692	2302	1778	1968	2371	2571
NTE	0	6444	2749	6630	3917	805	6557	2529	3065	1400	472	1266	1152	375	1955	2930	816	236	1438	1293	76	246	199	719	118	1306	2689	920	1687	2683

References

Araque, A., Parpura, V., Sanzgiri, R. P., & Haydon, P. G. (1999). Tripartite synapses: glia, the unacknowledged partner. *Trends in neurosciences*, *22*(5), 208–215.

Arellano, J. I., Benavides-Piccione, R., DeFelipe, J., & Yuste, R. (2007). Ultrastructure of dendritic spines: correlation between synaptic and spine morphologies. *Frontiers in neuroscience*, *1*, 10.

Asrican, B., Lisman, J., & Otmakhov, N. (2007). Synaptic strength of individual spines correlates with bound ca2+–calmodulin-dependent kinase ii. *The Journal of Neuroscience*, *27*(51), 14007–14011.

Azevedo, F. A., Carvalho, L. R., Grinberg, L. T., Farfel, J. M., Ferretti, R. E., Leite, R. E., ... others (2009). Equal numbers of neuronal and nonneuronal cells make the human brain an isometrically scaled-up primate brain. *Journal of Comparative Neurology*, *513*(5), 532–541.

Bair, W., Koch, C., Newsome, W., & Britten, K. (1994). Power spectrum analysis of bursting cells in area mt in the behaving monkey. *The Journal of neuroscience*, *14*(5), 2870–2892.

Bartol, T. M., Bromer, C., Kinney, J. P., Chirillo, M. A., Bourne, J. N., Harris, K. M., & Sejnowski, T. J. (2015). Hippocampal spine head sizes are highly precise. *bioRxiv*, 016329.

Bear, M. F., & Malenka, R. C. (1994). Synaptic plasticity: Ltp and ltd. *Current opinion in neurobiology*, *4*(3), 389–399.

Bi, G.-q., & Poo, M.-m. (1998). Synaptic modifications in cultured hippocampal neurons: dependence on spike timing, synaptic strength, and postsynaptic cell type. *The Journal of neuroscience*, *18*(24), 10464–10472.

Bienenstock, E. L., Cooper, L. N., & Munro, P. W. (1982). Theory for the development of neuron selectivity: orientation specificity and binocular interaction in visual cortex. *The Journal of Neuroscience*, *2*(1), 32–48.

Bishop, C. (2007). *Pattern recognition and machine learning (information science and statistics), 1st edn. 2006. corr. 2nd printing edn.* Springer, New York.

Bliss, T., Collingridge, G., & Morris, R. (2014). Synaptic plasticity in health and disease: introduction and overview. *Philosophical Transactions of the Royal Society of London B: Biological Sciences*, *369*(1633), 20130129.

Bliss, T. V., & Lømo, T. (1973). Long-lasting potentiation of synaptic transmission in the dentate area of the anaesthetized rabbit following stimulation of the perforant path. *The Journal of physiology*, *232*(2), 331–356.

Bosch, M., Castro, J., Saneyoshi, T., Matsuno, H., Sur, M., & Hayashi, Y. (2014). Structural and molecular remodeling of dendritic spine substructures during long-term potentiation. *Neuron*, *82*(2), 444–459.

Braitenberg, V. (2001). Brain size and number of neurons: an exercise in synthetic neuroanatomy. *Journal of computational neuroscience*, *10*(1), 71–77.

Branco, T., Clark, B. A., & Häusser, M. (2010). Dendritic discrimination of temporal input sequences in cortical neurons. *Science*, *329*(5999), 1671–1675.

Cerovic, M., dIsa, R., Tonini, R., & Brambilla, R. (2013). Molecular and

cellular mechanisms of dopamine-mediated behavioral plasticity in the striatum. *Neurobiology of learning and memory*, *105*, 63–80.

Christopher deCharms, R., & Merzenich, M. M. (1996). Primary cortical representation of sounds by the coordination of action-potential timing. *Nature*, *381*, 13.

Cooper, L. N., & Bear, M. F. (2012). The bcm theory of synapse modification at 30: interaction of theory with experiment. *Nature Reviews Neuroscience*, *13*(11), 798–810.

Czarnecki, A., Birtoli, B., & Ulrich, D. (2007). Cellular mechanisms of burst firing-mediated long-term depression in rat neocortical pyramidal cells. *The Journal of physiology*, *578*(2), 471–479.

DeFelipe, J., Marco, P., Busturia, I., & Merchán-Pérez, A. (1999). Estimation of the number of synapses in the cerebral cortex: methodological considerations. *Cerebral Cortex*, *9*(7), 722–732.

deKay, J. G., Chang, T. C., Mills, N., Speed, H. E., & Dobrunz, L. E. (2006). Responses of excitatory hippocampal synapses to natural stimulus patterns reveal a decrease in short-term facilitation and increase in short-term depression during postnatal development. *Hippocampus*, *16*(1), 66–79.

Deng, W., Aimone, J. B., & Gage, F. H. (2010). New neurons and new memories: how does adult hippocampal neurogenesis affect learning and memory? *Nature Reviews Neuroscience*, *11*(5), 339–350.

Denk, W., Strickler, J. H., & Webb, W. W. (1990). Two-photon laser scanning fluorescence microscopy. *Science*, *248*(4951), 73–76.

De Robertis, E. D., & Bennett, H. S. (1955). Some features of the submicroscopic morphology of synapses in frog and earthworm. *The Journal of biophysical and biochemical cytology*, *1*(1), 47–58.

Dobrunz, L. E., & Stevens, C. F. (1999). Response of hippocampal synapses to natural stimulation patterns. *Neuron*, *22*(1), 157–166.

Edelmann, E., & Lessmann, V. (2011). Dopamine modulates spike timing-

dependent plasticity and action potential properties in ca1 pyramidal neurons of acute rat hippocampal slices. *Front Synaptic Neurosci*, *3*(6).

Eichenbaum, H. (1997). Declarative memory: Insights from cognitive neurobiology. *Annual review of psychology*, *48*(1), 547–572.

Ellis-Davies, G. C. (2007). Caged compounds: photorelease technology for control of cellular chemistry and physiology. *Nature methods*, *4*(8), 619–628.

Engert, F., & Bonhoeffer, T. (1999). Dendritic spine changes associated with hippocampal long-term synaptic plasticity. *Nature*, *399*(6731), 66–70.

Erdil, E., Yağcı, A. M., Argunşah, A. O., Ramiro-Cortés, Y., Hobbiss, A. F., Israely, I., & Ünay, D. (2012). A tool for automatic dendritic spine detection and analysis. part i: Dendritic spine detection using multi-level region-based segmentation. In *Image processing theory, tools and applications (ipta), 2012 3rd international conference on* (pp. 167–171).

Faisal, A. A., Selen, L. P., & Wolpert, D. M. (2008). Noise in the nervous system. *Nature Reviews Neuroscience*, *9*(4), 292–303.

Farley, B., & Clark, W. (1954). Simulation of self-organizing systems by digital computer. *Transactions of the IRE Professional Group on Information Theory*, *4*(4), 76–84.

Feldman, D. E. (2009). Synaptic mechanisms for plasticity in neocortex. *Annual review of neuroscience*, *32*, 33.

Ferster, D., & Spruston, N. (1995). Cracking the neuronal code. *Science*, *270*(5237), 756.

Fifková, E., Anderson, C. L., Young, S., & Van Harreveld, A. (1982). Effect of anisomycin on stimulation-induced changes in dendritic spines of the dentate granule cells. *Journal of neurocytology*, *11*(2), 183–210.

Figurov, A., Pozzo-Miller, L. D., Olafsson, P., Wang, T., Lu, B., et al. (1996). Regulation of synaptic responses to high-frequency stimulation and ltp by neurotrophins in the hippocampus. *Nature*, *381*(6584), 706–709.

Fonseca, R. (2012). Activity-dependent actin dynamics are required for the maintenance of long-term plasticity and for synaptic capture. *European Journal of Neuroscience*, *35*(2), 195–206.

Fonseca, R., Nägerl, U. V., Morris, R. G., & Bonhoeffer, T. (2004). Competing for memory: hippocampal ltp under regimes of reduced protein synthesis. *Neuron*, *44*(6), 1011–1020.

Foster, M. (1895). *A text-book of physiology*. Lea Bros & Company.

Frerking, M., Schulte, J., Wiebe, S., & Stäubli, U. (2005). Spike timing in ca3 pyramidal cells during behavior: implications for synaptic transmission. *Journal of neurophysiology*, *94*(2), 1528–1540.

Friauf, E., Fischer, A. U., & Fuhr, M. F. (2015). Synaptic plasticity in the auditory system: a review. *Cell and tissue research*, *361*(1), 177–213.

Froemke, R. C. (2015). Plasticity of cortical excitatory-inhibitory balance. *Annual review of neuroscience*, *38*, 195.

Froemke, R. C., & Dan, Y. (2002). Spike-timing-dependent synaptic modification induced by natural spike trains. *Nature*, *416*(6879), 433–438.

Froemke, R. C., Tsay, I. A., Raad, M., Long, J. D., & Dan, Y. (2006). Contribution of individual spikes in burst-induced long-term synaptic modification. *Journal of neurophysiology*, *95*(3), 1620–1629.

Fulton, J. F. (1960). Ramon y cajal, sherrington and the neurone doctrine. *Basic Research in Cardiology*, *33*(1), 154–158.

Gähwiler, B. (1981). Organotypic monolayer cultures of nervous tissue. *Journal of neuroscience methods*, *4*(4), 329–342.

Goldberg, I. G., Allan, C., Burel, J.-M., Creager, D., Falconi, A.,

Hochheiser, H., ... Swedlow, J. R. (2005). The open microscopy environment (ome) data model and xml file: open tools for informatics and quantitative analysis in biological imaging. *Genome biology*, *6*(5), R47.

Govindarajan, A., Israely, I., Huang, S.-Y., & Tonegawa, S. (2011). The dendritic branch is the preferred integrative unit for protein synthesis-dependent ltp. *Neuron*, *69*(1), 132–146.

Gundlfinger, A., Breustedt, J., Sullivan, D., & Schmitz, D. (2010). Natural spike trains trigger short-and long-lasting dynamics at hippocampal mossy fiber synapses in rodents. *PLoS One*, *5*(4), e9961.

Gundlfinger, A., Leibold, C., Gebert, K., Moisel, M., Schmitz, D., & Kempter, R. (2007). Differential modulation of short-term synaptic dynamics by long-term potentiation at mouse hippocampal mossy fibre synapses. *The Journal of physiology*, *585*(3), 853–865.

Gustafsson, B., & Wigström, H. (1990). Long-term potentiation in the hippocampal ca1 region: its induction and early temporal development. *Progress in brain research*, *83*, 223–232.

Harris, K. M., & Stevens, J. K. (1989). Dendritic spines of ca 1 pyramidal cells in the rat hippocampus: serial electron microscopy with reference to their biophysical characteristics. *The Journal of neuroscience*, *9*(8), 2982–2997.

Harvey, C. D., & Svoboda, K. (2007). Locally dynamic synaptic learning rules in pyramidal neuron dendrites. *Nature*, *450*(7173), 1195–1200.

Harvey, C. D., Yasuda, R., Zhong, H., & Svoboda, K. (2008). The spread of ras activity triggered by activation of a single dendritic spine. *Science*, *321*(5885), 136–140.

Hassouna, S. M., & Farag, A. A. (2007). Multistencils fast marching methods: A highly accurate solution to the eikonal equation on cartesian domains. *Pattern Analysis and Machine Intelligence, IEEE Transactions on*, *29*(9), 1563–1574.

Hawes, S. L., Gillani, F., Evans, R. C., Benkert, E. A., & Blackwell, K. T. (2013). Sensitivity to theta-burst timing permits ltp in dorsal striatal adult brain slice. *Journal of neurophysiology*, *110*(9), 2027–2036.

Hebb, D. O. (1949). *The organization of behavior: A neuropsychological approach*. John Wiley & Sons.

Herikstad, R., Baker, J., Lachaux, J.-P., Gray, C. M., & Yen, S.-C. (2011). Natural movies evoke spike trains with low spike time variability in cat primary visual cortex. *The Journal of Neuroscience*, *31*(44), 15844–15860.

Hestrin, S., Sah, P., & Nicoll, R. A. (1990). Mechanisms generating the time course of dual component excitatory synaptic currents recorded in hippocampal slices. *Neuron*, *5*(3), 247–253.

Hill, T. C., & Zito, K. (2013). Ltp-induced long-term stabilization of individual nascent dendritic spines. *The Journal of Neuroscience*, *33*(2), 678–686.

Holderith, N., Lorincz, A., Katona, G., Rózsa, B., Kulik, A., Watanabe, M., & Nusser, Z. (2012). Release probability of hippocampal glutamatergic terminals scales with the size of the active zone. *Nature neuroscience*, *15*(7), 988–997.

Holtmaat, A. J., Trachtenberg, J. T., Wilbrecht, L., Shepherd, G. M., Zhang, X., Knott, G. W., & Svoboda, K. (2005). Transient and persistent dendritic spines in the neocortex in vivo. *Neuron*, *45*(2), 279–291.

Huganir, R. L., & Nicoll, R. A. (2013). Ampars and synaptic plasticity: the last 25 years. *Neuron*, *80*(3), 704–717.

Ito, M., & Kano, M. (1982). Long-lasting depression of parallel fiber-purkinje cell transmission induced by conjunctive stimulation of parallel fibers and climbing fibers in the cerebellar cortex. *Neuroscience letters*, *33*(3), 253–258.

Izhikevich, E. M., & Desai, N. S. (2003). Relating stdp to bcm. *Neural*

computation, *15*(7), 1511–1523.

Kasai, H., Fukuda, M., Watanabe, S., Hayashi-Takagi, A., & Noguchi, J. (2010). Structural dynamics of dendritic spines in memory and cognition. *Trends in neurosciences*, *33*(3), 121–129.

Kimmel, R., & Sethian, J. (1996). Fast marching methods for computing distance maps and shortest paths. *CPAM Report*, *669*.

Kremkow, J., Perrinet, L. U., Monier, C., Alonso, J.-M., Aertsen, A., Fregnac, Y., & Masson, G. S. (2016). Push-pull receptive field organization and synaptic depression: Mechanisms for reliably encoding naturalistic stimuli in v1. *Frontiers in Neural Circuits*, *10*, 37.

Lee, K. S., Schottler, F., Oliver, M., & Lynch, G. (1980). Brief bursts of high-frequency stimulation produce two types of structural change in rat hippocampus. *Journal of Neurophysiology*, *44*(2), 247–258.

Lee, S.-J. R., Escobedo-Lozoya, Y., Szatmari, E. M., & Yasuda, R. (2009). Activation of camkii in single dendritic spines during long-term potentiation. *Nature*, *458*(7236), 299–304.

Leon-Garcia, A. (2008). *Probability, statistics, and random processes for electrical engineering*. Pearson/Prentice Hall.

Lisman, J., & Spruston, N. (2005). Postsynaptic depolarization requirements for ltp and ltd: a critique of spike timing-dependent plasticity. *Nature neuroscience*, *8*(7), 839–841.

Lisman, J., & Spruston, N. (2010). Questions about stdp as a general model of synaptic plasticity. *Spike-timing dependent plasticity*, *26*, 53.

Lisman, J. E., & McIntyre, C. C. (2001). Synaptic plasticity: a molecular memory switch. *Current Biology*, *11*(19), R788–R791.

London, M., & Häusser, M. (2005). Dendritic computation. *Annu. Rev. Neurosci.*, *28*, 503–532.

López-Muñoz, F., Boya, J., & Alamo, C. (2006). Neuron theory, the cornerstone of neuroscience, on the centenary of the nobel prize award

to santiago ramón y cajal. *Brain research bulletin*, *70*(4), 391–405.

Losonczy, A., & Magee, J. C. (2006). Integrative properties of radial oblique dendrites in hippocampal ca1 pyramidal neurons. *Neuron*, *50*(2), 291–307.

Losonczy, A., Makara, J. K., & Magee, J. C. (2008). Compartmentalized dendritic plasticity and input feature storage in neurons. *Nature*, *452*(7186), 436–441.

Lowel, S., & Singer, W. (1992). Selection of intrinsic horizontal connections in the visual cortex by correlated neuronal activity. *Science*, *255*(5041), 209–212.

Magee, J. C. (2000). Dendritic integration of excitatory synaptic input. *Nature Reviews Neuroscience*, *1*(3), 181–190.

Mahan, A. L., & Ressler, K. J. (2012). Fear conditioning, synaptic plasticity and the amygdala: implications for posttraumatic stress disorder. *Trends in neurosciences*, *35*(1), 24–35.

Mainen, Z. F., & Sejnowski, T. J. (1995). Reliability of spike timing in neocortical neurons. *Science*, *268*(5216), 1503–1506.

Makridakis, S. (1993). Accuracy measures: theoretical and practical concerns. *International Journal of Forecasting*, *9*(4), 527–529.

Malenka, R. C., & Bear, M. F. (2004). Ltp and ltd: an embarrassment of riches. *Neuron*, *44*(1), 5–21.

Maletic-Savatic, M., Malinow, R., & Svoboda, K. (1999). Rapid dendritic morphogenesis in ca1 hippocampal dendrites induced by synaptic activity. *Science*, *283*(5409), 1923–1927.

Markram, H., Gerstner, W., & Sjöström, P. (2012). Spike-timing-dependent plasticity: a comprehensive overview. *Front Synaptic Neurosci*, *4*, 8.

Markram, H., Lübke, J., Frotscher, M., & Sakmann, B. (1997). Regulation of synaptic efficacy by coincidence of postsynaptic aps and epsps. *Science*, *275*(5297), 213–215.

Matsuzaki, M., Honkura, N., Ellis-Davies, G. C., & Kasai, H. (2004). Structural basis of long-term potentiation in single dendritic spines. *Nature*, *429*(6993), 761–766.

McCulloch, W. S., & Pitts, W. (1943). A logical calculus of the ideas immanent in nervous activity. *The bulletin of mathematical biophysics*, *5*(4), 115–133.

McHugh, T. J., Blum, K. I., Tsien, J. Z., Tonegawa, S., & Wilson, M. A. (1996). Impaired hippocampal representation of space in ca1-specific nmdar1 knockout mice. *Cell*, *87*(7), 1339–1349.

Mehta, M. R., Quirk, M. C., & Wilson, M. A. (2000). Experience-dependent asymmetric shape of hippocampal receptive fields. *Neuron*, *25*(3), 707–715.

Meyer, D., Bonhoeffer, T., & Scheuss, V. (2014). Balance and stability of synaptic structures during synaptic plasticity. *Neuron*, *82*(2), 430–443.

Middleton, S. J., & McHugh, T. J. (2016). Silencing ca3 disrupts temporal coding in the ca1 ensemble. *Nature neuroscience*.

Migliore, M., De Simone, G., & Migliore, R. (2015). Effect of the initial synaptic state on the probability to induce long-term potentiation and depression. *Biophysical journal*, *108*(5), 1038–1046.

Migliore, M., & Lansky, P. (1999). Long-term potentiation and depression induced by a stochastic conditioning of a model synapse. *Biophysical journal*, *77*(3), 1234–1243.

Mimaroglu, S., & Erdil, E. (2011). Combining multiple clusterings using similarity graph. *Pattern Recognition*, *44*(3), 694–703.

Mulkey, R. M., Endo, S., Shenolikar, S., Malenka, R. C., et al. (1994). Involvement of a calcineurin/inhibitor-1 phosphatase cascade in hippocampal long-term depression. *Nature*, *369*(6480), 486–488.

Nimchinsky, E. A., Yasuda, R., Oertner, T. G., & Svoboda, K. (2004). The number of glutamate receptors opened by synaptic stimulation

in single hippocampal spines. *The Journal of neuroscience*, *24*(8), 2054–2064.

Ogawa, H., & Umesono, K. (1998). Intracellular localization and transcriptional activation by the human glucocorticoid receptor-green fluorescent protein (gfp) fusion proteins. *Acta histochemica et cytochemica*, *31*(4), 303–308.

Okamoto, K.-I., Nagai, T., Miyawaki, A., & Hayashi, Y. (2004). Rapid and persistent modulation of actin dynamics regulates postsynaptic reorganization underlying bidirectional plasticity. *Nature neuroscience*, *7*(10), 1104–1112.

O'Keefe, J., & Dostrovsky, J. (1971). The hippocampus as a spatial map. preliminary evidence from unit activity in the freely-moving rat. *Brain research*, *34*(1), 171–175.

Otmakhov, N., Griffith, L. C., & Lisman, J. E. (1997). Postsynaptic inhibitors of calcium/calmodulin-dependent protein kinase type ii block induction but not maintenance of pairing-induced long-term potentiation. *The Journal of neuroscience*, *17*(14), 5357–5365.

Otmakhova, N. A., & Lisman, J. E. (1996). D1/d5 dopamine receptor activation increases the magnitude of early long-term potentiation at ca1 hippocampal synapses. *The Journal of neuroscience*, *16*(23), 7478–7486.

Otsu, N. (1975). A threshold selection method from gray-level histograms. *Automatica*, *11*(285-296), 23–27.

Palade, G. (1954). Electron microscope observations of interneuronal and neuromuscular synapses. In *Anatomical record* (Vol. 118, pp. 335–336).

Paulsen, O., & Sejnowski, T. J. (2000). Natural patterns of activity and long-term synaptic plasticity. *Current opinion in neurobiology*, *10*(2), 172–180.

Pfister, J.-P., & Gerstner, W. (2006). Triplets of spikes in a model of spike

timing-dependent plasticity. *The Journal of neuroscience*, *26*(38), 9673–9682.

Pike, F. G., Meredith, R. M., Olding, A. W., & Paulsen, O. (1999). Postsynaptic bursting is essential for hebbianinduction of associative long-term potentiation at excitatory synapses in rat hippocampus. *The Journal of physiology*, *518*(2), 571–576.

Prut, Y., Slovin, H., & Aertsen, A. (1995). Dynamics of neuronal interactions in monkey cortex in relation to behavioural events. *Nature*, *373*, 9.

Ramiro-Cortés, Y., & Israely, I. (2013). Long lasting protein synthesis-and activity-dependent spine shrinkage and elimination after synaptic depression. *PLoS One*, *8*(8), e71155.

Redondo, R. L., & Morris, R. G. (2011). Making memories last: the synaptic tagging and capture hypothesis. *Nature Reviews Neuroscience*, *12*(1), 17–30.

Rosanova, M., & Ulrich, D. (2005). Pattern-specific associative long-term potentiation induced by a sleep spindle-related spike train. *The Journal of Neuroscience*, *25*(41), 9398–9405.

Rosenblatt, F. (1958). The perceptron: a probabilistic model for information storage and organization in the brain. *Psychological review*, *65*(6), 386.

Sabbatini, R. (2003). Neurons and synapses. the history of its discovery. *Brain & Mind Magazine*, *17*.

Schiller, J., Schiller, Y., & Clapham, D. E. (1998). Nmda receptors amplify calcium influx into dendritic spines during associative pre- and postsynaptic activation. *Nature neuroscience*, *1*(2), 114–118.

Scoville, W. B., & Milner, B. (1957). Loss of recent memory after bilateral hippocampal lesions. *Journal of Neurology, Neurosurgery & Psychiatry*, *20*(1), 11–21.

Segal, M. (2004). History of neuroscience: Dendritic spines of memory.

IBRO History of Neuroscience.

Sheng, M., & Kim, M. J. (2002). Postsynaptic signaling and plasticity mechanisms. *Science*, *298*(5594), 776–780.

Sigurdsson, T., Doyère, V., Cain, C. K., & LeDoux, J. E. (2007). Long-term potentiation in the amygdala: a cellular mechanism of fear learning and memory. *Neuropharmacology*, *52*(1), 215–227.

Smith, M. A., Ellis-Davies, G. C., & Magee, J. C. (2003). Mechanism of the distance-dependent scaling of schaffer collateral synapses in rat ca1 pyramidal neurons. *The Journal of physiology*, *548*(1), 245–258.

Soille, P. (2013). *Morphological image analysis: principles and applications*. Springer Science & Business Media.

Song, S., & Abbott, L. F. (2001). Cortical development and remapping through spike timing-dependent plasticity. *Neuron*, *32*(2), 339–350.

Song, S., Miller, K. D., & Abbott, L. F. (2000). Competitive hebbian learning through spike-timing-dependent synaptic plasticity. *Nature neuroscience*, *3*(9), 919–926.

Staubli, U., & Lynch, G. (1987). Stable hippocampal long-term potentiation elicited by thetapattern stimulation. *Brain research*, *435*(1), 227–234.

Stäubli, U., & Scafidi, J. (1999). Time-dependent reversal of long-term potentiation in area ca1 of the freely moving rat induced by theta pulse stimulation. *The Journal of neuroscience*, *19*(19), 8712–8719.

Stevens, C., & Zador, A. (1996). Information through a spiking neuron. *Advances in neural information processing systems*, 75–81.

Stoppini, L., Buchs, P.-A., & Muller, D. (1991). A simple method for organotypic cultures of nervous tissue. *Journal of neuroscience methods*, *37*(2), 173–182.

Sutton, M. A., & Schuman, E. M. (2006). Dendritic protein synthesis, synaptic plasticity, and memory. *Cell*, *127*(1), 49–58.

Svoboda, K., & Yasuda, R. (2006). Principles of two-photon excitation

microscopy and its applications to neuroscience. *Neuron*, *50*(6), 823–839.

Tonnesen, J., Katona, G., Rózsa, J., Nagerl, U., et al. (2014). Spine neck plasticity regulates compartmentalization of synapses. *Nature neuroscience*, *17*(5), 678–685.

Touretzky, D. S. (1996). *Advances in neural information processing systems 8: Proceedings of the 1995 conference* (Vol. 8). Mit Press.

Troy, J., & Robson, J. (1992). Steady discharges of x and y retinal ganglion cells of cat under photopic illuminance. *Visual neuroscience*, *9*(06), 535–553.

Tsodyks, M. V., & Markram, H. (1997). The neural code between neocortical pyramidal neurons depends on neurotransmitter release probability. *Proceedings of the National Academy of Sciences*, *94*(2), 719–723.

Tunstall, B., Agnew, Z. K., Panzeri, S., & Gigg, J. (2010). Naturalistic stimulus trains evoke reproducible subicular responses both within and between animals in vivo. *Hippocampus*, *20*(2), 252–263.

Van Harreveld, A., & Fifkova, E. (1975). Swelling of dendritic spines in the fascia dentata after stimulation of the perforant fibers as a mechanism of post-tetanic potentiation. *Experimental neurology*, *49*(3), 736–749.

Vinje, W. E., & Gallant, J. L. (2002). Natural stimulation of the nonclassical receptive field increases information transmission efficiency in v1. *The Journal of Neuroscience*, *22*(7), 2904–2915.

Wallisch, P., Lusignan, M. E., Benayoun, M. D., Baker, T. I., Dickey, A. S., & Hatsopoulos, N. G. (2014). *Matlab for neuroscientists: an introduction to scientific computing in matlab*. Academic Press.

Wang, J.-H., & Kelly, P. T. (1996). The balance between postsynaptic ca (2+)-dependent protein kinase and phosphatase activities controlling synaptic strength. *Learning & Memory*, *3*(2-3), 170–181.

Wang, S.-H., Redondo, R. L., & Morris, R. G. (2010). Relevance of synaptic tagging and capture to the persistence of long-term potentiation and everyday spatial memory. *Proceedings of the National Academy of Sciences*, *107*(45), 19537–19542.

Wells, W. M., Viola, P., Atsumi, H., Nakajima, S., & Kikinis, R. (1996). Multi-modal volume registration by maximization of mutual information. *Medical image analysis*, *1*(1), 35–51.

Whitlock, J. R., Heynen, A. J., Shuler, M. G., & Bear, M. F. (2006). Learning induces long-term potentiation in the hippocampus. *science*, *313*(5790), 1093–1097.

Winder, D. G., Mansuy, I. M., Osman, M., Moallem, T. M., & Kandel, E. R. (1998). Genetic and pharmacological evidence for a novel, intermediate phase of long-term potentiation suppressed by calcineurin. *Cell*, *92*(1), 25–37.

Woods, G., & Zito, K. (2008). Preparation of gene gun bullets and biolistic transfection of neurons in slice culture. *JoVE (Journal of Visualized Experiments)*(12), e675–e675.

Zador, A. M., & Dobrunz, L. E. (1997). Dynamic synapses in the cortex. *Neuron*, *19*(1), 1–4.

Apoio financeiro da FCT e do FSE no âmbito do
Quadro Comunitário de Apoio, Bolsa n^o SFRH/BD/51264/2010

ITQB-UNL | Av. da República, 2780-157 Oeiras, Portugal
Tel (+351) 214 469 100 | Fax (+351) 214 411 277

www.itqb.unl.pt